NASA TECHNICAL NOTE

NASA TN D-7432

NASA TN D-7432

OPTIMIZATION OF WAVE CANCELLATION IN VARIABLE POROSITY TRANSONIC WIND TUNNEL FLOWS

by John William Davis

George C. Marshall Space Flight Center
Marshall Space Flight Center, Ala. 35812

NATIONAL AERONAUTICS AND SPACE ADMINISTRATION • WASHINGTON, D. C. • NOVEMBER 1973

TECHNICAL REPORT STANDARD TITLE PAGE

1. REPORT NO.	2. GOVERNMENT ACCESSION NO.	3. RECIPIENT'S CATALOG NO.
NASA TN D-7432		

4. TITLE AND SUBTITLE	5. REPORT DATE
Optimization of Wave Cancellation in Variable Porosity Transonic Wind Tunnel Flows	November 1973
	6. PERFORMING ORGANIZATION CODE
7. AUTHOR(S)	8. PERFORMING ORGANIZATION REPORT #
John William Davis	M108
9. PERFORMING ORGANIZATION NAME AND ADDRESS	10. WORK UNIT NO.
George C. Marshall Space Flight Center Marshall Space Flight Center, Alabama 35812	11. CONTRACT OR GRANT NO.
12. SPONSORING AGENCY NAME AND ADDRESS	13. TYPE OF REPORT & PERIOD COVERED
National Aeronautics and Space Administration Washington, D. C. 20546	Technical Note
	14. SPONSORING AGENCY CODE

15. SUPPLEMENTARY NOTES

Prepared by Aero-Astrodynamics Laboratory, Science and Engineering

16. ABSTRACT

A technique has been developed which is capable of determining the optimum wall configuration for a variable porosity perforated wall transonic wind tunnel. The technique is based on a mathematical model arrived at by considering the results of theory and past experimental investigations. A performance index was determined as a function of the significant wind tunnel parameters by comparing a formulation of this mathematical model, using MSFC 14 inch Trisonic Wind Tunnel experimental results, to interference free results. The resulting relationship was then used to determine the combination of wind tunnel parameters which should yield minimum reflected wave interference.

A theoretical development of wall porosity requirements for thick wall inclined hole test sections is included which follows the trends and generally the magnitude of available experimental data. This theory is useful in studying the present variable porosity case, but also should be of value in studies concerning the wave cancellation process for fixed porosity walls.

To implement this optimization procedure a multiple regression technique for Pth degree polynomials is developed to evaluate the mathematical models. This powerful general purpose tool can be used in any scientific endeavor where the process can be measured of for which experimental data exist. Using this regression technique many phenomena can be correlated or suspected laws or relationships investigated and optimizations determined other than those developed in the course of this study.

17. KEY WORDS	18. DISTRIBUTION STATEMENT

19. SECURITY CLASSIF. (of this report)	20. SECURITY CLASSIF. (of this page)	21. NO. OF PAGES	22. PRICE
Unclassified	Unclassified	136	Domestic, $4.50 Foreign, $7.00

For sale by National Technical Information Service, Springfield, Virginia 22151

PREFACE

The objective of this research was to develop a scientific procedure by which the transonic flow wave cancellation problem can be studied mathematically and which can be used to predict optimum values of wind tunnel parameters for a variable porosity transonic wind tunnel that can be expected to yield minimum reflected wave interference on the aerodynamic test model. The significant parameters are identified by means of an analysis of thin wall and thick wall theory for perforated wall wave cancellation and by a review of past experimental work.

By means of a quasi-linear multiple regression technique, a mathematical model was developed which predicts local model pressure ratios as a function of the significant wind tunnel parameters including Mach number and wall porosity using experimental data from the National Aeronautics and Space Administration (NASA), Marshall Space Flight Center (MSFC), 14-Inch Trisonic Wind Tunnel Facility (TWT). Using the same multiple regression technique, an empirical model was developed which predicts local model pressure ratios as a function of Mach number and distance along the model using experimental data for a very small model tested in a large wind tunnel which can be assumed to have negligible wave interference.

At any model station, the numerical difference in these physical models represents the error due to wave interference. Hence, the total error may be

obtained as a function of the significant wind tunnel parameters by integrating this difference over the length of the model. This error can be used as an index of performance. By this means an algebraic relation is determined which can be used to obtain the values of the transonic wind tunnel parameters which should be expected to yield minimum wave interference. The method of steepest ascent (descent) is used to determine these optimum values.

Optimum wall porosity values have been determined for the Marshall Space Flight Center 14-Inch Trisonic Wind Tunnel based on existing data. Although the data evaluated were measured over a range of wall porosities too small to allow firm quantitative conclusions, results of confirmation wind tunnel tests based on data from the transonic optimization procedure agree closely with the results predicted by the performance index. It is, therefore, reasonable to conclude that the optimization procedure developed does, in fact, provide a useful means to minimize wave interference and, with future refinements using statistically designed experiments, should prove to be a powerful tool in advancing variable porosity transonic wind tunnel technology. Results obtained using this technique can be expected to provide better simulation with less experimental testing than previous trial-and-error methods.

It is noted that this work was originally published as a doctorial thesis submitted to Oklahoma State University in July, 1972 and the support, encouragement, and advice by Dr. J. R. Norton and Dr. W. B. Brooks in the course of this study are gratefully acknowledged.

TABLE OF CONTENTS

TABLE OF CONTENTS (Concluded)

LIST OF ILLUSTRATIONS

LIST OF ILLUSTRATIONS (Concluded)

LIST OF TABLES

DEFINITION OF SYMBOLS

Symbol	Definition
A	cross-sectional area
A_0	model equation intercept coefficient
B_N	matrix quantity
B_P	model equation coefficients
b_{NP}	regression model coefficients
C_P	model equation coefficients
C_p	pressure coefficient
D	model diameter
D_p	model equation coefficients
d_h	perforated hole diameter
E	root mean square error
E_M	root mean square error at given Mach number
E_P	model equation coefficients
F	F statistic
h	distance between streamlines
L	length over which wave cancellation process occurs
l	model length
M	Mach number
M_f	minimizing function

DEFINITION OF SYMBOLS (Continued)

Symbol	Definition
$\dot{m}$	mass flow
N	number of independent variables
n	number of data points or perforated holes
P	static pressure or degree of equation
P_t	stagnation pressure
P(F)	probability at given F value
Q	significance level at given F value
q	dynamic pressure
R	multiple correlation coefficient
S_{N_y}	matrix quantity
S_{NN}	matrix quantity
S_{YY}	total sum of squares
S(RES)	residual sum of squares
S(REG)	regression sum of squares
s	variance
t_w	thickness of perforated test section walls
V	velocity
V_1	numerator degrees of freedom
V_2	denominator degrees of freedom

DEFINITION OF SYMBOLS (Continued)

Symbol	Definition
W_p	wall porosity
w	width of perforated opening
X	model location measured from the nose
Xd_h	distance between perforated wall hole centers
Y	value of dependent variable
$\overline{Y}$	average of observed values of dependent variable
y	difference in observed and mean values of dependent variable
Z_N	value of Nth independent variable
z_{NP}	difference in observed and mean values to the Pth power for the Nth independent variable
β	shock wave angle
Γ	integral function
γ	ratio of specific heats
δ^*	boundary layer displacement thickness
Θ	flow deflection angle across wave
Θ_w	test section wall convergence or divergence angle
λ	optimization function
ρ	density
$\lvert\epsilon\rvert_{AVG}$	average absolute percent error
$\sum'$	$\sum_{i=1}^{n}$, summation from the 1st to the nth term
χ^2	chi-square distribution

DEFINITION OF SYMBOLS (Concluded)

Superscript	Definition
C	calculated value
'	reference data value

Subscript	
h	conditions at perforated holes
i	i = 1, 2, ..., n
IN	inclined holes
NH	normal holes
W	conditions at the wall
∞	free stream condition

OPTIMIZATION OF WAVE CANCELLATION IN VARIABLE POROSITY TRANSONIC WIND TUNNEL FLOWS

SECTION I.

INTRODUCTION

A. Problem Statement

The basic principle of utilizing secondary mass flow through a partially open wall, by means of some form of auxiliary suction, to achieve useful transonic testing was discovered by Wright and Ward [1] at the NASA Langley Research Center (LRC) in 1950, largely by accident, in the course of boundary layer removed tests. While the basic technique has been very successful, advances have historically been based on trial and error experimental testing because of the complexities and limitations of transonic flow theory. No comprehensive theory has yet been developed which is capable of guiding the development of transonic wind tunnels, and such facilities have generally lagged behind work in the subsonic and supersonic speed regimes where a solid theoretical basis exists. While it is unlikely that a breakthrough can be made in transonic flow theory per se, it shall be the objective of this study to determine an orderly empirical procedure by which the transonic flow wave cancellation problem can be studied mathematically and which leads to the determination of optimum operating parameters for any given modern-day variable porosity transonic wind tunnel.

B. Method of Attack

As a means of developing an insight to the problem, the historical development and the operating principles of transonic wind tunnels are reviewed, with special emphasis on the perforated wall transonic wind tunnel in general use at the present time. The significant parameters at work in the process of cancelling incident wave systems from test models by proper suction through a perforated wall are identified by analyzing the theory for thin and thick walls and by reviewing past experimental work.

Having identified the parameters involved in the wave cancellation process, a mathematical model is developed using a quasilinear multiple-regression technique which relates conditions existing over a typical model to the significant wind tunnel parameters.

A wave cancellation performance index is determined by comparing the mathematical model with an experimental interference-free reference standard (small model tested in a large wind tunnel) with the resulting error related to the tunnel operating parameters. Then having represented the wave cancellation process by a logical mathematical model, a procedure is developed to determine the wind tunnel parameters at which the performance index is a minimum and hence the optimum wind tunnel configuration which should yield minimum reflected wave interference.

To establish the validity of the optimization technique, wind tunnel tests can be performed to experimentally confirm the variation of the performance index. Having established the validity of the technique, the method can then be applied to actual transonic wind tunnel optimization.

C. Explanation of Test Results

A search of the literature revealed that, in the judgment of the author, the best data for use as an interference-free reference standard were those of Capone and Coates [2], as discussed in Section VI. These data were obtained at zero degrees angle of attack for a 0.0062 percent blockage (ratio of model cross-sectional area to test section cross-sectional area) 20 deg cone-cylinder model tested in the LRC 16-Foot Transonic Tunnel. Observed wave interference in this study was negligible. A single row of static pressure orifices aligned at zero deg roll angle was used in this investigation, and the measured local pressures were nondimensionalized to the typical ratio of local static pressure to tunnel stagnation pressure. Data were evaluated at Mach numbers of 1.000, 1.038, 1.104, 1.151, and 1.208.

To relate the influence of wall porosity and free stream Mach number, existing data from the NASA MSFC TWT were used. The data used were those of Simon (MSFC Test TWT-546 unpublished) and of DeHart [3]. The model was a 0.902 percent blockage (1.500 inch diameter) 20 degree cone-cylinder instrumented with static pressure orifices in a similar manner as the LRC 16-ft test model, although the orifice locations were not at the same non-dimensional (X/D) positions. These data were obtained using a variable porosity transonic test section in which both the wall porosity and wall angle could be varied. Data were evaluated at Mach numbers of 1.00, 1.05, 1.10, 1.15, and 1.20.

D. Results of the Study

By analyzing the theory for perforated wall wave cancellation and reviewing past experimental work, the significant transonic wave cancellation parameters are identified and formulated into an analytic result for thick walls, which compares favorably with experimental results. These theoretical results have been used to guide the development of a complex mathematical model by which the transonic flow wave cancellation problem can be studied mathematically.

A quasi-linear multiple regression technique has been developed with which the behavior of indentified independent variables can be related to a given dependent variable. The resulting surface fit can be used to summarize trends for a given phenomenon and to seek mathematical information concerning optimum values. It also provides a means of predicting similar phenomena. This technique has much significance in all fields where processes can be observed or for which experimental data exist.

Using this multiple regression technique, an analytic representation of the pressure ratio existing over a 20 deg cone-cylinder model has been formulated which is free from wave interference and which can be used as a reference for future investigations. In a similar manner a mathematical model is developed which describes the pressure ratio of a 20 deg cone-cylinder model as a function of Mach number, wall porosity, wall angle, and model location. By means of these two relations, a performance index has been determined which relates the error from the reference value to the significant wind tunnel parameters.

From the relation for the performance index, optimum values of wall porosity have been determined as a function of Mach number for the MSFC TWT variable porosity test section for Mach numbers from 1.0 to 1.2, which should yield minimum reflected work interference. These results compare favorably with the thick wall theory for perforated wall wave cancellation developed and with the present tunnel settings which have been determined by trial-and-error methods. Further, confirmation tests based on results of the optimization technique agree with the predicted performance index which serves to establish the validity of the technique. Thus, the basic technique developed appears to have considerable usefulness in studying the complex problem of transonic wave cancellation and, with future refinements using statistically designed experiments, should prove to be a powerful tool in advancing variable porosity transonic wind tunnel technology. Results obtained using this technique can be expected to provide better simulation with less experimental testing than previous trial-and-error methods. By this means, calibration testing to minimize reflected wave interference should be greatly reduced, resulting in large savings of money and manpower. Better definition of the optimum tunnel configuration should also be expected.

SECTION II.

REVIEW OF TRANSONIC WIND TUNNEL DEVELOPMENT

A. General Background

A transonic wind tunnel is an experimental facility intended to simulate the flow over scaled aerodynamic test models that would be experienced by the full scale vehicle during free flight through the atmosphere at Mach numbers from approximately 0.5 to 1.5.

In transonic flow the difference between the free stream velocity and the speed of sound is small compared to the magnitude of either, and the changes in these parameters are of comparable magnitude. This is contrasted to subsonic flow, where the velocity is lower than the sonic speed and where changes in Mach number are primarily due to changes in free stream velocity at essentially constant sonic speeds, and to supersonic flow where the magnitude of the free stream velocity is substantially larger than the local sonic speed with changes in Mach number occurring through substantial variations of both parameters. In the transonic Mach number range, not only do compressibility effects become important, compared to lower subsonic Mach number where the flow is incompressible, but also the flow at near sonic speeds is extremely complex because of the mixed type of flow which may exist with local supersonic flow fields contained in subsonic flow regions or local subsonic flow fields embedded

in supersonic flow regions. These unusual difficulties affect both the design of aircraft and the experimental facilities with which to test them. The complex nature of the flow makes it difficult to establish simple transonic theories and, consequently, aircraft designers must depend more on experimental wind tunnel testing to establish aerodynamic information than in other speed ranges where theoretical methods are more useful.

In the transonic speed range, model-generated shock and expansion wave systems are steeply inclined with respect to the model and, under normal circumstances, would be expected to reflect off the tunnel walls at such an angle that wave disturbances would be reflected back to the model. The transonic wind tunnel must be designed to compensate for these many and complex problems if it is to provide proper free flight aerodynamic simulation.

Because of the complexity of transonic simulation, the development of suitable transonic test techniques has lagged developments in the subsonic and supersonic speed regimes where a solid theoretical basis exists. However, starting in the late 1940's, some progress began, and in the 1950's successful development of numerous test facilities was seen.

Generally, the primary difficulties in the development of a given transonic wind tunnel test technique are:

1. The establishment of useable test section flow at Mach numbers above approximately 0.75 due to the influence of the tunnel boundary layer on choking the test section flow.

2. The elimination of systems of shock waves and expansion waves which originate at the model, travel to the tunnel wall, reflect, and impinge upon the model causing erroneous data.

In the first difficulty, the formation of a test section boundary layer prohibits the further acceleration of the test media beyond this Mach number by limiting the effective area of the test section. This boundary layer may be eliminated by removing a portion of the test section flow through slots or holes installed in the test section walls, thus allowing acceleration of the test gas to Mach 1.0 (assuming an area ratio of 1.0 between the nozzle throat and the test section). Further increase in the removal of gas through the test section walls will then produce supersonic Mach numbers in the test section. At near sonic and supersonic speeds, the second problem mentioned above, namely the errors introduced by reflected wave systems, becomes evident. Again, by removing flow through slotted or perforated walls, it is possible to cancel waves at the walls by taking advantage of the reflective properties of shock and expansion waves from solid surfaces and free jet boundaries as discussed later. However, if such a procedure is to be completely successful, a continuous adjustment of wall open area (or, more specifically, wall porosity) must be made throughout the test Mach number range, as discussed in Sections III and IV. In recent years the introduction of the variable porosity wall has allowed considerable refinement in wave cancellation capabilities.

B. Transonic Facility Development

During the development of subsonic wind tunnels it was determined that the influence of the test section walls produced changes in the nature of the test section flow which significantly influenced experimental measurements; i. e., the conditions measured on a fixed model in a tube of flowing air did not correspond exactly to the case where the aircraft is moving through the atmosphere. Techniques for correcting test data were devised by such investigators as Theodorsen [4] and Goodman [5], and developments in this area still continue, for example, the recent work of Pindzola and Lo [6]. However, the need to minimize wall corrections has long been recognized. Goethert [7] has noted that wind tunnel velocity corrections increase with the third power of the Prandtl factor $\sqrt{1 - M_\infty^2}$. Thus, the importance of such corrections grew with the need for testing at higher velocities. One should note at this point that no satisfactory method has yet been derived to correct wind tunnel test results for boundary effects at near sonic test conditions [8].

Several investigators, such as Kondo [9] and Wieselburger [10], have noted that it should be possible to minimize or completely eliminate the need for wind tunnel velocity corrections by using a ventilated test section wall configuration with suitable longitudinal slots. By bleeding air from the test section through the slots, the combined influence of the solid wall and the open jets could produce a wind tunnel flow which inherently requires no corrections for the influence of the test section walls.

To study this phenomenon, Wright and Ward [1] built, at LRC, a small 12-in. diameter model tunnel having eight longitudinal slots, with a ratio of

slot open area to total test section area of 12.5 percent. Tests indicated that velocity corrections did, in fact, become very small with this configuration. However, a discovery of even greater importance was noted in the course of these tests. The slotted test section configuration greatly relieved the problem of test section choking and the attendant limitations on free stream Mach number. Thus, it was possible to operate the slotted wall wind tunnel with large model blockage to Mach numbers very close to 1.0. Further, the installation of additional plenum flow capacity could allow such a facility to be operated at supersonic speeds as well. These results, obtained in 1948, were of great importance for they represented the first truly successful transonic wind tunnel test technique. This development showed that a single wind tunnel could accomplish useful testing over the subsonic, transonic, and supersonic speed ranges although the slotted-wall configuration has only limited wave cancellation capability, as discussed below.

Many slotted-wall wind tunnels have been built since this discovery; detailed experimental work has shown that they provide reliable data throughout the subsonic speed range. However, while the technique is successful in overcoming the problem of boundary layer growth in the test section and does provide for the establishment of useful test section flow at transonic Mach numbers, the slotted-wall wind tunnel has shown only limited potential for eliminating shock wave and expansion wave reflections from the wall. This serious shortcoming tends to limit the use of slotted wind tunnels in the supersonic speed range to very low supersonic Mach numbers. At the higher supersonic Mach numbers,

such facilities tend to have the same limitations as closed solid wall wind tunnels [7].

It was shown both theoretically and experimentally by the staff of the Cornell Aeronautical Laboratory that shock waves could be cancelled satisfactorily, using a wall fabricated from a porous medium through which test section air could be removed, when the shock intensity and wall porosity were properly matched [11]. However, such walls were not very practical because of material limitations and because of the difficulty in matching the porosity requirements to changes in free stream Mach number.

Later investigations at the Arnold Engineering Development Center showed that systems of reflecting shock waves and expansion waves could be effectively cancelled at wind tunnel walls if a perforated configuration was used [12]. This type of installation consists of a large number of small (normally round) openings in the wall rather than the slots or porous medium in the methods previously discussed. Such a configuration can provide a fine grain with which to cancel the effects of impinging wave systems. It is mainly this type of test technique which is used in present day facilities. This approach will be considered in more detail in the next Section.

While the perforated-wall wind tunnel concept represented a significant advance in transonic testing technique, several investigators, for example, Estabrooks [12], Chew [13], and Felix [14], have established that interference-free pressure distributions in the transonic speed range cannot be produced in a transonic wind tunnel employing fixed porosity walls. To provide optimum wave cancellation, the wall porosity should increase with increasing free stream

Mach number. To meet this need, the NASA Marshall Space Flight Center developed a test technique using variable porosity perforated walls for transonic wind tunnels [14]. The concept is quite simple (see Figure 1) for the system implemented in the Marshall Space Flight Center 14-Inch Trisonic Wind Tunnel. The inner wall nearest the flow is fixed, and the outer wall nearest the plenum chamber is continuously movable in the axial direction, thus permitting each hole opening, and hence the wall porosity, to vary from zero to the maximum value incorporated in the specific wall configuration (5.4 percent for the MSFC TWT transonic test section). Subsequently, tunnels employing this concept have been developed at the Arnold Engineering Development Center, the Air Force Academy, and the Lockheed-Georgia Company. Also, a high Reynolds Number Wind Tunnel with variable porosity walls has been developed at the Marshall Space Flight Center. This variable porosity concept has proved most effective in minimizing reflected wave interference. However, the procedure for optimizing the walls has proved to be exceedingly difficult using largely trial-and-error procedures.

C. Present State-of-the-Art

Slotted-wall wind tunnels continue to be used by many in the field primarily in the subsonic speed range where they have been shown to provide reliable data. However, such facilities have only limited capability for cancelling wave reflections, and this shortcoming tends to limit their usefulness in the transonic speed range to very low supersonic Mach numbers.

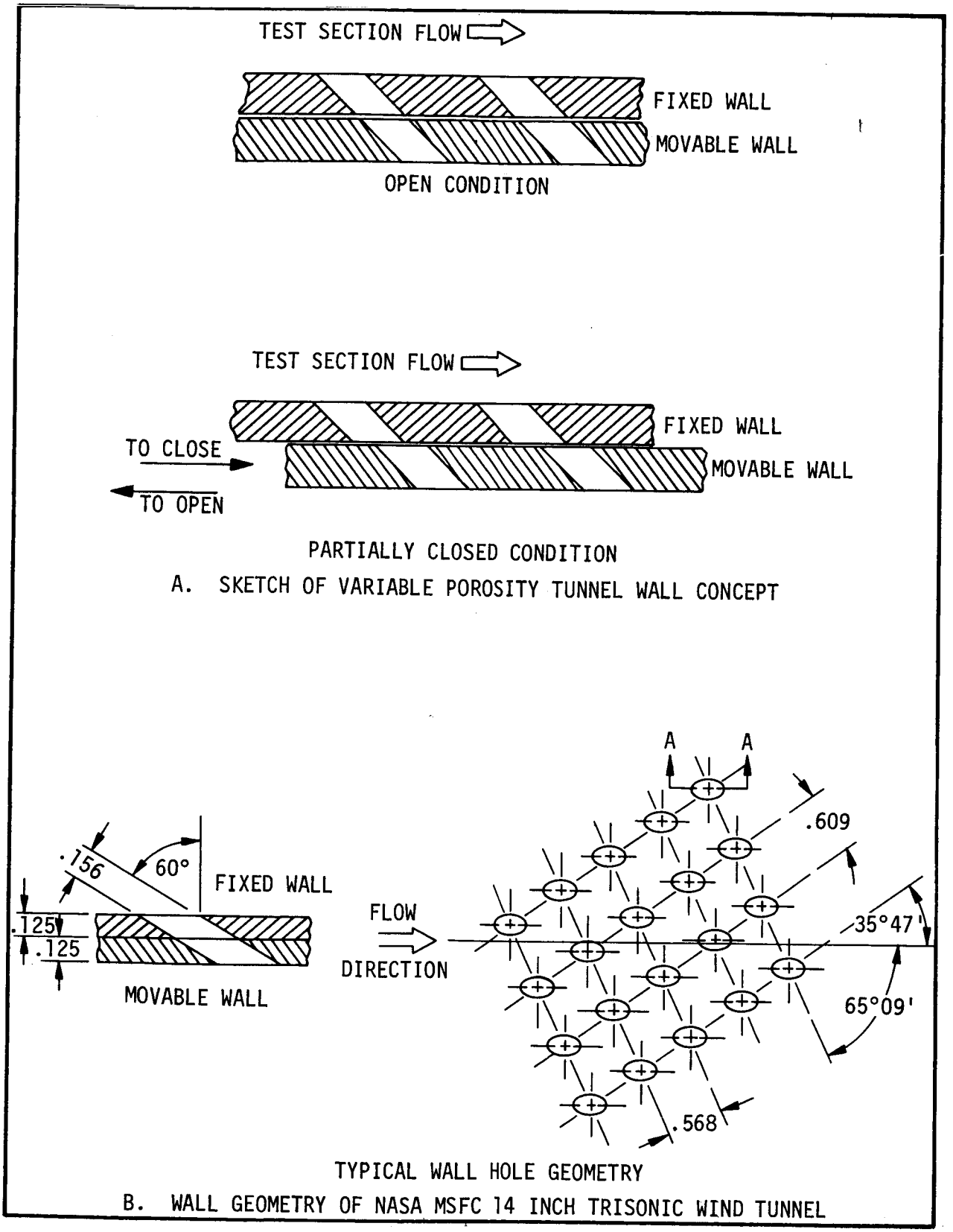

Figure 1. NASA MSFC variable porosity transonic test section concept.

Most modern day transonic wind tunnels employ the perforated wall concept. This type of tunnel has been found to be considerably more effective in the cancellation of model induced waves at the test section walls than longitudional slotted tunnels, and thus it is preferred where testing at Mach numbers larger than one is desired. However, such facilities are more limited at subsonic Mach numbers where flow distortions from the conditions which would exist in free flight are more severe than for slotted tunnels [7]. Generally speaking, subsonic testing in longitudional slotted-wall wind tunnels is superior to testing in perforated-wall wind tunnels. For economic reasons and for mechanical simplicity, it has been standard practice to use single fixed porosity walls in perforated wall facilities. Where the perforations are incorporated normal to the flow, the usual wall porosity selected is about 22 percent. However, many tunnels use holes inclined to the flow because of the inherent advantages discussed in the next section. Such facilities usually employ walls with about 6 to 8 percent open area for holes inclined at 60 deg. If the model size is kept small with respect to the tunnel size, it is usually assumed that the effects of reflected wave interference are negligible. Such an assumption is usually reasonable if the model blockage is 1 percent or less, although such difficulties are compounded in the critical Mach number range from approximately 1.0 to 1.25 [15].

The most recent extension of the state-of-the-art in transonic wind tunnel testing has been through the use of variable porosity perforated walls. Evaluation tests have indicated that the use of such walls greatly improves the ability to produce reasonably accurate data throughout the transonic Mach

number range, especially in the critical Mach number range from 1.0 to 1.25. Further, such a facility has much flexibility in adjusting to radically different model shapes.

SECTION III.

PERFORATED WALL TRANSONIC WIND TUNNEL CONCEPT

A. Introduction

In supersonic flow, wind tunnel models produce shock and expansion waves, which in general travel to the test section wall, reflect from this boundary and return toward the model. Unless the model is small with respect to the tunnel size, or unless the Mach number is sufficiently large that the wave angle allows the wave to pass aft of the model, the reflected wall will impinge upon the model and induce disturbances which invalidate the simulation of the free-flight condition.

B. Wave Reflection

As shown in Figure 2, waves are reflected from solid boundaries with the same sign and intensity as the original wave. That is, shock waves reflect as shock waves and expansion waves reflect as expansion waves, since the flow direction must be maintained parallel to the wall. However, waves reflect from a free boundary with opposite sign but equal intensity due to the requirement that static pressure must be constant along the free boundary. Then, in this case shock waves reflect from the free boundary as expansion waves and expansion waves reflect as shock waves.

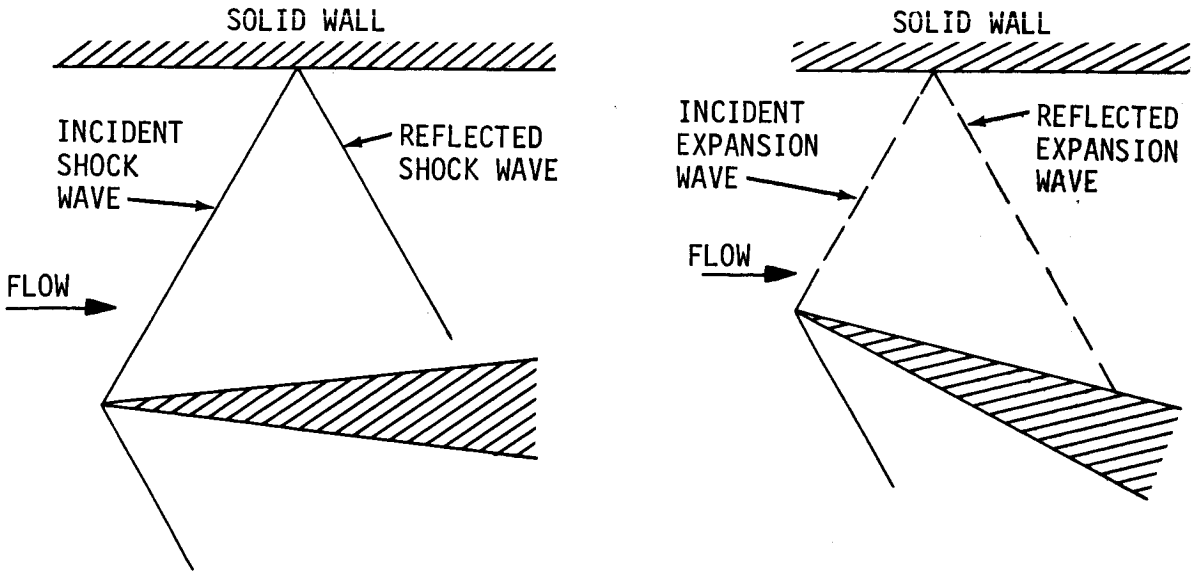

A. SOLID WALL CASE

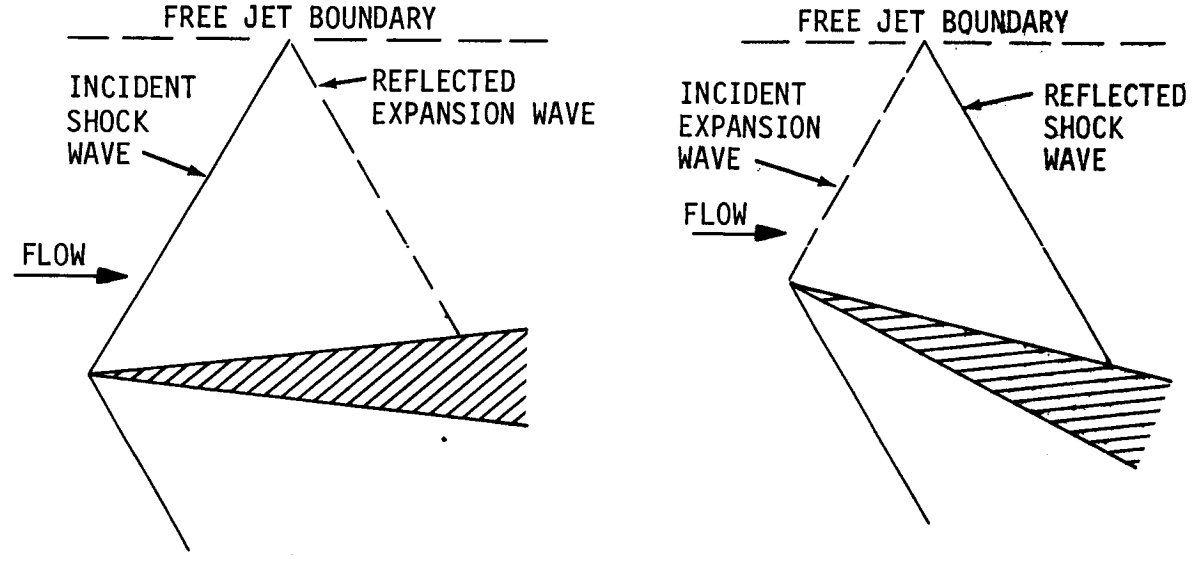

B. FREE JET BOUNDARY CASE

Figure 2. Wave reflections from solid and free jet boundaries.

Thus, since solid and free jet boundaries result in wave reflections having opposite characteristics, it is possible to eliminate wave reflection from wind tunnel walls if a proper balance of open and solid wall area can be utilized.

In this report, the ratio of open area of the wall to total wall area will be termed "wall porosity," where open area is calculated on the basis of the total hole area measured perpendicular to the axis of the hole.

C. Perforated Wall Concept

In the perforated-wall wind tunnel, the wall porosity is achieved by drilling a great number of holes, normally circular, in the wall to achieve a fine grain cancellation effect. These holes are usually arranged in a symmetrical pattern; often taper strips are used in the upstream portion of the test section to prevent abrupt changes in porosity.

A typical perforated-wall test section configuration is shown in Figure 3. Flow normally enters the test section from a sonic (area ratio 1.0) nozzle, although testing with converging-diverging nozzles is also possible. Suction is applied to the plenum chamber by exhausters, vacuum storage, or ejector pumping by the main stream flow. Initially, the effect of this plenum suction is to bleed off or remove the tunnel wall boundary layer. The resulting increase in stream tube area allows the test section flow to be accelerated above the normal choking Mach number to Mach 1.0. Further flow removal through the perforated wall will produce supersonic Mach numbers. Also the flow through the partially open wall produces a free jet boundary which may be used to cancel waves.

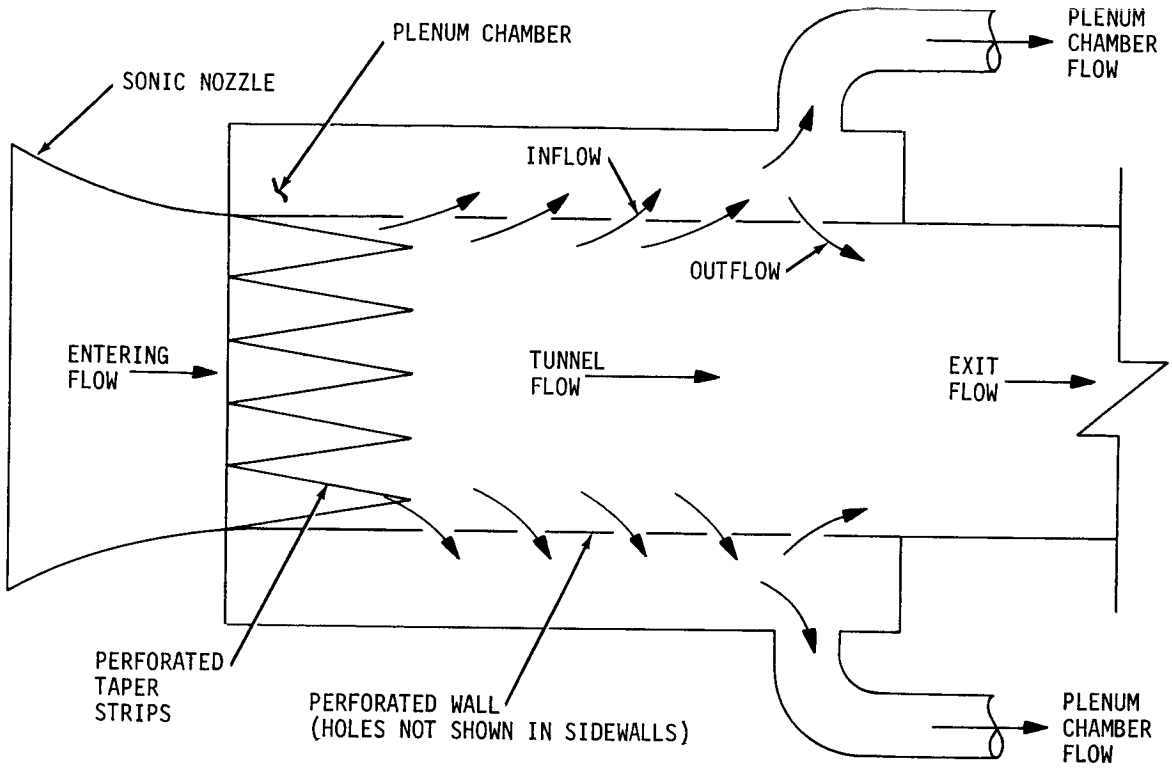

Figure 3. Perforated wall transonic test section.

D. Model Size Criteria

It is obvious that both the shape and the size of wind tunnel models being tested influence the wall cancellation properties of the given test section wall. The shape of the model affects not only the strength of the waves and hence the amount of flow which must cross the wall to the plenum chamber to cancel the waves but also the type of mixed wave system present. Two-dimensional configurations have different criterion than do axisymmetric configurations or three-dimensional models. The elimination of wave systems is particularly difficult for models having sharp corners, such as cone-cylinders where a centered expansion fan is produced. In general, gradual changes in model

shape can be expected to produce less difficult cancellation problems, although perfect cancellation is possible only in the simplest of models.

Davis and Graham [15] investigated cone-cylinders of 0.9, 1.5, 2.9, 4.4, and 5.9 percent tunnel blockage at zero angle of attack. These results indicate that serious wall interference occurs at blockages larger than approximately two percent. However, as shown by Davis [16], interference is less severe for models with more gradual transition of shape, such as the AGARD B winged ogive-cylinder model.

E. Wave Reflection From Partially Open Walls

Typical shock wave reflections from partially open walls are indicated in Figure 4. When the plenum flow passes through the test section wall a pressure drop is produced across the wall. If the pressure drop across the wall is exactly equal to the rise in pressure across the oblique shock waves, then the primary shock wave will not be reflected [7]. On the other hand, if the wall porosity is less than the no-reflection case, a shock wave will be partially reflected since the mass flow through the wall will be too low to align the flow parallel to the wall. A pressure adjustment in the form of a shock wave is then required. Alternatively, if the porosity is too large, an expansion wave will be partially reflected since the mass flow through the wall will be too high, and the corresponding pressure adjustment requires an expansion process.

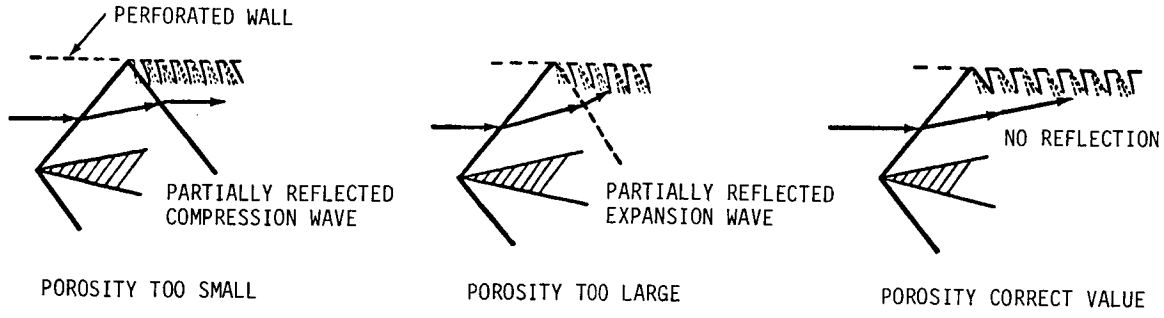

Figure 4. Wave reflection from partially open walls.

F. Wave Cancellation

The foregoing arguments concerning shock reflection for partially open walls are based on considerations at relatively large distances downstream of the shock wave. Considering the process near the wall, if the incident wave strikes a portion of the wall which is effectively solid, it will be reflected in like sense, as discussed in Section III. Should the incident wave strike an effectively open element of the wall, it will be reflected in opposite sense; i.e., a shock wave will reflect as an expansion wave and vice versa. In general, pressure equilibrium will not be achieved immediately, and a system of expansion and shock waves are produced which tend to cancel each other near the wall. The distance from the wall within which this decay occurs depends upon how fine grain a wall is incorporated and, hence, upon the size of the perforated holes. This process is indicated in Figure 5 for points close to the wall. As the secondary plenum flow passes through the perforated wall, expansion waves form at the leading edges of the holes, and shock waves form at the trailing edges. The interaction of the expansion and shock wave systems from the wall

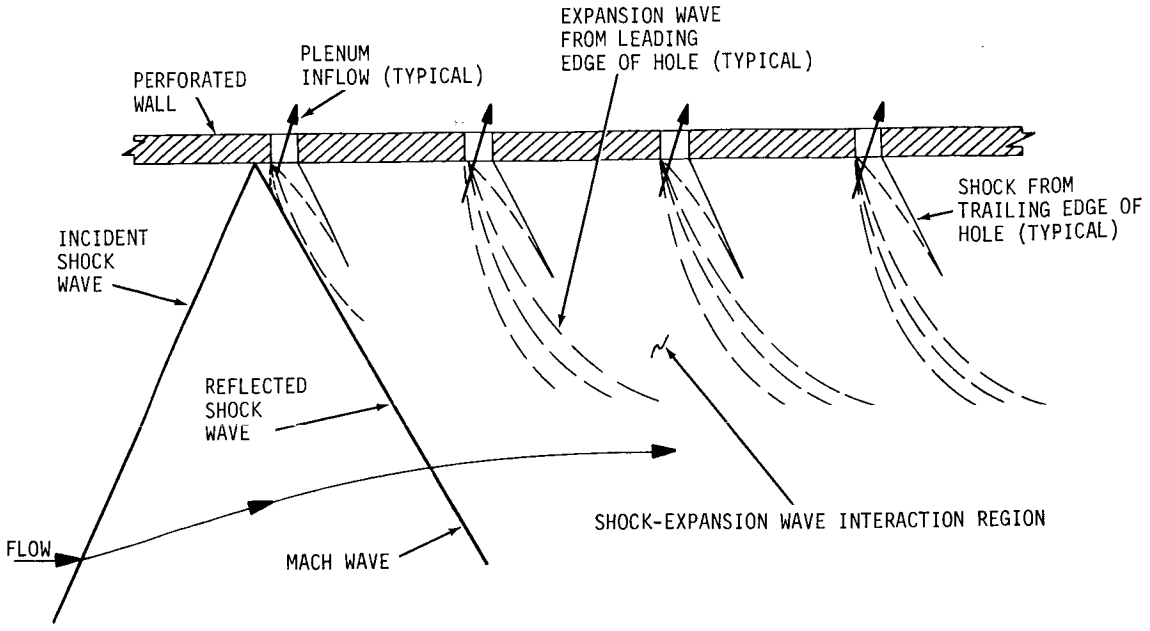

Figure 5. Wave process near the wall.

holes causes them to cancel each other, so that hopefully the wave system gradually disappears near the surface of the wall. In addition the interaction of the incident wave with the wave system emanating from the holes, which eventually overtakes the reflected wave, should cause the gradual weakening of the reflected wave to near zero strength for properly configured walls, as shown in Figure 5.

Gardener [17] investigated the decay of flow disturbances for various perforated walls. Figure 6 shows results for Mach 1.20 which indicate that appreciable local Mach number disturbances (and hence static pressure disturbances) occur near the wall for straight holes. Initially, the disturbances decay very rapidly, and at a distance of approximately 24 hole diameters, reach a constant value. The Mach number variation gradually loses intensity as the distance from the wall increases, so that at a distance of approximately

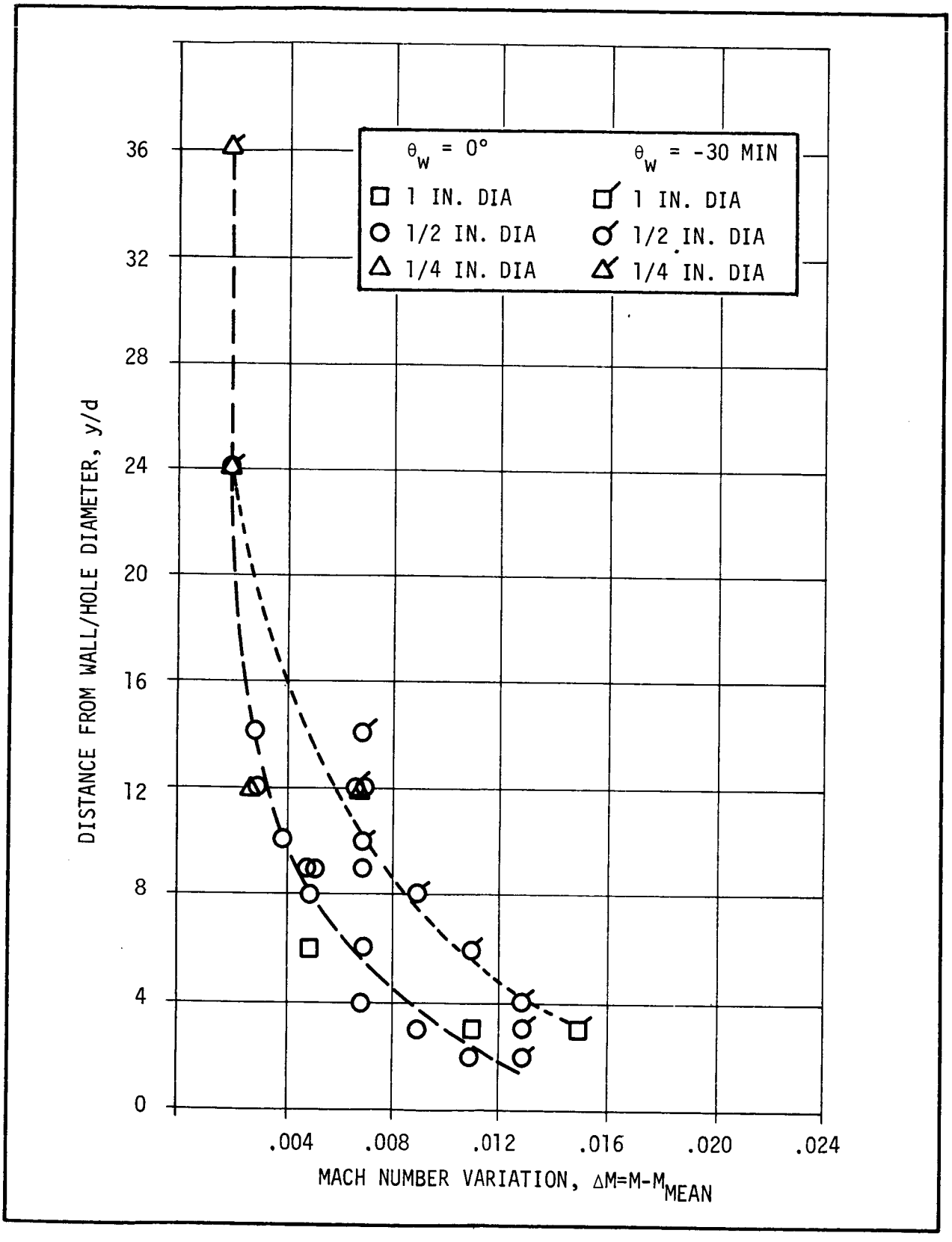

Figure 6. Decay of flow disturbances produced by various perforated walls with straight holes at M = 1.20 [17].

9 to 14 hole diameters, depending on wall angle, the Mach number variation falls to $\pm$ 0.005. Results at lower Mach numbers indicate less severe disturbances. Tests using walls with 60 deg inclined holes indicated similar results.

Then the flow near the wall is highly nonuniform, but this nonuniformity disappears with increasing distance from the wall. The effective thickness of this nonuniform flow region near the wall should be proportional to the diameter of the wall openings such that a fine-grain configuration using many small holes should be superior to a coarse-grain design having fewer and larger holes. Of course, the design of the test section must be such that the nonuniform layer does not reach the model.

G. Influence of Inclined Holes on Wave Reflection

A typical partially reflected wave system emanating from a cone-cylinder model is shown in Figure 7. Successful testing of such a model requires the cancellation of both shock and expansion waves at the wall. As will be shown in Section IV, an ideal perforated wall is capable, within the limitations of linear theory for thin walls, of eliminating reflections of both shock and expansion waves provided the flow inclination is small and pressure-drops for both the waves and the wall are linear. In order to eliminate both shock and expansion waves for thin walls with two-dimensional models, it is necessary for a wall to have the same pressure-drop characteristics for both inflow to the test section and outflow from it. In real flow, conventional straight-hole perforated walls do not process linear wall-pressure drop characteristics having the same slope for both inflow and outflow primarily due to test section boundary layer effects.

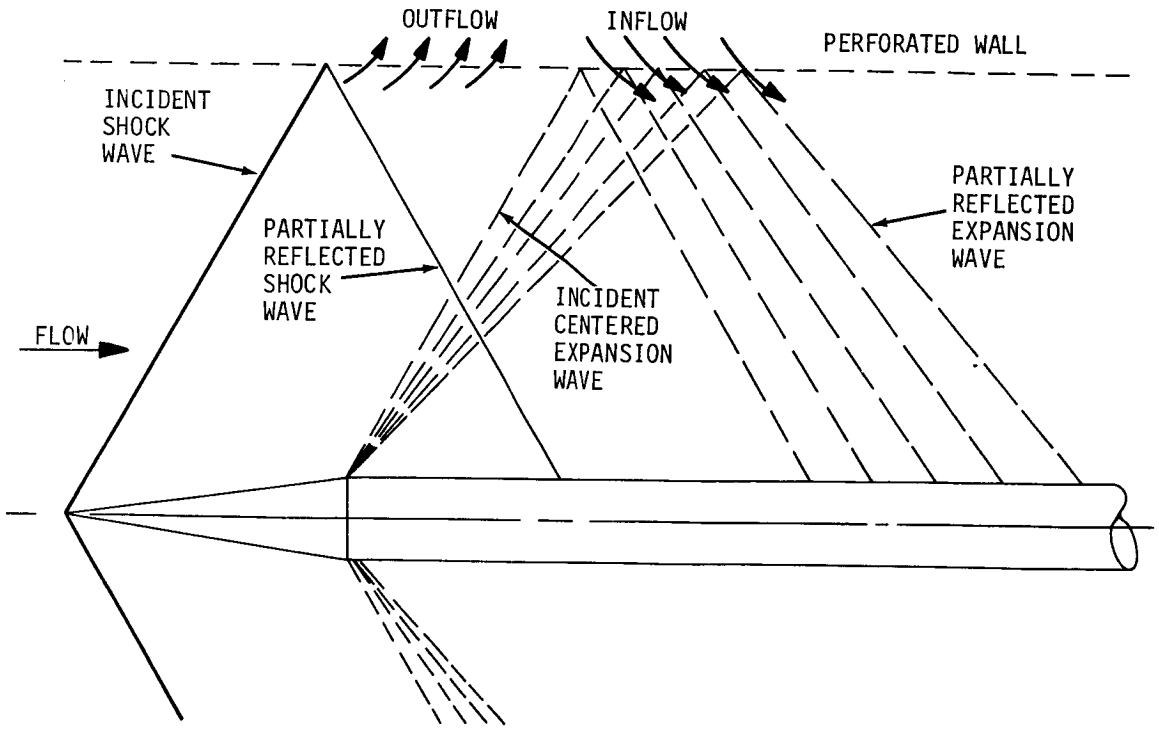

Figure 7. Partially cancelled wave system for a cone-cylinder model.

However, as indicated in Figure 8, it is possible to devise walls with a more or less equal pressure drop for both inflow and outflow. As shown by Chew [13], when holes were inclined at angles of 0 (straight holes), 30, 45, and 60 degrees, respectively, to the wall, the resistance to outflow was considerably reduced as the angle of the holes is inclined in the direction of the flow. In addition, as shown in Figure 8, at wall porosities of both 6 and 12 percent, a steeper slope is observed for 60 deg inclined holes in the negative flow or inflow region yielding a more linear wall characteristic when compared with the irregular curve produced by straight holes in the inflow region.

The basic principle of the inclined hole is illustrated in Figure 9. A differential resistance is developed by virtue of the fact that, for outflow regions, the flow has an easy path with minimum turning into the plenum chamber; whereas, in regions of inflow to the test section the flow must turn through an angle

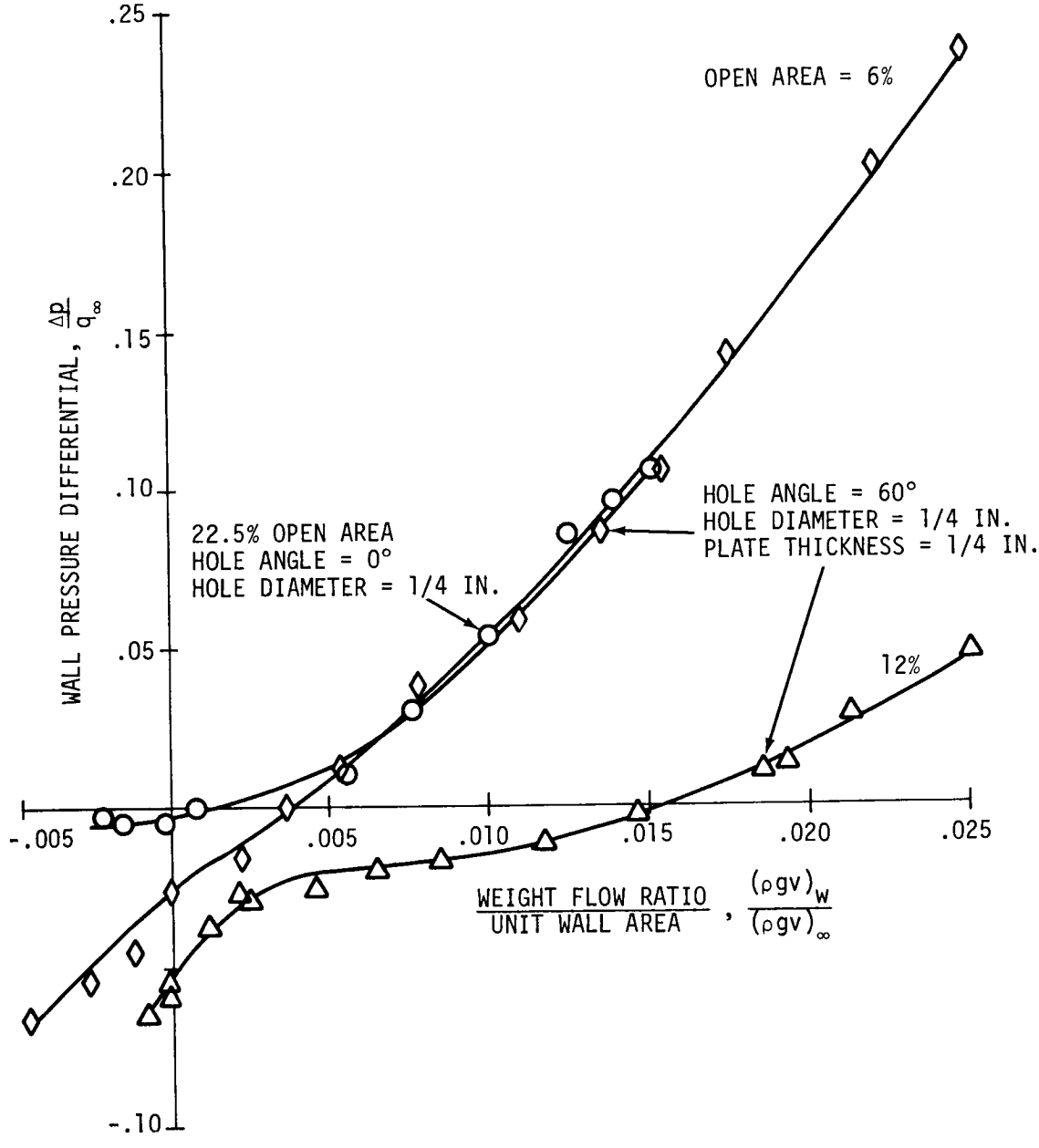

Figure 8. Comparison of wall pressure differential for straight and inclined holes at M = 1.00 [13].

greater than 90 deg and overcome a significant component of the dynamic pressure of the main stream flow.

Walls incorporating inclined holes match more closely the required characteristics for cancelling simultaneously both shock and expansion waves.

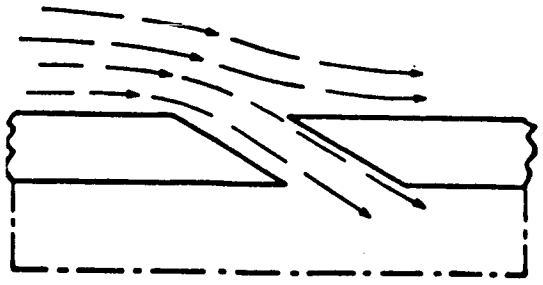

FLOW OUT OF TEST SECTION

FLOW INTO TEST SECTION

Figure 9. Differential resistance for inflow and outflow through a perforated wall with inclined holes.

Not only is the wall-pressure drop more nearly linear but also the resistance to inflow back to the test section helps to maintain a constant test section Mach number throughout the length of the test section. However, such a wall can at best only approach the complete elimination of complex wave systems, and suitable design compromises have to be reached.

H. Effect of Wall Thickness

As shown in Figure 10, a somewhat different flow pattern should be expected through thin perforated walls as compared with thick walls. When a perforated wall is thin compared with the diameter of the wall openings, a pressure drop is produced which, as shown in Figure 11, is reasonably linear

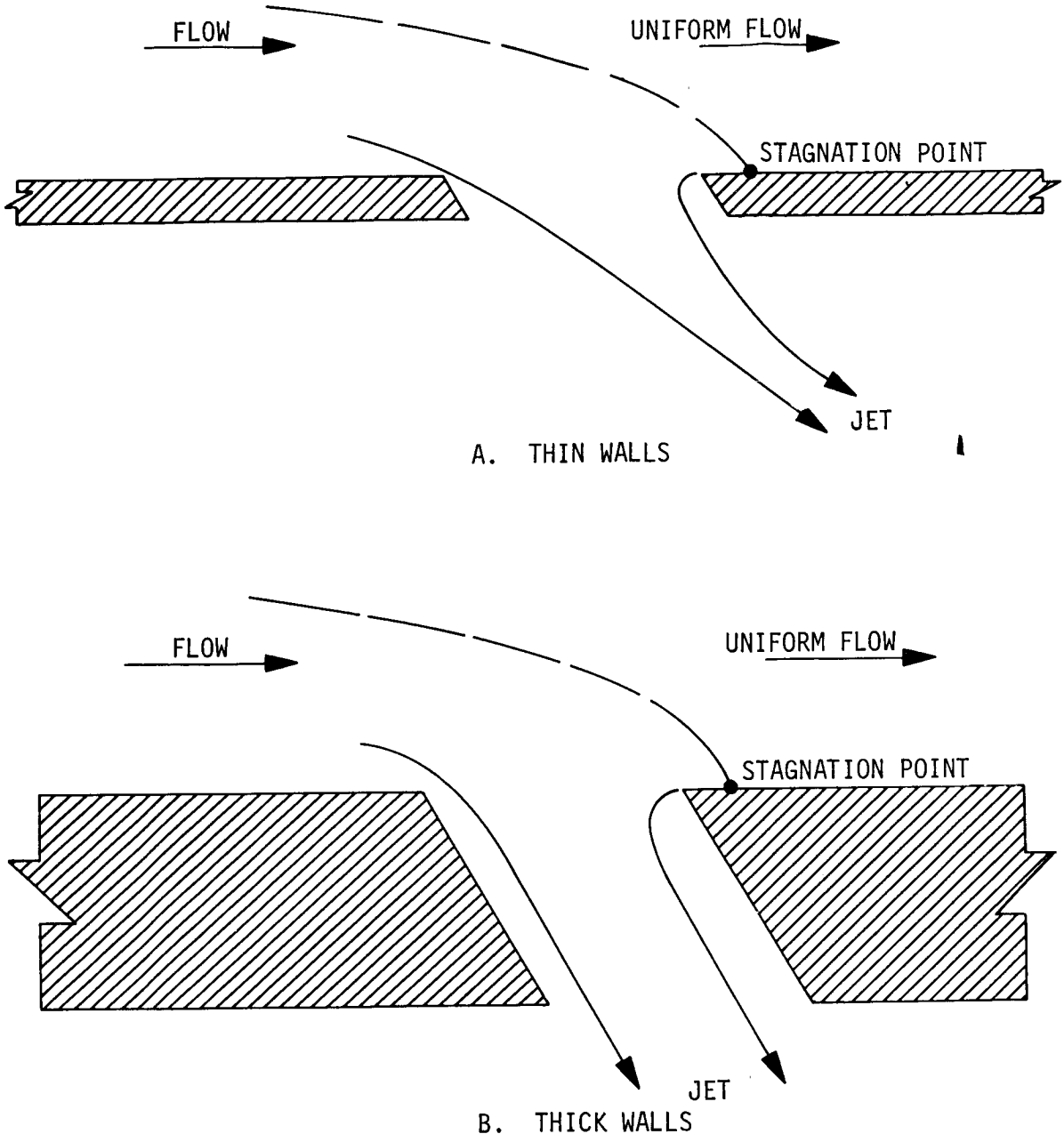

Figure 10. Flow pattern for thin and thick perforated walls with inclined holes.

and larger in magnitude than for thicker walls. However, as shown in Figure 10, when the walls are thick, when compared with the hole diameter, the flow pattern is modified since the lengthened hole tends to guide the flow similar to a channel. In this case, the individual channels or holes may act as diffusers

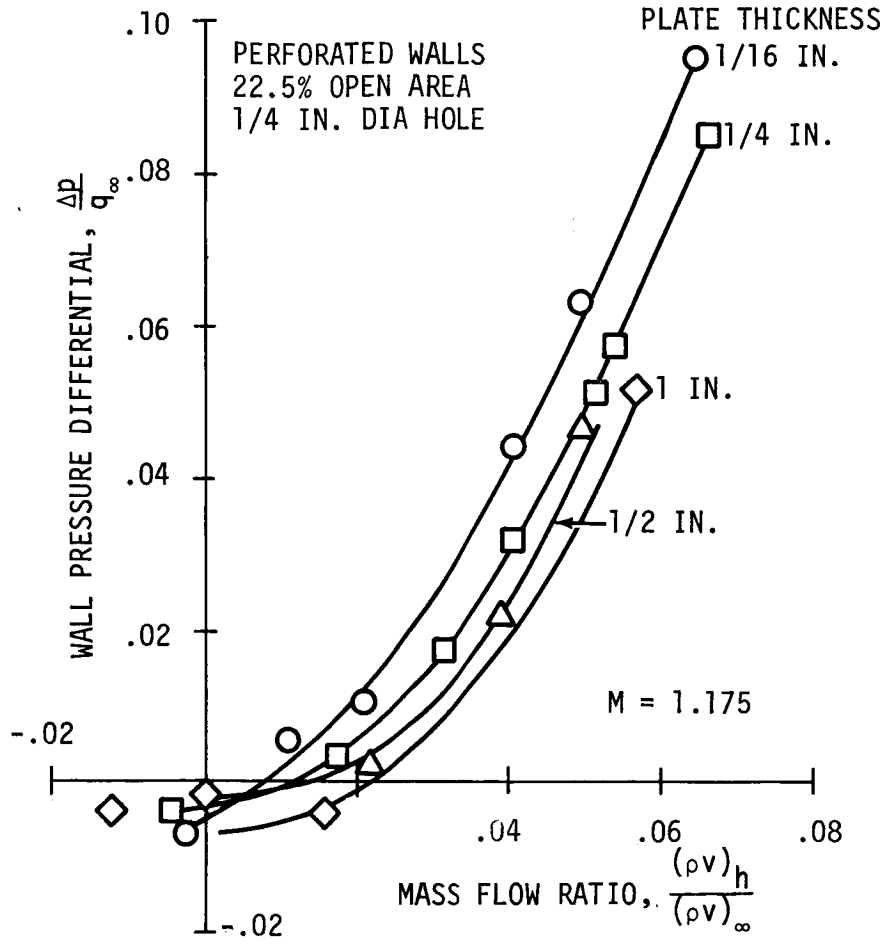

Figure 11. Influence of wall thickness for perforated walls with $\frac{1}{4}$ in. diameter straight holes [18].

such that the pressure drop across the wall would be reduced. Then, in general, one expects thin walls to behave more linearly and, thus, to be more capable of eliminating reflected waves. The boundary condition for perfect wave cancellation with thin walls is determined by the pressure-matching condition discussed under the heading "Model Size Criteria" with the flow angle behind the reflected wave unspecified. However, for thick walls, the boundary condition is fixed by the angle of the holes with respect to the flow, which is coincident with the flow angle behind the reflected wave, since it is assumed that the flow

is perfectly guided through the holes and no pressure-matching constraint is required.

The data shown in Figure 11 are for a Mach number of 1.175. However, similar results were obtained by Chew [18] at both higher and lower Mach numbers including the subsonic range. The walls used to obtain these data incorporated common $\frac{1}{4}$-in. diameter holes. The problem of hole diameter per se will now be discussed.

I. Hole Size Requirements

As previously discussed, the requirement that the system of waves generated by the edges of the hole openings be cancelled before reaching the model generally results in a fine-grain configuration. That is, for a constant wall porosity, the use of more holes of small diameter should achieve cancellation of the waves nearer the wall.

The desirability of the fine-grain wall configuration, however, conflicts with the need previously discussed for thin (linear) walls, since, other things being equal, fine-grain walls tend to behave as thick walls. Further, structural requirements dictate to some degree the basic wall thickness, particularly in variable porosity tunnels. Based on data such as those shown in Figure 11, most tunnel designers have concluded that the wall thickness should not be greater than the diameter of the perforated hole opening (however, most variable porosity designs can only approach this goal because of stress constraints). Chew [18] investigated a series of walls having holes with different diameters, but with the ratio of hole diameter to wall thickness being constant. As shown

in Figure 12, for a hole diameter/plate thickness ratio of 1.0, the walls exhibited more linear characteristics as hole diameter increased. Although, those data were obtained at Mach 1.10, similar results were obtained throughout the transonic range. However, it is noted that these results can be greatly influenced by the test section boundary layer, as discussed in the next section.

J. Boundary Layer Influence on Wave Reflection

In real flow it is difficult to achieve linear wall characteristics having the same slope for both inflow and outflow, as required for the elimination of wave reflections. This difficulty is due primarily to the boundary layer developed along the test section. Furthermore, the initial impingement of the primary wave occurs at the edge of the boundary layer rather than at the wall. Thus, a more complex disturbance region of shock wave boundary layer interaction can occur than has been postulated thus far. However, if the boundary layer is thinned sufficiently by plenum suction and by sufficient wall angle change (to be discussed later), the influence of the boundary layer can be practically eliminated so that wave reflection can be insignificant, provided the other considerations discussed are properly accounted for. Chew (19) investigated pressure drop across perforated walls as a function of boundary layer displacement thickness. Figure 13 shows the measured relationship at Mach 1.20 for $\frac{1}{8}$-in. diameter holes and a $\frac{1}{8}$-in. thick wall. These results indicate that when the boundary layer thickness is larger than the diameter of the holes, the wall characteristics become nonlinear, and, hence, wave reflection for complex wave systems should be expected. Then, for effective

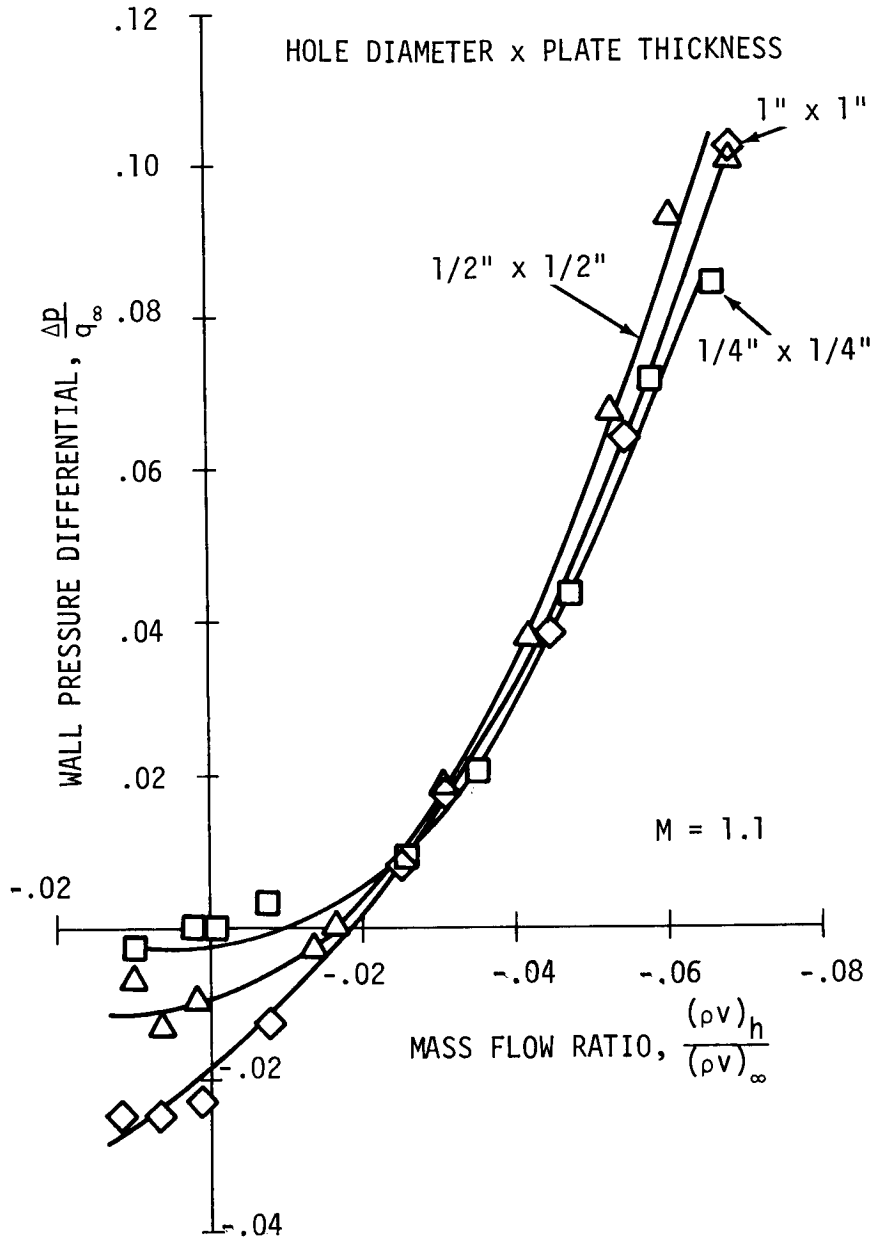

Figure 12. Influence of hole size for perforated straight hole walls when the ratio of hole diameter to wall thickness is unity [17].

cancellation of waves impinging on perforated walls, the boundary layer must be kept thin.

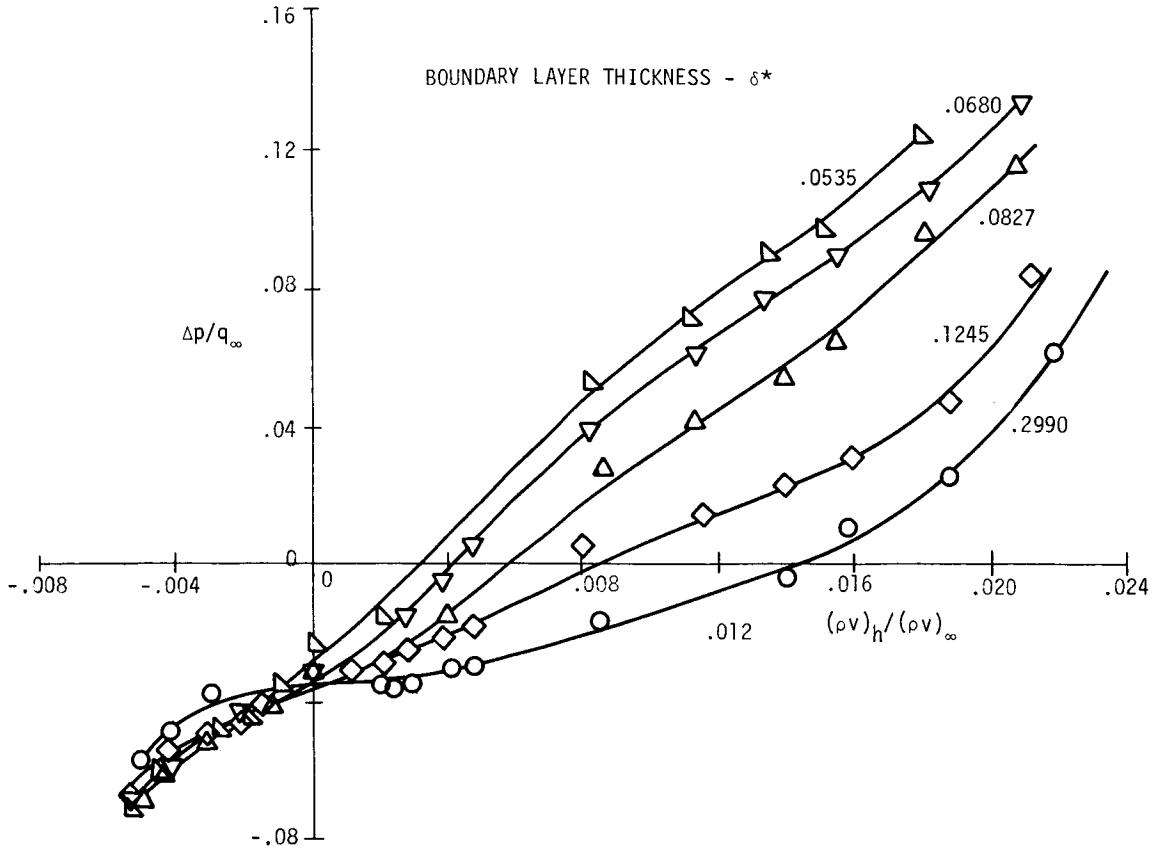

Figure 13. Influence of boundary layer displacement thickness for perforated walls with 60 deg inclined holes, hole diameter $\frac{1}{8}$-in., wall thickness $\frac{1}{8}$-in., wall porosity 6 percent at Mach number 1.20 [19].

K. Wall Convergence and Divergence

There are two means of reducing the boundary layer thickness along perforated transonic wind tunnel walls; plenum suction through the wall and modification of the wall angle. While it is necessary to keep the wall boundary layer displacement thickness thin along the length of the test section, experience has shown that thinning entirely by plenum suction can introduce disturbances. To augment this process, two-dimensional tunnels usually employ variable angle walls capable of either converging or diverging slightly from the parallel position. Assuming that the pressure in the plenum chamber is constant,

the boundary layer thickness tends to grow along the length of parallel walls. As the boundary layer grows, the effective stream tube grows smaller so that, for supersonic free stream Mach numbers, the Mach number decreases and the static pressure rises. This condition causes a larger differential pressure across the wall and, hence, more mass flow through the wall, which tends to thin the boundary layer as desired. However, alternately the walls may be converged slightly, which also reduces the effective steam tube size, such that the net effect is to thin the boundary layer by a similar process as previously noted. This converged wall procedure has been found to be especially effective in eliminating reflections of expansion waves.

Again a trade-off is required, for often walls which are too converged for complete shock wave cancellation are not converged enough for complete expansion wave cancellation and no perfect solution can then be found. Hence, the ability to converge and diverge test section walls is extremely important when model configurations require the elimination of both compression and expansion waves (as in most cases).

L. Summary Remarks

For realistic models, the best one can hope for is to arrive at a suitable compromise which can satisfactorily minimize wave reflections from the test section walls. Then the transonic perforated-wall wind tunnel is really a trade-off of factors, such as Mach number, wall porosity, flow angle, linear wall characteristics, fine grain cancellation, boundary layer thickness, wall angle, etc. In truth, each new model of different size, shape, or angle-of-

attack requirement represents a new problem, and probably some new combination of tunnel parameters is required for minimum interference. It is for this reason that the variable porosity test section wall, which shall be ultimately treated, represents such a versatile tool since it can be optimized for any configuration.

SECTION IV.

THEORETICAL ANALYSIS OF THE TRANSONIC PERFORATED-WALL WAVE CANCELLATION PROBLEM

A. Introduction

To minimize reflected wave interference, a criterion of judgment must be determined which is capable of measuring the error introduced over the length of the model by the reflected wave process. That is, a performance index may be defined as a function of the important parameters at work in the wave cancellation process which can be used to determine the optimum wind tunnel configuration for any given test condition. A study of the theory of wave cancellation can be expected to yield an insight to this problem and to provide a guide to the basic flow mechanisms involved. Results of such a study, together with the experimentally determined relationships discussed in Section III, should provide a reasonably comprehensive basis for the development of a model relationship capable of describing the essential features of the wave-reflection, partial-reflection, wave-cancellation process as it influences wave interference on wind-tunnel models. Such a model relationship of this process would be extremely valuable in providing a basic understanding of the physical nature of the process and the importance of the many variables at work, and a

means of minimizing wave disturbances on models by the proper selection of the wind tunnel configuration.

Then as a means of better understanding this problem, the theory of wave cancellation for perforated transonic wind tunnel walls will now be considered. The analysis will treat only those conditions somewhat downstream of the point of wave impingement on the test section wall where the initial imbalance of the wave has been eliminated by the formation of a system of interacting secondary waves originating at the wall perforations, as previously discussed. The need for linear wall characteristics and the means for achieving them are shown in Section III.

B. Linear Theory of Wave Cancellation for Thin Walls

Where entropy changes are neglected and the compressibility equations are linearized, Goethert [7], assuming that traverse slots behave similarly to perforated holes, has shown the following relationship between pressure changes behind the wave and behind the perforated wall for supersonic flow passing the wall at small oblique angles:

$$\frac{P_3 - P_1}{q_1} = \frac{-2}{\sqrt{M_1^2 - 1}} \left(\frac{1}{W_p} - 1 \right) \Theta_1 = K\Theta_1 \qquad (1)$$

The physical relationship of this situation is indicated in Figure 14, and one notes the following limitations in the application of equation (1):

1. Walls must be thin with respect to perforated hole size,
2. Incident wave must be relatively weak with small turning angles,

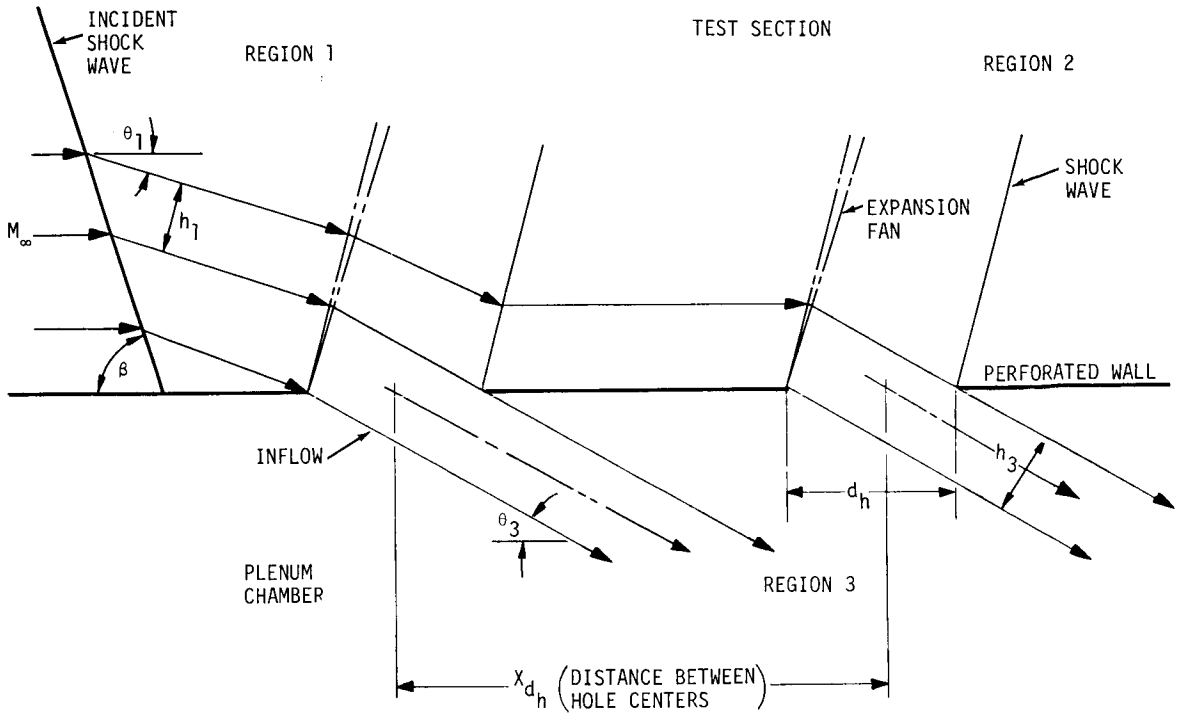

Figure 14. Wave system model for the no-reflection case with straight holes.

3. Free stream flow limited to the low supersonic speed range, so that flow is very nearly isentropic and follows the linearized Prandtl-Glauert theory,

4. The region of interest must be located a reasonable distance behind the point of impingement of the incident wave on the wall, and must be located outside the region of the shock-expansion wave interaction near the wall, and

5. The factor K in equation (1) tends to go to infinity at Mach numbers approaching 1.0. In actual flow, K maintains some finite value.

Further, Goethert [7] notes the following condition for no reflection from the wall:

$$\frac{P_1 - P_3}{q_\infty} = \frac{\Delta P_{wave}}{q_\infty} , \qquad (2)$$

which is based on the physical criteria discussed in Section III.

Assuming weak incident waves where $M_\infty \sin\beta$ is only slightly greater than unity, the linearized equation denoting pressure changes for weak shock and expansion waves is given by the following approximate relationship which uses only the first term in the solution for weak waves obtained in Reference 20:

$$\frac{P_1 - P_\infty}{P_\infty} = \frac{\gamma M_\infty^2}{\sqrt{M_\infty - 1}} \Theta_1 \quad . \tag{3}$$

Assuming that M_1 is approximately equal to M_∞ (weak waves), equation (3) becomes,

$$\frac{P_1 - P_\infty}{P_\infty} = \frac{\gamma M_1^2}{\sqrt{M_1^2 - 1}} \Theta_1 \quad . \tag{4}$$

Dividing the numerator and denominator of the left side of equation (4) by P_∞ yields

$$\frac{P_1}{P_\infty} - 1 = \frac{\gamma M_1^2}{\sqrt{M_1^2 - 1}} \Theta_1 \quad . \tag{5}$$

The pressure coefficient across the wave is defined by

$$C_p = \frac{\Delta P_{wave}}{q_\infty} = \frac{P_1 - P_\infty}{q_\infty} = \frac{2}{\gamma M_\infty^2}\left(\frac{P_1}{P_\infty} - 1\right) \quad . \tag{6}$$

With the assumption that $M_1 = M_\infty$, equation (5) is substituted into equation (6) to obtain

$$\frac{\Delta P_{wave}}{q_\infty} = \frac{2\Theta_1}{\sqrt{M_1^2 - 1}} \tag{7}$$

By setting equation (1) equal to equation (7), as specified by equation (2), the following results:

$$\frac{2}{\sqrt{M_1^2 - 1}}\left(\frac{1}{W_p} - 1\right) \quad \Theta_1 = \frac{2\Theta_1}{\sqrt{M_1^2 - 1}} \quad , \tag{8}$$

which when simplified yields

$$W_p = 0.50 \quad . \tag{9}$$

Thus, the wall porosity obtained from linearized theory, which is necessary to provide complete wave cancellation for thin walls, is 50 percent open area. Further, this result obtained for idealized walls is independent of Mach number, pressure, and the angle of flow deflection across the wave, and hence the wave intensity. In fact, this solution indicates that the wall porosity for a perforated wall should be 50 percent for all conditions independent of all parameters. Of course, such a characteristic is highly desired in that one wall geometry should be capable of meeting the test requirements for all models, Mach numbers, and flow conditions.

However, wind tunnel designers have long used wall porosities of approximately 22 percent for straight-hole test section walls and approximately 6 percent for inclined-hole configurations, since they have been shown to exhibit superior cancellation characteristics relative to walls of 50 percent porosity as predicted by the linear theory. Figure 15 compares linear thin wall theory with the most desirable wall porosity for a 20 deg cone-cylinder model determined by trial-and-error experiments for the MSFC 14-Inch Trisonic Wind Tunnel

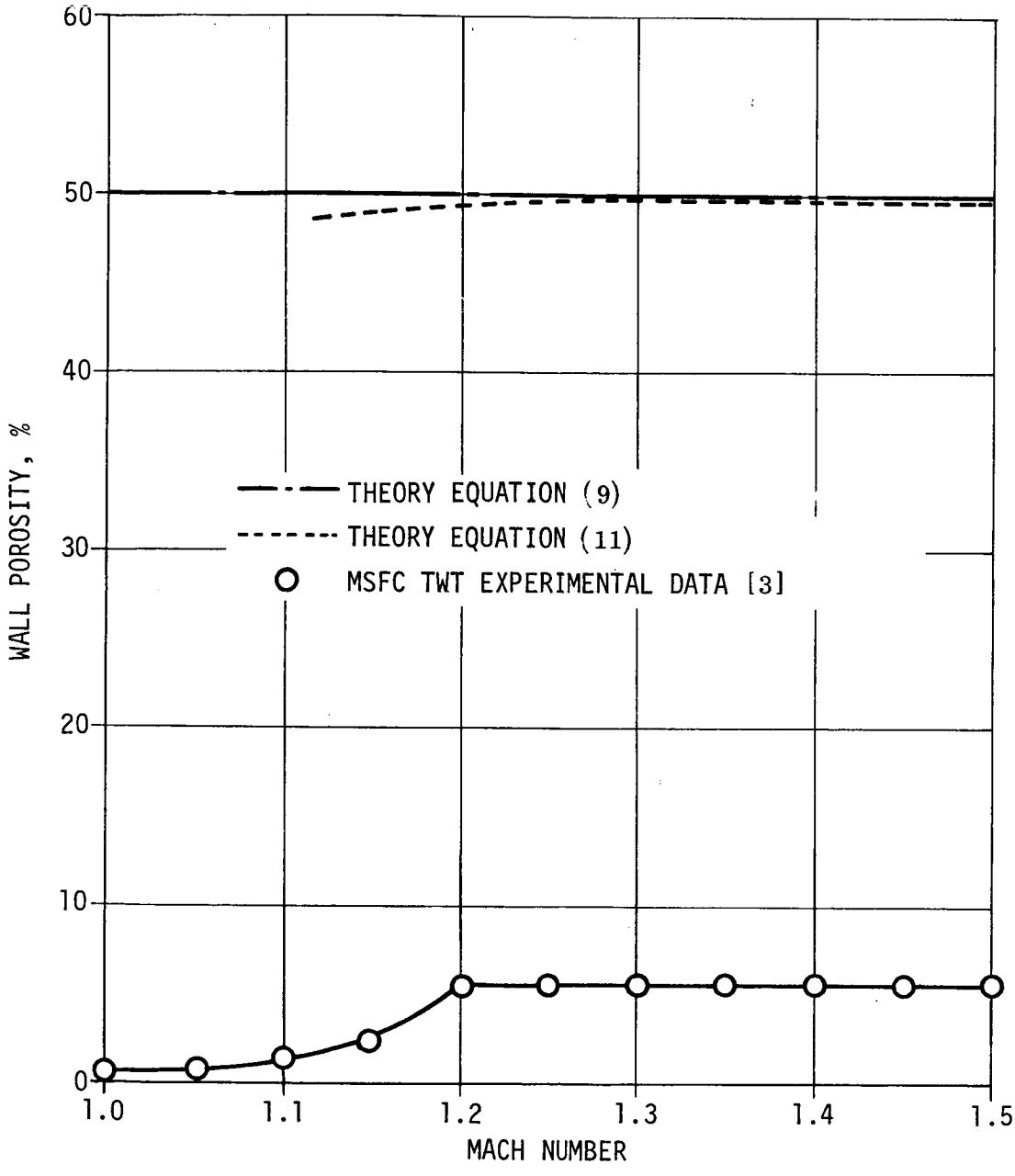

Figure 15. Comparison of theoretical and experimental optimum wall porosity determinations for straight holes, $\gamma = 1.4$.

variable porosity walls (3). As shown in Figure 15, it is clear that the linear theory for thin walls fails to correlate with the experimental data for real walls. It should be noted at this point that the TWT test section walls had a maximum porosity of 5.4 percent. This is why the experimentally determined curve

becomes flat (fully open holes) at Mach number 1.2. Although this thin wall theory does establish useful trends and denotes the importance of the wall porosity parameter, this approach fails to properly account for known real flow conditions. The two possible sources of error are the approximate relationship for pressure changes across waves [equation (3)] and the K factor in equation (1). Each potential problem area will be investigated separately.

C. Theory of Wave Cancellation for Thin Walls Using Exact Form of Shock Wave Relationship

The solution previously developed for thin walls used an approximate relationship [equation (3) for pressure changes across waves]. An attempt to improve the theoretical relationship by considering an exact expression for pressure change across a shock wave will now be treated.

From NACA Report 1135 [20], the exact solution for conditions across a shock wave is given by

$$\frac{\Delta P_{\text{shock wave}}}{q_\infty} = \frac{4(M_1^2 \sin^2\beta - 1)}{(\gamma + 1) M_1^2} \quad . \tag{10}$$

An analysis similar to that given in the previous section results in the following relationship for the wall porosity:

$$W_p = \left\{ 1 + \left[\frac{4(M_\infty^2 \sin^2\beta - 1)}{(\gamma + 1) M_\infty^2} \right] \left[\frac{(M_\infty^2 - 1)^{1/2}}{2\Theta_1} \right] \right\}^{-1} \quad . \tag{11}$$

Equation (11) specifies the wall porosity for perfect cancellation in terms of the free stream Mach number, the shock wave angle, and the flow deflection angle across the oblique shock wave. The wave angle and the flow deflection angle in turn are a function of the model shape under investigation in the given test and the free stream Mach number.

To assess the validity of equation (11), one can evaluate this relation for a 20 deg cone-cylinder and again compare the results with experimental measurements from Reference 3. Shown in Table 1 are the wave angle, flow deflection angle, and the Mach number behind the oblique shock, as well as the evaluation of equations (7) and (10) for a range of Mach numbers from 1.1159 (the lowest free stream Mach number at which the flow over the surface of the cone is supersonic) to 1.50. The cone-cylinder flow parameter results in Table 1 were determined by the method of characteristic in References 15 and 21.

Using the values in Table 1, the wall porosity as given by equation (11) was calculated as shown in Figure 15. These thin wall analytical results indicate the general trend of increasing wall porosity with Mach number for perfect wave cancellation that is exhibited by the experimental data. However, the quantitative values tend to agree with the theoretical results obtained from equation (9) and approach a wall porosity of 50 percent at the higher Mach numbers, as would be suspected for this type of analysis. Therefore, since solutions using approximate and exact results for conditions across a shock wave yield similar results for the wave cancellation relationship, the

lack of agreement with experimental data for known real wall conditions must be involved in the K factor of equation (1), which will be considered next.

TABLE 1

FLOW PARAMETERS FOR A 20 DEGREE CONE-CYLINDER AT ZERO ANGLE OF ATTACK

M_∞	β (degrees)	Θ_1 (radians)	M_1	$\frac{\Delta P_{wave}}{q_\infty}$ Equation (IV-7)	$\frac{\Delta P_{wave}}{q_\infty}$ Equation (IV-10)	Percent Error of Equation (IV-7)
1.1159	65.259	0.008519	1.0908	0.03441	0.03631	5.241
1.115	61.683	0.008599	1.1273	0.03028	0.03142	3.619
1.20	57.489	0.008990	1.1787	0.02711	0.02782	2.578
1.30	51.163	0.010210	1.2784	0.02458	0.02504	1.825
1.50	42.669	0.013648	1.4734	0.02441	0.02487	1.817

D. Comparison of Experimental and Theoretical K Values

Goethert [7] notes that equation (1) has increasingly large errors as Mach numbers near 1.0 are approached, since for linearized flow as Mach numbers approach 1.0, the K factor tends to go to infinity. Of course, in real flow the K factor maintains a finite value. Thus, since as shown by equation (1),

$$K = \frac{2}{\sqrt{M_1^2 - 1}} \left(\frac{1}{W_p} - 1 \right) \quad , \tag{12}$$

then the wall porosity must be reduced as Mach numbers near 1.0 are approached in order for K to maintain a finite value. This trend follows that exhibited by the experimental data shown in Figure 15.

To obtain a more quantitative evaluation of this relationship, values of K were calculated from equation (12) and compared with values determined from the experimental data of Chew [18] for 22.5 percent open area $\frac{1}{16}$-in. diameter normal holes with the following results:

Mach Number	K (Experiment)	K_{IV-12}
1.0	5.60	∞
1.10	6.33	15.03
1.175	10.59	11.16

It is clear that K maintains a finite value at Mach numbers near 1.0 and that the trend of the experimentally determined K values decreases as Mach 1.0 is approached. This trend is opposite that indicated by equation (12). As Mach number increases, the error between the experimental and theoretical results decreases such that reasonable agreement between theory and experiment is exhibited at Mach number 1.175, apparently indicating that this expression is useful at higher transonic Mach numbers.

Then it must be concluded that the K factor in equation (1) does not accurately represent the physical situation except at the higher transonic Mach numbers and that the thin wall theory is not useful in the critical low transonic

speed range. Therefore, a thick wall representation of the wave cancellation flow phenonemon will now be considered.

E. Theory of Wave Cancellation for Thick Walls

Postulating a perfectly guided thick wall flow cancellation model as shown in Figure 16, the following derivation is obtained. On a unit basis, the mass flow through a perforated hole in the test section wall is given by

$$\dot{m} = \rho_2 V_2 A_2 = \rho_2 V_2 \sin \Theta_2 w \quad , \tag{13}$$

where ρ_2 and V_2 are specified by Prandtl-Meyer theory for a given incident wave condition.

For perfect wave cancellation, the mass flow rate out of the tunnel wall must equal the outflow along the disturbance. Thus, since the wall porosity is equal to $\sum W/L$,

$$\rho_\infty V_\infty h = \rho_2 V_2 \sin \Theta_2 \, LW_p \quad . \tag{14}$$

Further, as may be seen in Figure 16, the required turning angle through the Prandtl-Meyer expansion fan is given by

$$\tan(\Theta_2 - \Theta_1) = \frac{h}{L + h/\tan\beta} \quad . \tag{15}$$

Equation (15) may be solved for h as follows:

$$h = L \frac{\tan(\Theta_2 - \Theta_1) \tan\beta}{\tan\beta - \tan(\Theta_2 - \Theta_1)} \tag{16}$$

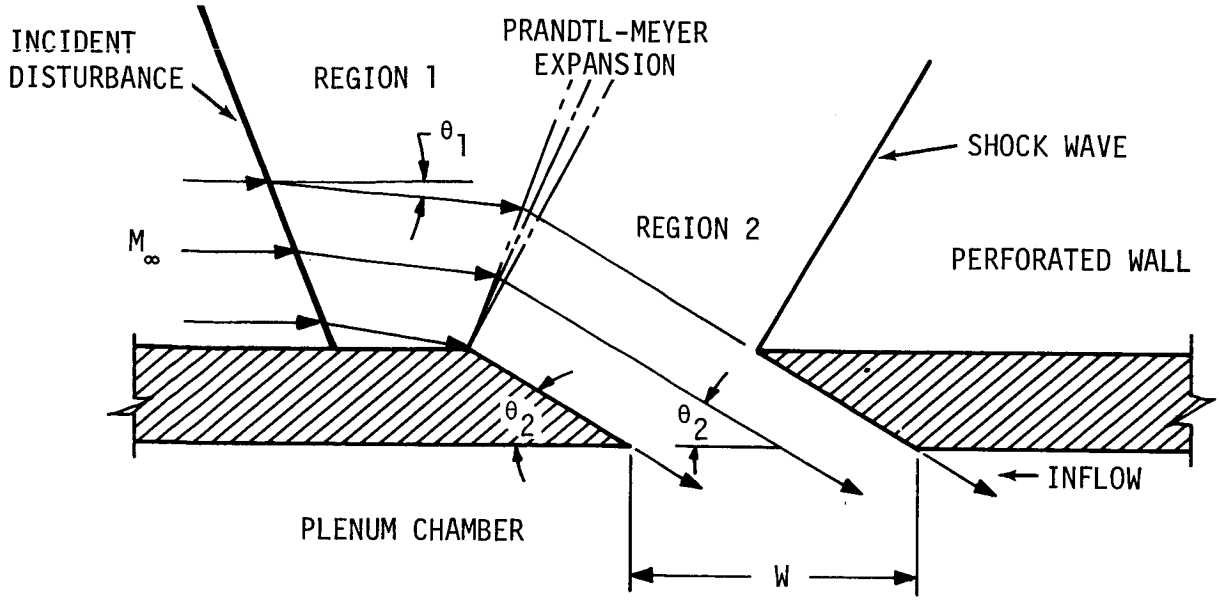

A. WAVE SYSTEM MODEL

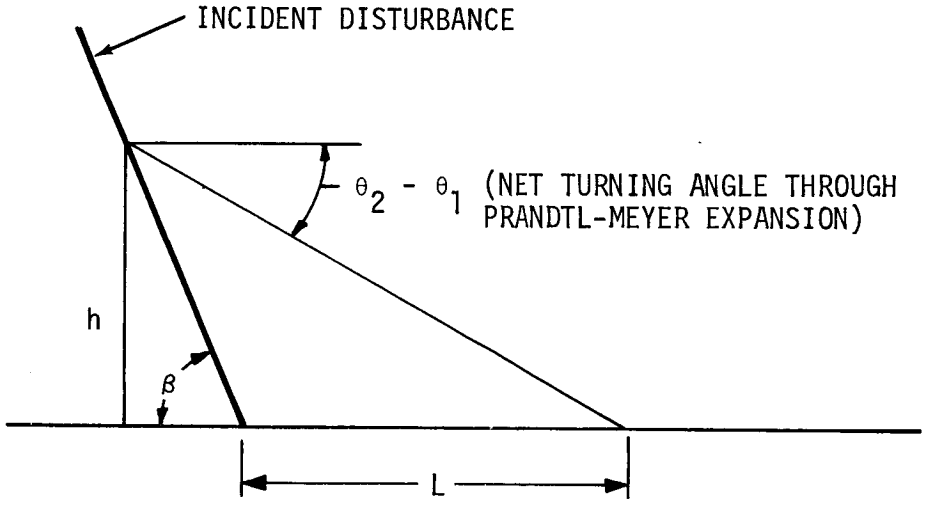

B. WAVE SYSTEM GEOMETRICAL RELATIONSHIP

Figure 16. Wave system model for fully cancelled wave with 60 deg inclined holes.

Substituting equation (16) into equation (14) and solving for wall porosity yields

$$W_p = \frac{\rho_\infty V_\infty}{\rho_2 V_2} \left[\frac{\tan(\Theta_2 - \Theta_1)\tan\beta}{\tan\beta - \tan(\Theta_2 - \Theta_1)} \right] \frac{}{\sin\Theta_2} \quad . \tag{17}$$

Equation (17) indicates that the required wall porosity for perfect wave cancellation is a function of the density ratio and velocity ratio across the wave system, the incident wave angle and the turning angle through the wave, (each of which are functions of Mach number and model shape), and the hole inclination angle, which is constant for a given wall configuration. Thus, the model shape and the free stream Mach number which influence the wave angle and the flow deflection angle, as well as the perforated wall configuration, are important parameters in the wave cancellation process.

Figure 17 shows the comparison between this result for a 20 deg cone-cylinder (obtained using the flow parameters shown in Table 1), and the previously mentioned MSFC 20 deg cone-cylinder experimental data, as well as AEDC-PWT 4-Ft. data for 60 deg inclined holes [22]. Equation (17) provides a much improved correlation between theory and experiment wherein not only is the trend of increasing wall porosity with increasing Mach number established, but also the analytical values are of the same order of magnitude as the measured result. However, good agreement is obtained only at the lower transonic Mach numbers. As Mach number increases, the analytical results fall progressively lower than the experimental values. The nonlinear variation of wall porosity with respect to Mach number shown in Figure 17 for equation (28) is similar to that indicated by the experimental data.

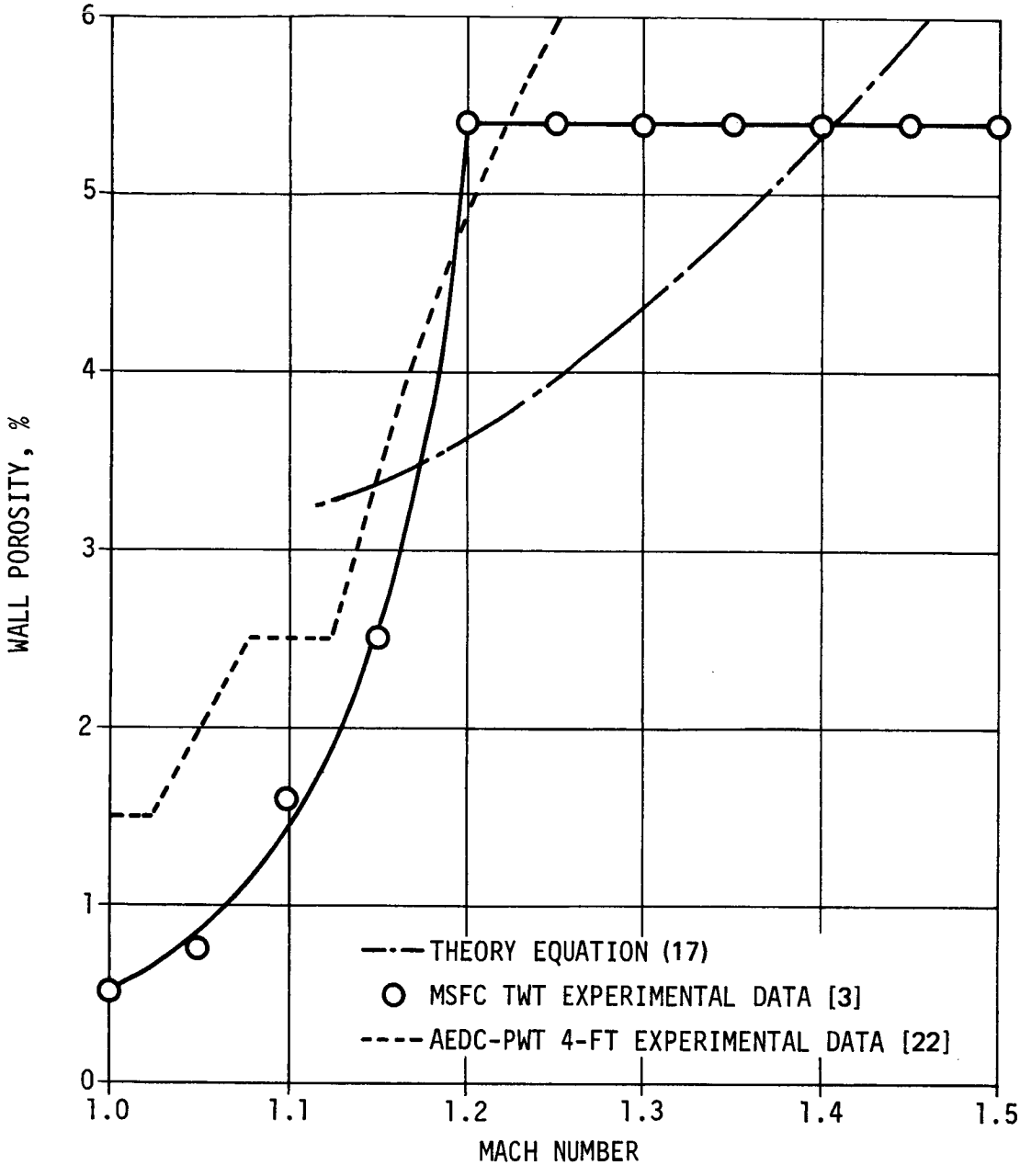

Figure 17. Comparison of theoretical and experimental optimum wall porosity determinations for 60 deg inclined holes, $\gamma = 1.4$.

Since it is clear that these results yield improved agreement with experimental measurements when compared with those derived in the two previous sections, it is therefore concluded that the thick wall model more nearly represents the true physical situation.

F. Summary of Theoretical Methods

It has been shown that, while the linearized thin wall wave cancellation theory does yield some insight into the problem, the wall porosity specified by this theory is much higher than known real wall conditions, especially in the critical low transonic speed range. On the other hand, the thick wall theory developed shows reasonable agreement with experimental results, both in magnitude and trend, with the predicted values of wall porosity being generally lower than known real wall conditions. Thus, it may be concluded that the wave cancellation process for real walls is more nearly represented by the thick wall theory but that the physical representation is not as good as should be desired since the experimental results fall between the predictions of the two theories.

Parameters identified as important to the wave cancellation process are wall porosity, free stream Mach number, perforated hole inclination angle, oblique shock wave angle, and flow deflection angle through the model-induced wave system. However, the relationship for complex model shapes and sizes and the influence of other parameters, such as Reynolds number, have not been identified. To meet these needs, the next section will treat a method which is capable of handling all important parameters and which is not burdened by the limitations of linearization procedures.

SECTION V.

OPTIMIZATION OF VARIABLE POROSITY TRANSONIC WIND TUNNEL FLOWS

A. Introduction

As previously discussed, the variable porosity perforated-wall transonic wind tunnel test technique seems to offer much promise for correctly adjusting wall porosity with respect to Mach number such that waves are effectively cancelled at the wall. The ability to easily reconfigure the wall geometry allows flexibility in matching wall characteristics to varying Mach number requirements. Furthermore, this capability allows the investigator to determine the best tunnel settings for each test Mach number instead of having to arrive at a single design compromise to accommodate all test conditions as required for fixed-porosity transonic wind tunnels. Also, variable porosity walls offer an improved test procedure for complex models generating both shock and expansion waves in that it is possible to minimize combined disturbances over the model surface [14].

Since the requirements for successful transonic testing are many and often diverse, it is inevitable that a trade-off is required among the various important variables. The variable porosity concept allows this trade-off to be

made for each test, instead of for each wind tunnel, and in effect it allows the redesign of the wall configuration to meet the needs of each experimental investigation.

What is needed, then, is a scientific procedure by which this problem can be studied and which leads to optimization of the tunnel configuration with minimum test time and expense.

B. Development of a Suitable Wave Cancellation Model Relationship

In order to determine the influence of the important parameters in the wave cancellation process, it will be necessary to compare experimental results to a known interference-free standard for a specific aerodynamic test model. A 20 deg (total included angle) cone-cylinder model shall be considered as a basis for optimization of the tunnel configuration. This shape is particularly useful in that it provides a difficult test of the wall cancellation characteristics with respect to both the bow shock wave and the strong centered expansion fan originating at the discontinuity between the cone and cylinder portions of the model. Data are available for the 20 deg cone-cylinder configuration for very small models tested in large wind tunnels which should be virtually interference-free, and the simple nature of the shape provides ready theoretical prediction of actual surface conditions for subsonic and supersonic Mach numbers, as shown by Davis and Graham [15]. Thus, a ready standard of comparison is available.

In principle, the technique developed herein can treat any model size or shape, but the present work will be restricted to a 20 deg cone-cylinder model at zero angle of attack. A single model size and hence blockage ratio will be used. The usual wall interference parameter employed by investigators has been the blockage parameter (i.e., the ratio of the cross-sectional area of the model to the wind tunnel test section cross-sectional area). As noted by Ferri [23], the tendency of those working in this field has been to test models of sufficiently low blockage that the necessity of making theoretical corrections to the data is avoided, because of the uncertainty existing in such corrections, and to use a single zero angle-of-attack criterion for all angles of attack. The present approach is consistent with the present state-of-the-art except that it will not be required that the model be ultra small. Rather, the tunnel configuration will be varied to minimize interference to the fixed size and shape model.

Now consider a typical pressure distribution measured along the length of such a model. An improperly set transonic tunnel wall configuration can produce both reflected shock and expansion wave disturbances along the model as shown in Figure 7. Since it is desired to eliminate wave disturbances at all points on the model, the local model pressure ratio can be determined by regression analysis as a function of the important parameters, including distance along the model, and compared with the interference-free results. Such mathematical relationships can be determined by the method developed in the Appendix where the important tunnel parameters are those identified in Sections III and IV.

The parameters selected for analysis are thus free stream Mach number, wall porosity, wall angle, and the nondimensional location along the model. The analysis developed in Section IV suggests that nonlinear relationships should be used and that perhaps a second order relationship will be satisfactory. However, experience has shown that higher order equations are required to adequately describe the relationship when the regression technique developed in the Appendix is used.

Thus, the following model equation is suggested for the wave cancellation optimization process:

$$\left[\frac{P}{P_t}\right]_{\text{experiment}} = A_0 + B_1 M + B_2 M^2 + \ldots + B_p M^p + C_1 W_p + C_2 W_p^{\,2} + \ldots + C_p W_p^{\,p} + D_1 \Theta_w + D_2 \Theta_w^{\,2} + \ldots + D_p \Theta_w^{\,p} + E_1\left(\frac{X}{D}\right) + E_2\left(\frac{X}{D}\right)^2 + \ldots + E_p\left(\frac{X}{D}\right)^p \qquad (18)$$

The interference-free reference data can be treated in a similar manner as shown below:

$$\left(\frac{P}{P_t}\right)_{\text{reference}} = A_1' + B_1' M + B_2' M^2 + \ldots + B_p' M^p + C_1'\left(\frac{X}{D}\right) + C_2'\left(\frac{X}{D}\right)^2 + \ldots + C_p'\left(\frac{X}{D}\right)^p . \qquad (19)$$

The wave cancellation model selected [equation (18)] fails to show the interdependence of Mach number and wall porosity determined in Sections III and IV, as may be seen when the partial derivatives of the pressure ratio with respect to Mach number and wall porosity are evaluated. An attempt was made to include the linear cross products of Mach number, wall porosity, and wall angle in equation (18). This procedure is developed in Reference 24. For this case, the surface fits failed to adequately describe the input data, evidently because of the strong correlation between Mach number and wall porosity and because attempts to isolate the optimum values proved meaningless. Therefore, equation (18) has been used in the form shown with the interdependence of Mach number, wall porosity, and wall angle being established by the mathematical formulation discussed in the next section. It should also be noted that equations (18) and (19) represent surfaces containing a family of curves of similar shape. This representation generally follows the trends discussed in Sections VI and VII.

Since widely different flow conditions exist over the cone and cylinder portions of the model, the quasi-linear multiple regression analysis is applied separately over each of these portions of the model for equations (18) and (19) to enhance the goodness of fit. Thus, the result is separate relationships for the cone and the cylinder.

Then, having reduced the wave cancellation process and the pressure distribution along the model to logical mathematical relationships, one can proceed to the development of a procedure to determine the tunnel configuration that will yield the minimum reflected wave interference.

C. Procedure for Minimizing Reflected Wave Interference

Upon establishing realistic model relationships for the wave cancellation process and the interference-free reference data, the constants in equations (18) and (19) can be evaluated by the quasi-linear multiple regression technique developed in the Appendix. Having determined these constants and investigated their suitability by assessing the average absolute percent error from the input data, the multiple correlation coefficient, and the F ratio, one now has mathematical relationships which can be attacked by the tools of calculus. That is, the specific wall porosity and the wall angle which can be expected to yield minimum reflected wave interference on the model for any given free stream Mach number can be determined. Future studies might also determine the physical tunnel parameters subject to the desired constraints of pressure and temperature as well as Mach number for facilities operating over a wide Reynolds number range, such as the NASA Marshall Space Flight Center High Reynolds Number Wind Tunnel.

To solve for these optimum tunnel settings, the root mean square (RMS) error relationship between the experimentally derived model relationship, equation (18), and the reference data, equation (19), integrated over the length of the model can be determined as follows:

$$E = \left[\int_0^{\left(\frac{X}{D}\right)_1} \left(\frac{P}{P_t}_{exp} - \frac{P}{P_\infty}_{ref} \right)^2 d\left(\frac{X}{D}\right) + \int_{\left(\frac{X}{D}\right)_1}^{\left(\frac{X}{D}\right)_l} \left(\frac{P}{P_t}_{exp} - \frac{P}{P_\infty}_{ref} \right)^2 d\left(\frac{X}{D}\right) \right]^{1/2} \tag{20}$$

where the partial integration is performed over the length of the cone 0 to $\left(\frac{X}{D}\right)_1$ and over the cylinder $\left(\frac{X}{D}\right)_1$ to $\left(\frac{X}{D}\right)_1$, considering all parameters except $\frac{X}{D}$ as constants.

After performing this integration, the problem of locating the minima of the RMS error relationship is reduced to a nonlinear function of several varibles as shown below:

$$E = F\left(M, W_p, \Theta_w\right) . \tag{21}$$

For a given Mach number, the value of the Mach number can be substituted into equation (21) such that the constrained function becomes

$$E_M = F\left(W_p, \Theta_w\right) \quad \text{at} \quad M = M_1 . \tag{22}$$

There are several methods for solving multi-dimensional static optimization problems such as those posed in minimizing the root mean square error function at a specific Mach number as specified by equation (22). The normal procedure is to solve for critial points using the necessary conditions for local extreme values as follows:

$$\frac{\partial E_M}{\partial W_p} = \frac{\partial E_M}{\partial \Theta_w} = 0 . \tag{23}$$

Solution to these equations yields the coordinates of the critial points. The sufficient conditions for E_M to have a local minimum are that at the critical points

$$\frac{\partial^2 E_M}{\partial W_p^2} \quad \text{and} \quad \frac{\partial^2 E_M}{\partial \Theta_w^2} > 0 \ . \tag{24}$$

If the values of the second partial derivatives are less than zero, a local maximum is indicated; if they are equal to zero, an inflection point is indicated. Hence, for nonlinear multivariate relations, one sees that it is possible to obtain more than one local minimum point (or maximum point, for that matter). Therefore, each of the minimum values determined must be evaluated by equation (22) to determine which yields the minimum RMS error value and, hence, the optimum values of wall porosity and wall angle for the specific Mach number in question.

However, the cross-product terms in the relation for root mean square error yield a set of simultaneous equations, equation (23), which can be cumbersome to solve. In the present investigation, a more easily implemented computer-oriented method will be used to determine the optimum values of the various tunnel configuration settings. This method is similar to that discussed by Pun [25] for steepest ascent (descent) search in multidimensional static optimization problems.

Given a performance index as a function of several variables, such as specified by equation (22), the problem is to determine in a minimum number of steps the values of the variables which result in a minimum value for the performance index. Again, it is recalled that the necessary condition for the performance index (E_M) to have a local extreme is that the partial derivatives with respect to each of the independent variables be identically equal to zero.

Arbitrary initial trial values of the independent variables can be assumed which shall be denoted by the subscript m. Then, in searching for minimum values, the following may be written:

$$W_{p_{m+1}} = W_{p_m} - \lambda \left[\frac{\partial E_M}{\partial W_p} \right]_m \tag{25}$$

and

$$\Theta_{w_{m+1}} = \Theta_{w_m} - \lambda \left[\frac{\partial E_M}{\partial \Theta_w} \right]_m , \tag{26}$$

where λ is a function to be determined and the two respective partial derivatives are assigned the values determined from the trial values of the independent variables. Then, if the trial value of the variables to be optimized is indeed a critial point, the partial derivatives of the error function will be equal to zero (as closely as desired) and the $m + 1$ trial values will be equal to the mth trial values.

To determine the value of λ, the relations for the independent variables, equations (25) and (26), may be substituted into equation (22) as follows:

$$E_M = F \left\{ W_{p_m} - \lambda \left[\frac{\partial E_M}{\partial W_p} \right]_m , \Theta_{w_m} - \lambda \left[\frac{\partial E_M}{\partial \Theta_w} \right]_m \right\} . \tag{27}$$

It is noted that equation (27) is a function of only one independent variable (λ), since all other terms are constants for a given trial value. Thus, the

value of λ which should yield the extreme values for root mean square can be determined by evaluating the necessary conditions for such an occurrence.

By forming the partial derivative of equation (27) with respect to λ and setting this relation equal to zero, a trial value of λ can be solved for by noting that all the parameters except λ are constants determined by the values of the independent variables at the mth trial. The exact form of this solution is dependent on the specific relationship involved but, in any case, the value of λ is easily obtained by digital computer procedures. Multi-valued solutions for λ are to be expected in this determination. Since the most rapid convergence to the minimum value is desired, all λ solutions in the equation of the performance index, equation (27), may be tested to determine which solution yields the minimum root mean square error. The use of other roots would either converge less rapidly or converge to points other than the minimum point. The solution for λ yielding the minimum value of RMS error is then selected for use in calculations for the given trial, equations (25) and (26).

Knowing λ, a new trial value can be readily obtained from equations (25) and (26) and the procedure repeated until the given critical point has been isolated as closely as desired. This technique has been found to converge reasonably rapidly. In application, this search technique leads only to a single local critical point. Thus, a grid search technique in a similar manner will then reveal all critical points which are either local maxima or minima in the range of interest. This technique is not able to determine saddle points if the partial derivatives are finite, and the search simply proceeds past such points.

Once the critical points are isolated, the indicated values for wall porosity and wall angle can be substituted into equation (22) and the value of the root mean square error of the performance index determined for each local extremum. Inspection of these results will then reveal the critical point which yields the minimum root mean square error. The wall porosity and wall angle which should produce the most optimum test conditions for the given Mach are specified by this minimum critical point.

A computer program has been developed using the methods developed in this chapter to determine the tunnel settings which should yield the best transonic testing configurations. Results obtained for the MSFC Trisonic Wind Tunnel Facility are discussed in Section VII.

D. Summary

Thus, a logical mathematical procedure has been developed which is capable of determining the values of the tunnel wall porosity and wall angle which can be expected to yield the minimum reflected wave interference over the length of the model for any given free-stream Mach number. Strictly speaking, the tunnel settings so derived are valid only for the same model size and shape. However, in practice, such tunnel settings could be expected to yield useful results for similar types of models.

The optimization procedure developed is straightforward in application, but the results can be no better than the experimental data from which they are derived. Also of importance is the selection of the proper model equation relationships. The present work considered those parameters identified as

significant by the theoretical and experimental studies indicated in Sections III and IV. In principle, it would be possible to extend this work to include additional parameters such as Reynolds number, angle of attack, etc., when such considerations seem necessary. Further, while the analysis presented considers only a single size and shape model, such a procedure can be applied to a wide range of model sizes and shapes to develop a family of tunnel settings for different types of tests. Thus, a powerful general-purpose tool is now available by which wave reflection can be minimized for a wide range of testing.

SECTION VI.

INTERFERENCE-FREE STANDARD

A. Introduction

The proposed scheme of variable porosity transonic tunnel flow optimization developed herein requires experimental data obtained from a 20 deg cone-cylinder model tested at zero angle of attack as a known interference-free standard. This model was selected for the following reasons:

1. It provides a difficult test of wall cancellation characteristics. The test is difficult because the incident wave system contains not only shock waves but also a strong centered expansion fan originating at the juncture between the cone and cylinder portions of the model, and

2. This general shape was representative of future testing requirements for launch vehicle configurations. Other types of models could also be considered in future investigations.

As noted in Section IV, the present calibration of the MSFC 14-Inch Trisonic Wind Tunnel Facility indicates that the maximum possible physical wall porosity of 5.4 percent is capable of optimum operation up to a maximum Mach number of 1.2 after which some uncancelled wave reflection should be expected. Therefore, for present purposes, a range of interest from Mach

1.0 to 1.2 is arbitrarily designated. Higher Mach numbers can be optimized in the future using this technique when higher porosity walls become available. Lower Mach numbers could also be treated.

B. Available Experimental Data

In an effort to establish an experimental interference-free standard, a literature search was made to determine what data are available. Table 2 presents some of the investigations studied. Previous studies concerning transonic interference-free data have almost universally used the data from Estabrooks [12] obtained in the Arnold Engineering Development Center 16-Foot Transonic Tunnel. These data are no longer available in tabulated form, making their use in this work undesirable because of the use of the computer in the analysis of the data. The more recent data from the AEDC 1-Foot and 4-Foot Transonic Tunnels were rejected because of relatively high percent blockages [26], [27], [28]. The data from the NASA Lewis Research Center 8 × 6 Foot Tunnel [29] are not useful because of extensive disturbances caused by nonporous sections of the tunnel. The more recent data of Hartley and Jacocks [30] from the AEDC 16-T for a 0.0625 percent model blockage provide a reasonable interference-free standard, although some wall interference was determined at Mach numbers between 0.95 and 1.05. Finally, it was concluded that the best available data for use as an interference-free standard were those of Capone and Coates [2] from the Langley Research Center 16-Foot Transonic Tunnel. These data were obtained at zero degrees angle of attack for a 0.0062 percent blockage model using a single row of static pressure orifices aligned

TABLE 2

SOURCES OF 20 DEGREE CONE-CYLINDER EXPERIMENTAL DATA

Reference	Investigator	Facility	Tunnel	Mach Range	Model Diameter	Percent Blockage
2	Capone and Coates	Langley	16-Foot Transonic	0.7-1.3	8.5 6.0 1.5	0.198 0.098 0.0062
12	Estabrooks	AEDC	1-Foot Transonic	0.7-1.4	2.708 1.1915 1.000	4.00 2.00 0.50
			16-Foot Transonic	0.7-1.4	1.915 21.600	0.008 1.00
26	Robertson and Chevalier	AEDC	1-Foot Transonic	0.5-1.2	1.0 1.5	0.50 1.23
27	Anderson, Anderson, and Credle	AEDC	1-Foot Transonic	0.6-1.3	1.354	0.945
28	Jacocks	AEDC	4-Foot Transonic	0.6-1.2	5.416	1.00
30	Hartley and Jacocks	AEDC	16-Foot Transonic	0.6-1.6	5.416	0.0625
29	Mitchel	Lewis	8 × 6 Foot	0.5-2.0	4.0 8.0 12.0 16.00	0.18 0.73 1.64 2.91
31	Erickson and Dowling	Convair	4 × 4 Foot	0.8-1.1	3.480	0.412

at zero degrees roll angle; they are assumed to be interference-free for practical purposes and, therefore, were adopted as the standard for the present investigation. It should be noted, however, that the model used in this investigation suffered from two construction abnormalities: The total included angle was not precisely 20 deg and the nose tip was not as sharp as some of the larger models. As noted by the authors these abnormalities caused deviations from the somewhat flat pressure distribution which normally exists over the cone. However, these errors are considered to be less significant than those in the next best choice, Hartley and Jacocks [30], where the effect of the reflected wave interference is integrated over the length of the cylinder.

Additional reports of some importance to this study, but not included in Table 2 are the cone-cylinder investigations from the MSFC 14-Inch TWT [15], [32], [33], and two studies from NASA-Ames Research Center [34], [35]. The NASA-Ames studies are of particular interest in that Schlieren photographs were taken and the data by Page [34] are the lowest percent blockage found in the open literature (0.005 percent). However, for this study, the cone half angle was 6 degrees 59 minutes, so the data were not useful for present purposes.

C. Regression Analysis for the Interference-Free Standard

Having chosen the LRC 16-Foot, 0.0062 percent blockage, 20 deg cone-cylinder data as the interference-free standard, the next problem is the determination of a mathematical model which describes the relationship of the local model pressure ratio with respect to axial variations along the model and with respect to Mach number variations from 1.0 to 1.2 at zero angle of attack.

Because of the different nature of the flow over the cone and cylinder portions of the model, separate relationships for each portion are determined in the following form:

$$\frac{P}{P_t} = A_0' + B_1'M + B_2'M^2 + \ldots + B_P'M^P + C_1'\left(\frac{X}{D}\right) + C_2'\left(\frac{X}{D}\right)^2 + \ldots + C_P'\left(\frac{X}{D}\right)^P \quad . \tag{28}$$

Using the data of Capone and Coates [2], second, third, and fourth order relations were obtained using the computer program discussed in Section V and the Appendix for X/D values from 1.063 to 2.813 in the case of the cone and for X/D values from 3.063 to 9.813 measured over the cylinder. To assess the goodness of fit, the experimental data were machine-plotted along with the values obtained from the fitted equations for each degree equation studied and for each Mach number at which reference data were available (Mach numbers, 1.000, 1.038, 1.104, 1.157, and 1.208). Results clearly indicated that the fourth order fit was superior. In addition, the standard deviation, the multiple correlation coefficient, the maximum percent error for any data point, the average absolute percent error for all data points, and the value of the F statistic were computed for each fit. These results are shown in Table 3 along with other statistical parameters.

In general, the fits were well-behaved with good correlation with the experimental data. A fourth order fit was selected, based on the above mentioned criteria, as the best representation of the data for both the cone and

TABLE 3

SURFACE FIT PARAMETERS FOR 20 DEGREE CONE-CYLINDER REFERENCE DATA IN THE MACH RANGE FROM 1.00 TO 1.20

Deg of Equation	s + -	R	Max Percent Error	Avg Percent Error	F	M
Cone Portion of Model						
2	0.1754	0.9387	9.587	2.404	88.94	40
3	0.1663	0.9587	7.113	2.345	63.46	40
4*	0.1297	0.9713	6.327	1.847	76.54	40
Cylinder Portion of Data						
2	0.1391	0.9608	16.09	2.293	544.8	140
3	0.0946	0.9824	11.69	1.492	739.0	140
4**	0.0722	0.9897	9.82	1.161	784.0	140

* Equation selected as best fit:

$$\frac{P}{P_t} = -0.4372 \times 10^1 + 0.6372M + 0.1589\times10^2M^2 - 0.1973 \times 10^2M^3 + 0.6649 \times 10^1M^4 + 0.3681 \times 10^1 \left(\frac{X}{D}\right) - 0.3217 \times 10^1 \left(\frac{X}{D}\right)^2 + 0.1197 \times 10^1 \left(\frac{X}{D}\right)^3 - 0.1614 \left(\frac{X}{D}\right)^4$$

** Equation selected as best fit:

$$\frac{P}{P_t} = -0.2138 \times 10^1 + 0.3226 \times 10^1M - 0.8607M^2 - 0.1967\times10^1M^3 + 0.9872M^4 + 0.7380 \left(\frac{X}{D}\right) - 0.1591\left(\frac{X}{D}\right)^2 + 0.1499 \times 10^{-1} \left(\frac{X}{D}\right)^3 - 0.5206 \times 10^{-3} \left(\frac{X}{D}\right)^4$$

cylinder portions of the model. The equations selected for further use are as follows:

1. Cone Portion of Model

$$\frac{P}{P_t} = -0.4372 \times 10^1 + 0.6372M^1 + 0.1589 \times 10^2M^2 - 0.1973 \times 10^2M^3 + 0.6649 \times 10^1M^4 + 0.3681 \times 10^1 \left(\frac{X}{D}\right) - 0.3217 \times 10^1 \left(\frac{X}{D}\right)^2 + 0.1197 \times 10^1 \left(\frac{X}{D}\right)^3 - 0.1614 \left(\frac{X}{D}\right)^4 . \quad (29)$$

2. Cylinder Portion of Model

$$\frac{P}{P_t} = -0.2138 \times 10^1 + 0.3226 \times 10^1M - 0.8607M^2 - 0.1967 \times 10^1M^3 + 0.9872M^4 + 0.7380 \left(\frac{X}{D}\right) - 0.1591 \left(\frac{X}{D}\right)^2 + 0.1499 \times 10^{-1} \left(\frac{X}{D}\right)^3 - 0.5206 \times 10^{-3} \left(\frac{X}{D}\right)^4 . \quad (30)$$

For each Mach number fitted, equations (29) and (30) were evaluated over the length of the model where data exist and were compared to the original experimental data as shown in Figure 18. Experimental data are shown only at Mach numbers 1.00, 1.104, and 1.208 for clarity. As may be seen, the fit over the cone portion of the model shows excellent agreement; although, as previously mentioned, the experimental data are not as flat as should be expected in this region. Over the cylinder portion of the model, the analytic surface fit shows good agreement with the experimental results, although just aft of the

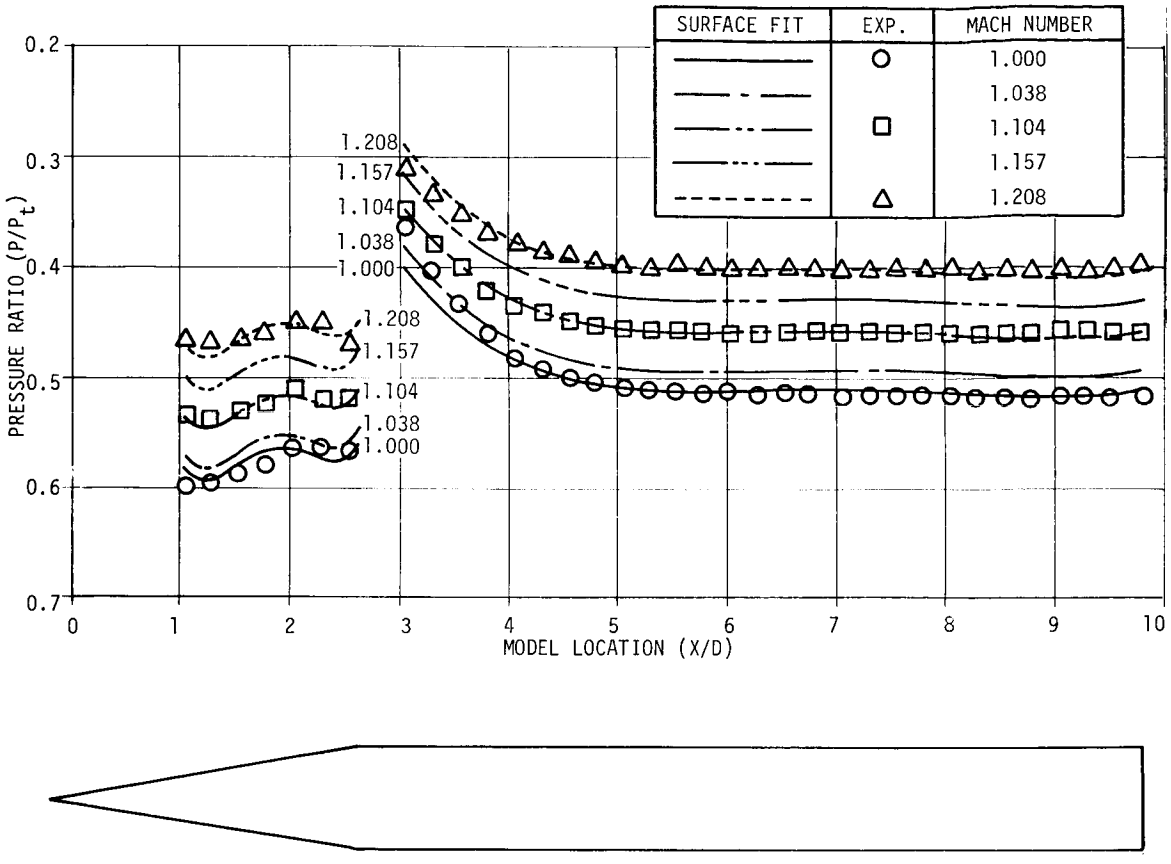

Figure 18. Comparison of surface fit and experimental results for LRC 20-deg cone cylinder reference data.

shoulder between the cone and cylinder, the indicated values are slightly lower than experiment at Mach 1.000, have excellent agreement at Mach 1.104, and are slightly higher than experiment at Mach 1.208. In each case the maximum percent error occurs at the extreme forward end of this cylinder fit.

For the cone portion of the model, the maximum error for any data point was 6.33 percent, the average absolute error was 1.85 percent, the standard deviation was ±0.01296, and the value of the F statistic was 76.54. Results for the cylinder portion of the model indicated a maximum error of 9.82

percent, an average absolute error of 1.16 percent, a standard deviation of ±0.00722, and an F statistic value of 784.0.

Considering the fitted expression for the pressure ratio existing over the cone, equation (29), the combined effect of all independent variable terms on the dependent variable may be tested to determine the usefulness of the result. That is, the null hypothesis may be tested that:

$$H_0: B'_1 = B'_2 = \ldots B'_P = 0$$

$$C'_1 = C'_2 = \ldots C'_P = 0 \quad .$$

At the 0.05 significance level with 28 numerator degrees of freedom and 11 denominator degrees of freedom, the F_{table} value is 4.65 [36]. Therefore, since $F > F_{table}$ $(76.54 > 4.65)$, the null hypothesis that there is no combined effect of the independent variables is rejected at the 0.05 significance level, and one observes that it is highly probably that the fitted expression does represent the measured pressure ratios over the cone.

Similarly, considering the surface fit over the cylinder portion of the model, equation (30), the F_{table} value at the 0.05 significance level with 128 numerator degrees of freedom and 11 denominator degrees is 4.34 [36]. Then since $F > F_{table}$ $(784 > 4.34)$, the null hypothesis that there is no combined effect of the independent variables is rejected at the 0.05 significance level, and one observes that it is highly probable that the fitted expression does represent the measured pressure ratio over the cylinder.

D. Summary

Thus, an analytic representation of the pressure ratio existing over the top surface of a 20-deg cone-cylinder model in the Mach number range from 1.0 to 1.2 at zero degrees angle of attack is now available, which is, for all practical purposes, interference-free and which can be used as a reference standard for the remainder of this study.

SECTION VII.

EVALUATION OF OPTIMIZATION TECHNIQUE USING MSFC 14-INCH TRISONIC WIND TUNNEL DATA

A. Introduction

In order to evaluate the usefulness of the optimization technique developed herein for variable porosity transonic wind tunnel flows, it is desirable to apply the method to an actual set of wind tunnel data. As stated earlier, an existing set of wind tunnel data obtained from the MSFC 14-Inch Trisonic Wind Tunnel for a 20-deg cone-cylinder at zero angle of attack will be used in the evaluation.

The data available to be used to determine the local model pressure ratio as a function of Mach number, model location, and the tunnel parameters is limited to a wall angle of -15 min in the Mach number range of interest (1.00 to 1.20). Therefore, for present evaluation purposes, the pressure ratio will be determined as follows:

$$\frac{P}{P_t} = F\left(M, W_p, \frac{X}{D}\right) \quad . \tag{31}$$

Shown in Table IV are the experimental results studied. The data are from TWT Test 475 as reported in Reference 3. Inspection of Table 4 reveals that data exist at only one wall porosity for each test Mach number. Then, to

TABLE 4

MSFC 14-INCH TRISONIC WIND TUNNEL DATA STUDIED (θ_w = - 15 minutes)

Test No.	Run No.	Mach No.	W_p (Percent)	P_t (psia)
475	19/0	1.003	0.75	20.01
475	20/0	1.001	0.75	30.02
475	21/0	1.058	0.75	20.01
475	21/1	1.058	0.75	20.02
475	21/2	1.058	0.75	20.02
475	22/0	1.057	0.75	30.02
475	23/0	1.103	1.60	20.02
475	24/0	1.099	1.60	30.02
475	25/1	1.141	2.00	20.02
475	26/0	1.153	2.00	32.02
475	27/0	1.209	5.40	20.02
546*	67	1.001	0.50	29.99
546*	68	1.000	1.10	30.00
546*	69	1.003	1.60	20.01

* Runs to confirm optimization results

accurately assess the quantitative influence of wall porosity on the wave cancellation problem by the method proposed, additional experimental results shall be required and the present investigation should be considered qualitative in nature. It is further noted that the Test 475 data were obtained at two different stagnation pressures, 20 and 30 psia, respectively, and it is assumed that the change in stagnation pressure, and hence Reynolds number, has negligible effect on measured results. This assumption is consistent with past experience as shown in Reference 3.

B. Regression Analysis for the 14-Inch Trisonic Wind Tunnel Data

A surface fit of the form shown in equation (31) was obtained using the computer program discussed in Section V and the Appendix for second, third, and fourth order polynomial relationships for X/D values from 0.913 to 2.721 in the case of the cone portion of the model and for X/D values from 2.821 to 11.765 measured over the cylinder, where the shoulder separating the cone from the cylinder was located at an X/D of 2.756.

Again, the experimental data were machine-plotted, along with the values obtained from the fitted regression equations for each Mach number analyzed to determine the goodness of fit. The plotted results again indicated that the fourth order fit was superior to lower order fits. In addition, the maximum percent error, the average percent error, the standard deviation, and the value of the F static were computed for each fit as shown in Table 5. These results clearly show the fourth order fit to be the best representation of the data except that for the cone, the F statistic does not increase with increasing order of the polynomial

TABLE 5

SURFACE FIT PARAMETERS FOR MSFC 14-INCH TRISONIC WIND TUNNEL DATA IN THE MACH NUMBER RANGE FROM 1.00 TO 1.20

Deg of Equation	s + -	R	Max Percent Error	Avg Percent Error	F	M
Cone Portion of Model						
2	0.01248	0.9680	6.052	1.609	276.7	99
3	0.01179	0.9723	5.307	1.615	195.5	99
4*	0.01121	0.9763	5.781	1.595	158.6	99
Cylinder Portion of Model						
2	0.02042	0.9152	18.63	3.575	368.2	363
3	0.01546	0.9529	14.15	2.683	435.7	363
4**	0.01143	0.9732	10.19	1.988	604.5	363

* Equation selected as best fit:

$$\frac{P}{P_t} = -0.3637\times10^{1} + 0.8396\times10^{1}M - 0.4725\times10^{1}M^2 - 0.8564M^3 + 0.8954M^4$$

$$+ 0.1110W_p - 0.4449\times10^{-1}W_p^2 - 0.1325\times10^{-1}W_p^3 + 0.3264\times10^{-2}W_p^4$$

$$+ 0.1208\times10^{1}\left(\frac{X}{D}\right) - 0.1189\times10^{1}\left(\frac{X}{D}\right)^2 + 0.4439\left(\frac{X}{D}\right)^3 - 0.6419\times10^{-1}\left(\frac{X}{D}\right)^4$$

** Equation selected as best fit:

$$\frac{P}{P_t} = 0.8396 - 0.2110\times10^{1}M + 0.5524M^2 - 0.1193M^3 + 0.2023M^4 + 0.1759W_p$$

$$- 0.7750\times10^{-1}W_p^2 - 0.5704\times10^{-2}W_p^3 + 0.2623\times10^{-2}W_p^4 + 0.5897\left(\frac{X}{D}\right)$$

$$- 0.1175\left(\frac{X}{D}\right)^2 + 0.1006\times10^{-1}\left(\frac{X}{D}\right)^3 - 0.3134\times10^{-3}\left(\frac{X}{D}\right)^4$$

(as was also the case with the reference data). To investigate this behavior, a computer dump was evaluated, and it was determined that the R value was indeed properly calculated. Evidently this unexpected behavior is due to the more erratic nature of the measured pressure ratios over the cone as an analysis of the computational process showed that the ratio of the denominator degrees of freedom of the numerator degrees of freedom increased more rapidly with increasing order of the equation than did the ratio of regression sum of squares to the residual sum of squares. Thus, a decreasing F value with order of equation is indicated for this case. A similar analysis for the cylinder showed that ratio of sums of squares increased more rapidly than the ratio of degrees of freedom with increasing order of the equation and hence the F value increased.

Overall the surface fits were well-behaved with good correlation with the TWT experimental data. Using the previously mentioned criteria, a fourth order fit was selected as the best representation of the data for both the cone and the cylinder portions of the model. The equations selected for further use are as follows:

1. Cone portion of model

$$\frac{P}{P_t} = -0.3637\times10^{1} + 0.8396\times10^{1}M - 0.4725\times10^{1}M^2 - 0.8564M^3 + 0.8954M^4$$

$$+ 0.1110W_p - 0.4449\times10^{-1}W_p^2 - 0.1325\times10^{-1}W_p^3 + 0.3264\times10^{-2}W_p^4$$

$$+ 0.1208\times10^{1}\left(\frac{X}{D}\right) - 0.1189\times10^{1}\left(\frac{X}{D}\right)^2 + 0.4439\left(\frac{X}{D}\right)^3 - 0.6419\times10^{-1}\left(\frac{X}{D}\right)^4 \quad (32)$$

2. Cylinder portion of model

$$\frac{P}{P_t} = 0.8396 - 0.2110\times10^{1}M + 0.5524\,M^2 - 0.1193\,M^3 + 0.2023\,M^4 + 0.1759\,W_p$$

$$- 0.7750\times10^{-1}W_p^2 - 0.5704\times10^{-2}W_p^3 + 0.2623\times10^{-2}W_p^4 + 0.5897\left(\frac{X}{D}\right)$$

$$- 0.1175\left(\frac{X}{D}\right)^2 + 0.1006\times10^{-1}\left(\frac{X}{D}\right)^3 - 0.3134\times10^{-3}\left(\frac{X}{D}\right)^4 \qquad (33)$$

As shown in Figure 19, equations (32) and (33) were evaluated for each Mach number fitted and compared with the experimental data. Experimental data are shown only at Mach numbers of 1.003, 1.103, and 1.209 for clarity. As was the case with the LRC reference data, the analytic surface fit shows good agreement with the experimental results, although near the shoulder between the cone and cylinder some deviation occurs.

For the cone portion of the model, the maximum percent error for any data point was 5.781 percent, the average absolute error was 1.595 percent, the standard deviation was ± 0.01121, the multiple correlation coefficient was 0.9763, and the value of the F statistic was 158.6. Results for the cylinder portion of the model indicate a maximum error for any data point of 10.19 percent, an average absolute error of 1.988 percent, a standard deviation of ± 0.01143, a multiple correlation coefficient of 0.9732, and an F static value of 604.5. As was the case with the reference data, a test of significance at the 0.05 level clearly showed that the null hypothesis (that there is no combined effect of the independent variables) should be rejected and that it is highly

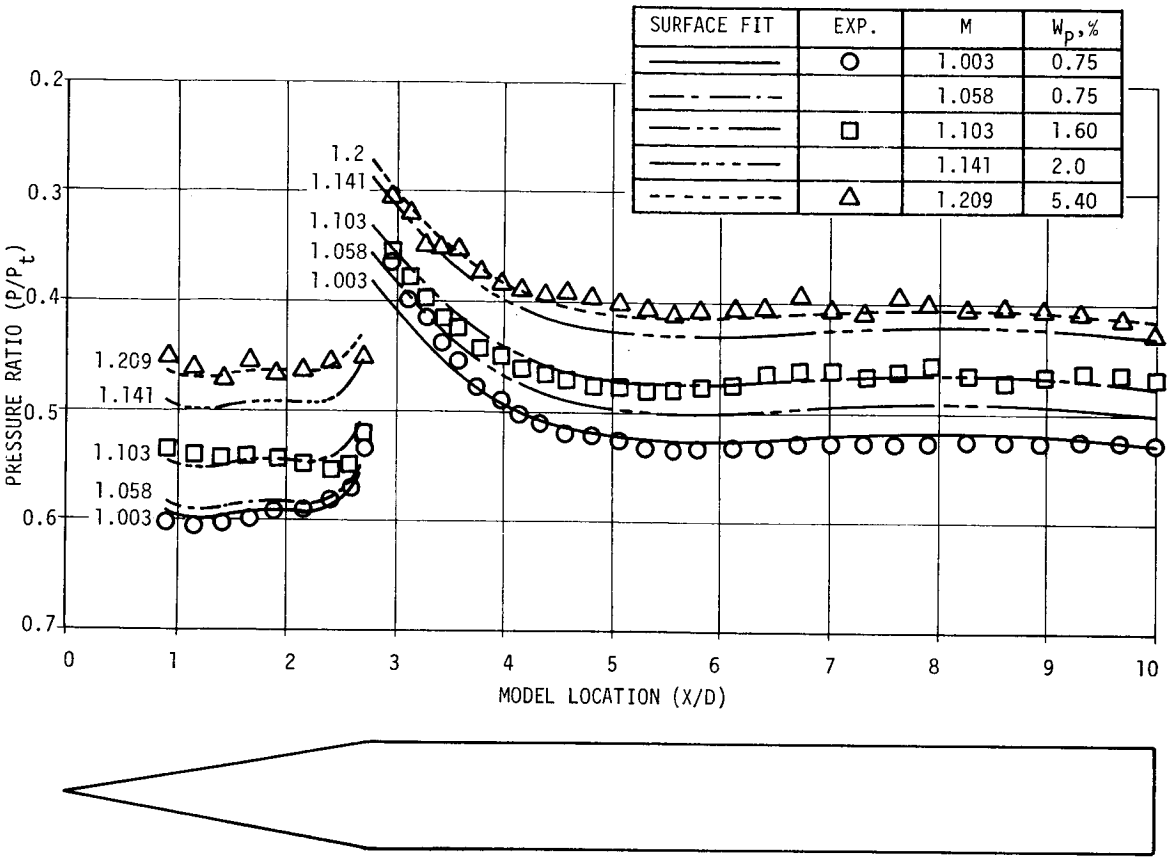

Figure 19. Comparison of surface fit and experimental results for MSFC TWT 20 deg cone cylinder data.

probable that the fitted expressions do represent the measured pressure ratios over the model.

C. Optimization of the Wind Tunnel Data

Now that reasonably accurate analytic representations of the TWT wind tunnel data have been determined incorporating the influence of wall porosity and similar relationships which are free of wave interference, the optimum value of wall porosity for a given Mach number which should produce minimum

wave interference on the aerodynamic test model can be obtained by the procedure developed in Section V.

Using the computer program discussed in Section V, all critical points in the physical range of wall porosity from 0 to 5.40 percent were identified for test Mach numbers of 1.00, 1.05, 1.10, 1.15, and 1.20. Furthermore, the square of the performance index E_M was plotted versus wall porosity for each Mach number and the nature of each critical point was identified. A typical plot of this relationship for Mach number 1.00 is shown in Figure 20. It is interesting to note that for this condition two critical points exist (wall porosities of 0.55 percent and 1.61 percent) with nearly equal performance index values between which exists a maximum point. The lower porosity value is nearly identical to the present TWT standard setting as determined by trial and error experiments, and the higher value is the critical point identified as optimum in the computer analysis (lower E_M value). This phenomenon will be discussed in more detail in the next section. The performance index curves at other Mach numbers showed similar trends except the minimum point having the lowest wall porosity had somewhat higher performance index values, and thus the optimum critical point identified in the analysis was more clearly defined. The values of each critical point are shown in Table 6. As shown in the table, the root having the lowest performance index value (and hence the optimum wall porosity) shows increasing wall porosity requirements with increasing Mach number. Further, the optimum condition switched to a different root (higher porosity value of the several indicated minima) at a Mach number of 1.2, reflecting the

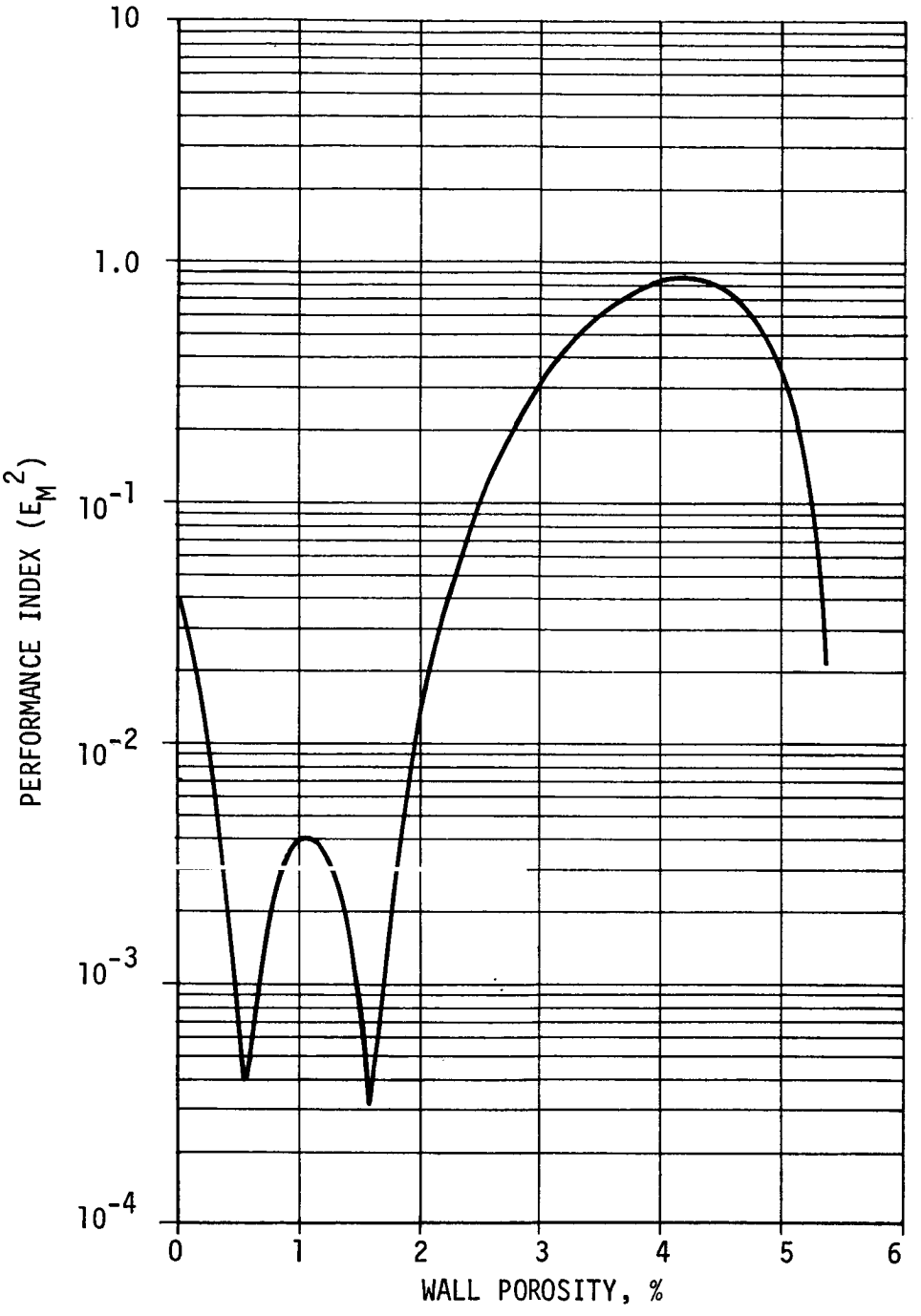

Figure 20. Variation of performance index at Mach number 1.0.

influence of the interdependence of Mach number and wall porosity built into equation (20).

TABLE 6

CRITICAL POINTS IDENTIFIED BY OPTIMIZATION PROGRAM

M	W_p	E_M^2	Type of Variation
1.00	0.555	0.3896×10^{-3}	Minimum Point
1.00	1.071	0.4022×10^{-2}	Maximum Point
1.00	1.610*	0.3145×10^{-3}	Minimum Value
1.00	4.196	0.8251	Maximum Point
1.05	0.538	0.8619×10^{-3}	Minimum Point
1.05	1.063	0.4885×10^{-2}	Maximum Point
1.05	1.638*	0.2276×10^{-3}	Minimum Value
1.05	4.197	0.8140	Maximum Point
1.10	0.422	0.1422×10^{-2}	Minimum Point
1.10	1.063	0.1033×10^{-2}	Maximum Point
1.10	1.766*	0.2507×10^{-3}	Minimum Value
1.10	4.194	0.7571	Maximum Point
1.15	0.260	0.1518×10^{-2}	Minimum Point
1.15	1.068	0.2355×10^{-1}	Maximum Point
1.15	1.940*	0.2318×10^{-3}	Minimum Value
1.15	4.196	0.6679	Maximum Point
1.20	0.087	0.7919×10^{-3}	Minimum Point
1.20	1.073	0.4901×10^{-1}	Maximum Point
1.20	2.129	0.9129×10^{-3}	Minimum Point
1.20	4.196	0.5627	Maximum Point
1.20	5.292*	0.2502×10^{-3}	Minimum Value

* Computer-identified optimum value.

In Figure 21 the optimized results for the MSFC TWT are compared to the present standard values and to the results from the AEDC 4-Foot tunnel as well as to the theory developed in Section IV for thick walls. In the low transonic speed range, the optimized values tend to agree with theory, equation (17) and with the AEDC results, and are somewhat higher than the MSFC data. However, at higher Mach numbers the computer selected optimum values, the AEDC data, and MSFC data tend to agree, each having a considerably larger change of wall porosity with respect to Mach number than the thick wall theory. Then overall, the optimized wall porosity values tend to qualitatively agree with previous experimental results and are generally of the same sort of quantitative value.

A further analysis was performed to determine if the optimized wall porosity values were indeed an improvement over the present settings. Using equations (32) and (33), plots of pressure ratio versus model station were made at the indicated optimum values and the present standard conditions and compared with interference-free reference values. In each case, the analytically obtained values represented an improvement over the present standard values. A typical plot of the results of Mach number 1.15 is shown in Figure 22.

D. Confirmation Wind Tunnel Tests

As a means of confirming the trends indicated by the mathematically determined optimum TWT performance index relationship, a short test was conducted in the MSFC TWT. Three runs were made at Mach number 1.0 at

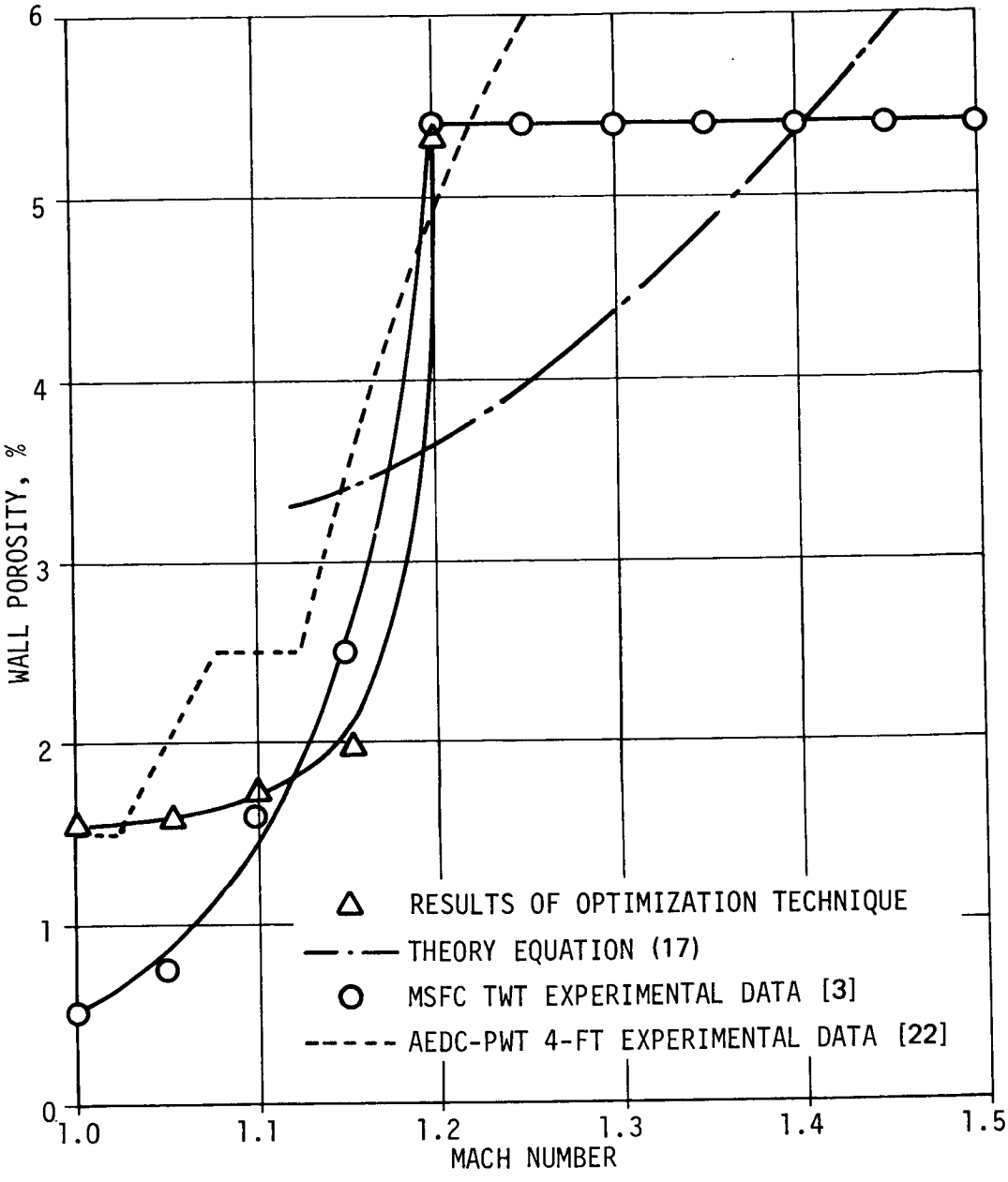

Figure 21. Comparison of computer optimum wall porosity values to theoretical and experimental results for 60 deg inclined holes.

wall porosities of 0.5, 1.1, and 1.6 percent, respectively, as shown in Table 4 for test 546. The 0.5 percent wall porosity represents both the present TWT standard value and the lower porosity minimum point previously discussed. As shown in Figure 20, the 1.1 percent wall porosity configuration represents

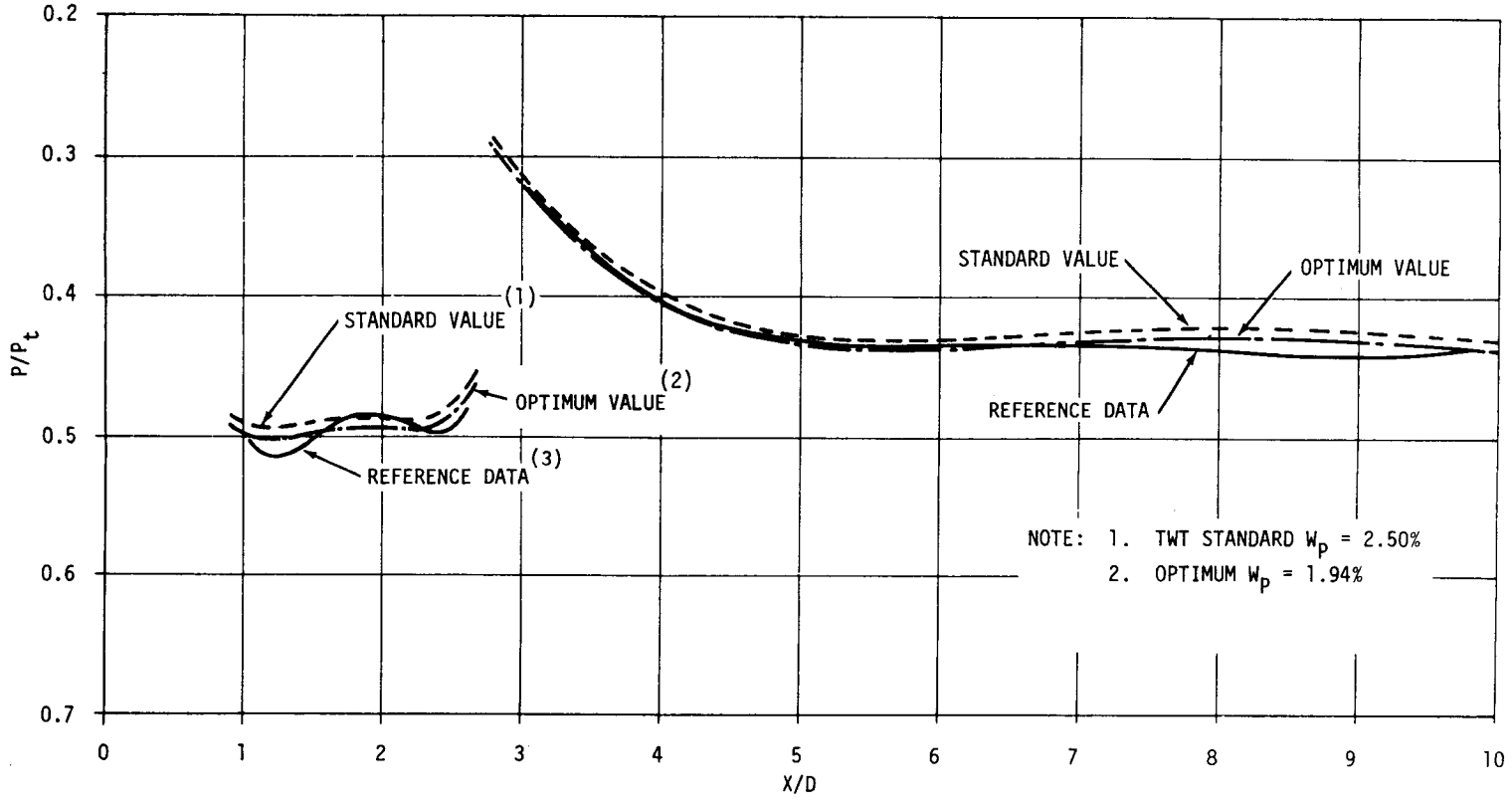

Figure 22. Comparison of the results of model equations (32) and (33) for present TWT standard optimum conditions and the computer-identified optimum values at M = 1.15.

a maximum performance index value, and the 1.6 percent porosity point is the computer-identified optimum value. Testing was limited to one Mach number because of tunnel time limitations, and it was therefore decided to test at Mach 1.0 since it represents a particularly difficult simulation condition and since two critical points were unusually near the same performance index value at this condition.

The results of this investigation are shown in Figure 23. The computer-determined optimum value of 1.6 percent wall porosity clearly falls closest to the interference-free results, although it is evident that a reflected shock wave impinges on the model at about model station 4.5. The minimum critical point of 0.5 percent porosity also gives a reasonable comparison with the reference data but is in all cases in poorer agreement, as predicted by the performance index values. The maximum point indicated at 1.1 percent porosity in all cases has the poorest agreement with the reference values, again as predicted by the performance index. It is, therefore, reasonable to conclude that the optimization procedure developed herein does, in fact, provide a useful tool to improve transonic wave interference.

E. Summary

It has been shown that the optimization technique developed for variable porosity walls can be expected to provide useful optimum values for given test conditions and that the utilization of this procedure should provide better simulation with less experimental testing than the previous trial-and-error methods. However, the technique is empirical in nature, and the results can be no better than the data on which they are based.

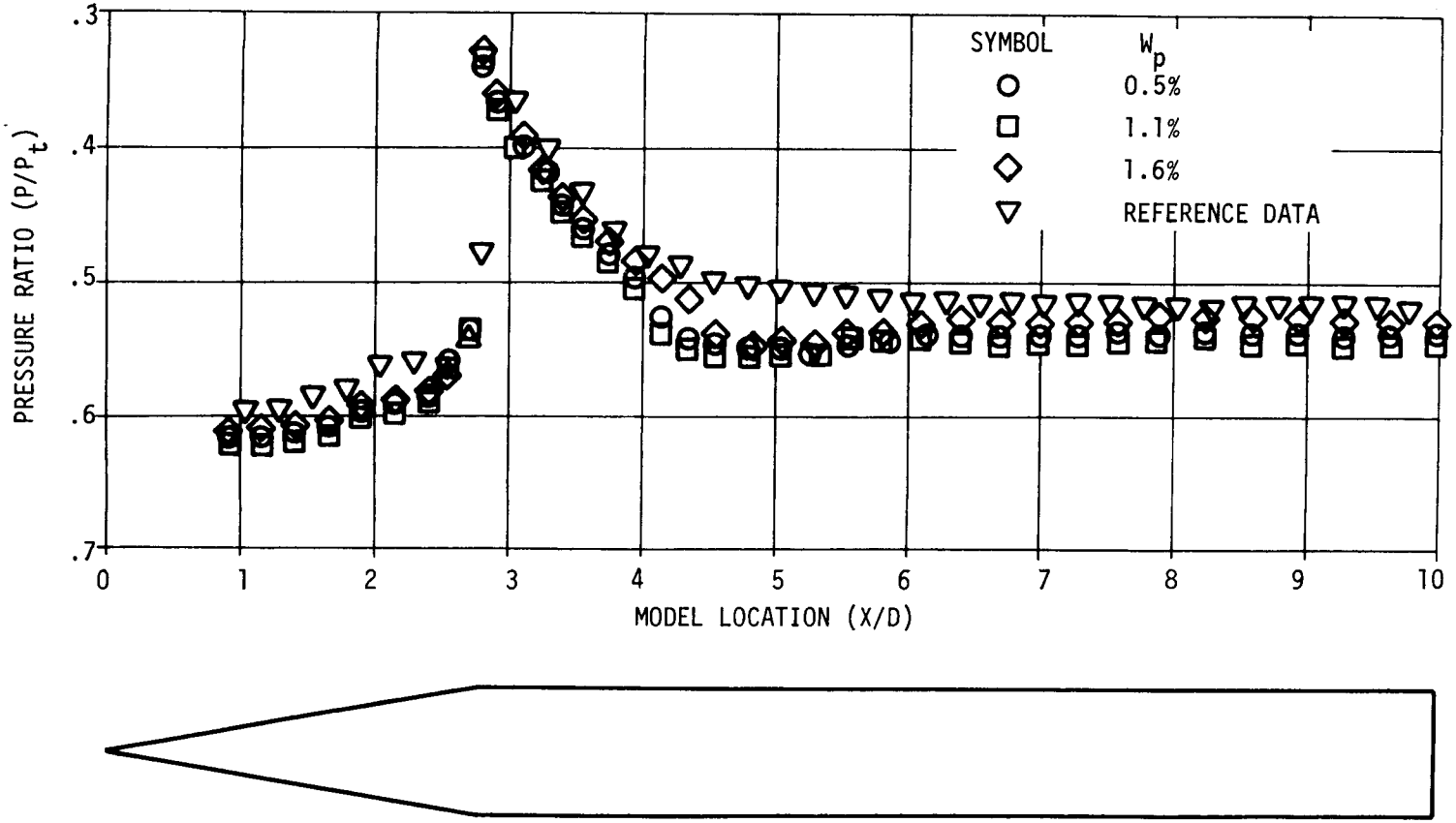

Figure 23. Experimental results at critical points identified by optimization technique for Mach number 1.0.

The present surface fits provide a good representation of the input data, and the indicated optimum wall porosity values follow the expected trends and show reasonable quantitative agreement with experimental results.

SECTION VIII.

CONCLUSIONS

A. General Remarks

During the course of this study, a technique has been developed which is capable of determining the optimum configuration for a variable-porosity perforated-wall transonic wind tunnel. The technique was based on a mathematical model arrived at by considering both the results of wave cancellation theory and past experimental investigations. Using experimental results from the MSFC 14-Inch Trisonic Wind Tunnel, the model was evaluated using a Pth degree multiple regression technique. A performance index was determined as a function of the significant wind tunnel parameters by comparing the mathematical model to interference-free results. The resulting relationship was then used to determine the combination of wind tunnel parameters which should yield minimum reflected wave interference using static optimization techniques.

The theoretical development of wall porosity requirements for thick wall inclined-hole test sections follows the trends and generally the magnitude of available experimental data. As such, the theory is useful not only in formulating the model relationship developed herein, but also may be of value in studies concerning the wave cancellation process for fixed-porosity test

sections. An analysis of the theory of wave cancellation for thin walls failed to correlate with experimental data for real walls and shows little usefulness in the low transonic speed range.

The multiple regression technique for Pth degree polynomials developed to evaluate the mathematical models is a powerful general purpose tool which could be used in any scientific endeaver where the process can be measured or for which experimental data exist. Using this procedure, many phenomena can be correlated or suspected laws or relationships investigated and optimizations determined other than those developed in the course of this study.

The optimization technique developed is empirical in nature, and the results can be no better than the data upon which they are based. The present evaluation of the technique is limited to determining the influence of wall porosity at a wall angle of -15 min due to the unavailability of data at other conditions for the TWT. Further, the evaluation must be considered qualitative in nature, until additional testing over a wider wall porosity range can be accomplished.

Confirmation wind tunnel tests based on results of the transonic optimization procedure at Mach number 1.0 agree closely with results predicted by the performance index. Both the predicted trends over the experimental model and the behavior at the indicated critical points showed close agreement with theory. It is, therefore, reasonable to conclude that the optimization procedure developed does, in fact, provide a useful means to minimize wave interference, and with future refinements using statistically designed experiments should prove to be a powerful tool in advancing variable porosity transonic wind tunnel

technology. Results obtained with this technique can be expected to provide better simulation with less experimental testing than previous trial-and-error methods.

E. Proposals for Future Investigation

In order to apply this technique to the MSFC TWT or other variable porosity wind tunnel, it will be necessary to conduct experimental tests over a wide range of wall porosities and wall angles such that the statistical influence of these parameters can be properly evaluated. It would be useful to extend the test Mach number range for these investigations such that the entire transonic speed range is covered. Analysis of these data should then provide accurate optimum porosity and wall angle values for each tunnel test condition. Again, confirmation tests should be used to evaluate the results.

Additional parameters worthy of future investigation include the effect of angle of attack, and model size and shape. Furthermore, the influence of Reynolds number could be evaluated. This would be of considerable importance in a facility such as the MSFC High Reynolds Number Wind Tunnel where Reynolds number can be varied over a wide range.

The present investigation tested the suitability of the various surface fits based on the combined effect of all the independent variables. A useful addition to the computer program would be the determination of partial F ratios and partial correlation coefficients by which the significance of individual independent variables could be tested.

As noted previously, the surface fits for the model relationships showed good agreement with the input data. However, near the shoulder between the cone and the cylinder some disagreement occurs. A possible refinement would be to break the model data down into smaller increments with the fits forced to be continuous at the common boundaries. Such a procedure might be difficult to implement, but potentially could improve the accuracy of the optimized results.

Two other modifications to this wave cancellation optimization technique potentially could improve the results in specific applications. First, the influence of Mach number can be decoupled from the regression equation by incorporating separate fits at each Mach number as shown in Reference 15. By this means, potential improvement of the surface fits should be possible, resulting in improved optimum values of the tunnel parameters. Also, the values of the performance index could be obtained directly by numerical integration of the differences between the measured pressure ratios for the wind tunnel data and the interference-free standard for a given test condition. These numerically integrated values of the performance index can then be fitted with respect to the important wave cancellation parameters and optimum values determined by the technique developed in Section V.

Since the interference-free reference data show some abnormalities over the cone portion of the model caused by model construction difficulties, additional tests of this type could be expected to further refine the indicated optimum results.

APPENDIX

MULTIPLE REGRESSION TECHNIQUE FOR Pth DEGREE POLYNOMIALS

A. Introduction

The investigation of physical processes and requirements for data analysis methods frequently require the use of models which describe the processes. The model can be formulated such that certain variables interact according to physical theories associated with the particular process, or it may contain identified independent variables and unknown parameters. The relationship of the parameters identified in the model can be determined using the statistical tool commonly referred to as regression analysis. In principle, it should be possible to establish complex curves or surfaces for quasi-linear multiple variable functions by regression techniques to summarize trends in data and to provide a means of predicting similar phenomena. Furthermore, such a technique might be used to establish unknown laws or relationships.

Most statistical textbooks treat the problem of linear multiple variable regression and of nonlinear regression of one independent variable. However, to study the complex problem of the optimization of transonic wind tunnel flows, a method capable of determining nonlinear regression of multiple independent variables is needed. By this means, an analytical representation of the experimental data is provided which can be used to optimize the wind tunnel flow.

B. Regression Analysis Technique Development

The general procedure in regression analysis is to take partial derivatives of a specific model-dependent minimizing function. The set of equations obtained by setting these partial derivatives equal to zero are frequently referred to as the normal equations. If the normal equations are not transcendental in any of the unknown parameters, they can be solved by the usual algebraic methods. It is this situation which is of concern here. First consider the following model:

$$Y_i^C = \left(b_{10} + b_{11} Z_{1i} + b_{12} Z_{1i}^2 + \ldots + b_{1P} Z_{1i}^P\right) + \left(b_{20} + b_{21} Z_{2i} + b_{22} Z_{2i}^2 + \ldots + b_{2P} Z_{2i}^P\right) + \ldots + \left(b_{N0} + B_{N1} Z_{Ni} + b_{N2} Z_{Ni}^2 + \ldots + b_{NP} Z_{Ni}^P\right) \quad (34)$$

where i = 1, 2 ..., nth set of data; P is the degree of polynomial; N is the number of independent variables, and the intercept $A_0 = b_{10} + b_{20} + \ldots + b_{N0}$.

For any given independent variable Z_N, the mean value is given by

$$\bar{Z}_N = \frac{\sum Z_{Ni}}{n} \quad . \quad (35)$$

Then, by adding and subtracting equal quantities in equation (34), namely, $b_{NP}Z_N^P$, equation (34) can be rewritten as follows where the quantities in parenthesis are identically equal to zero:

$$Y_i^C = \left[b_{10} + b_{11}Z_{1i} + \left(b_{11}\bar{Z}_1 - b_{11}\bar{Z}_1\right) + b_{12}Z_{1i}^2 + \left(b_{12}\bar{Z}_1^2 - b_{12}\bar{Z}_1^2\right)\right.$$

$$\left. + \ldots + b_{1P}Z_{1i}^P + \left(b_{1P}\bar{Z}_1^P - b_{1P}\bar{Z}_1^P\right)\right]$$

$$+ \left[b_{20} + b_{21}Z_{2i} + \left(b_{21}\bar{Z}_2 - b_{21}\bar{Z}_2\right) + b_{22}Z_{2i}^2 + \left(b_{22}\bar{Z}_2^2 - b_{22}\bar{Z}_2^2\right)\right.$$

$$\left. + \ldots + b_{2P}Z_{2i}^P + \left(b_{2P}\bar{Z}_2^P - b_{2P}\bar{Z}_2^P\right)\right]$$

$$+ \ldots + \left[b_{N0} + b_{N1}Z_{Ni} + \left(b_{N1}\bar{Z}_N - b_{N1}\bar{Z}_N\right) + b_{N2}Z_{Ni}^2 + \left(b_{N2}\bar{Z}_N^2\right.\right.$$

$$\left.\left. - b_{N2}\bar{Z}_N^2\right) + \ldots + b_{NP}Z_{Ni}^P + \left(b_{NP}\bar{Z}_N^P - b_{NP}\bar{Z}_N^P\right)\right] \qquad (36)$$

Regrouping equation (36) yields

$$Y_i^C = \left[b_{10} + b_{11}\bar{Z}_1 + b_{12}\bar{Z}_1^2 + \ldots + b_{1P}\bar{Z}_1^P\right] + \left[b_{11}\left(Z_{1i} - \bar{Z}_1\right)\right.$$

$$\left. + b_{12}\left(Z_{1i}^2 - \bar{Z}_1^2\right) + \ldots + b_{1P}\left(Z_{1i} - \bar{Z}_1^P\right)\right]$$

$$+ \left[b_{20} + b_{21}\bar{Z}_2 + b_{22}\bar{Z}_2^2 + \ldots + b_{2P}\bar{Z}_2^P\right] + \left[b_{21}\left(Z_{2i} - \bar{Z}_2\right)\right.$$

$$\left. + b_{22}\left(Z_{2i}^2 - \bar{Z}_2^2\right) + \ldots + b_{2P}\left(Z_{2i}^P - \bar{Z}_2^P\right)\right]$$

$$+ \ldots + \left[b_{N0} + B_{N1}\bar{Z}_N + b_{N2}\bar{Z}_N^2 + \ldots + b_{NP}Z_N^P\right] + \left[b_{N1}\left(Z_{Ni} - \bar{Z}_N\right)\right.$$

$$\left. + b_{N2}\left(Z_{Ni}^2 - \bar{Z}_N^2\right) + \ldots + b_{NP}\left(Z_{Ni}^P - \bar{Z}_N^P\right)\right] \quad . \qquad (37)$$

For convenience, the following quantities which are now grouped in equation (37) above are defined:

$$b_0 = \left(b_{10} + b_{11}\bar{Z}_1 + b_{12}\bar{Z}_1^{\,2} + \ldots + b_{1P}\bar{Z}_1^{\,P}\right) + \left(b_{20} + b_{21}\bar{Z}_2 + b_{22}\bar{Z}_2^{\,2} + \ldots + b_{2P}\bar{Z}_2^{\,P}\right) + \ldots + \left(b_{N0} + b_{N1}\bar{Z}_N + b_{N2}\bar{Z}_N^{\,2} + \ldots + b_{NP}\bar{Z}_N^{\,P}\right) , \tag{38}$$

$$\left.\begin{aligned}
z_{11_i} &= Z_{1i} - \bar{Z}_1 \\
z_{12_i} &= Z_{1i}^{\,2} - \bar{Z}_1^{\,2} \\
&\vdots \\
z_{1P_i} &= Z_{1i}^{\,P} - \bar{Z}_1^{\,P} \\
&\vdots \\
z_{21_i} &= Z_{2i} - \bar{Z}_2 \\
z_{22_i} &= Z_{2i}^{\,2} - \bar{Z}_2^{\,2} \\
&\vdots \\
z_{2P_i} &= Z_{2i}^{\,P} - \bar{Z}_2^{\,P} \\
&\vdots \\
z_{N1i} &= Z_{Ni} - \bar{Z}_N \\
z_{N2_i} &= Z_{Ni}^{\,2} - \bar{Z}_N^{\,2} \\
&\vdots \\
z_{NP_i} &= Z_{Ni}^{\,P} - \bar{Z}_N^{\,P}
\end{aligned}\right\} \tag{39}$$

so equation (37) can now be written in the following form:

$$Y_i^C = b_0 + \left(b_{11}z_{11_i} + b_{12}z_{12_i} + \ldots + b_{1P}z_{1P_i}\right)$$

$$+ \left(b_{21}z_{21_i} + b_{22}z_{22_i} + \ldots + b_{2P}z_{2P_i}\right)$$

$$+ \ldots + \left(b_{N1}z_{N1_i} + b_{N2}z_{N2_i} + \ldots + b_{NP}z_{NP_i}\right) \quad . \tag{40}$$

The classical form of the least squares minimizing is

$$M_f = \sum \left(Y_i - Y_i^C\right)^2 \quad . \tag{41}$$

This result follows from the least squares principle that the best representation of the data is that which makes the sum of the squares of the residuals a minimum. The condition which fulfills this requirement is that the partial derivatives of this function with respect to each of the unknowns be zero. Hence, the following normal equations for $i = 1, 2, \ldots, n$ are written:

$$\left.\begin{aligned} \frac{\partial M_f}{\partial b_0} &= 0 \\ \frac{\partial M_f}{\partial b_{11}} &= 0 \\ \frac{\partial M_f}{\partial b_{12}} &= 0 \\ \frac{\partial M_f}{\partial b_{1P}} &= 0 \end{aligned}\right\} \qquad \left.\begin{aligned} \frac{\partial M_f}{\partial b_{21}} &= 0 \\ \frac{\partial M_f}{\partial b_{22}} &= 0 \\ \frac{\partial M_f}{\partial b_{2P}} &= 0 \end{aligned}\right\} \qquad \left.\begin{aligned} \frac{\partial M_f}{\partial b_{N1}} &= 0 \\ \frac{\partial M_f}{\partial b_{N2}} &= 0 \\ \frac{\partial M_f}{\partial b_{NP}} &= 0 \end{aligned}\right\} \quad . \tag{42}$$

By substituting equation (40) into equation (41) and taking the partial derivative of this result with respect to b_0 and setting it equal to zero as per equation (42), the following result is obtained:

$$\frac{\partial M_f}{\partial b_0} = \sum \Big[- 2Y_i + 2b_0 + 2\left(b_{11}z_{11_i} + b_{12}z_{12_i} + \ldots + b_{1P}z_{1P_i}\right) + 2\left(b_{21}z_{21_i} + b_{22}z_{22_i} + \ldots + b_{2P}z_{2P_i}\right) + \ldots + 2\left(b_{N1}z_{N1_i} + b_{N2}z_{N2_i} + \ldots + b_{NP}z_{NP_i}\right)\Big] = 0 \; . \tag{43}$$

Dividing equation (43) by 2 and expanding yields

$$\frac{\partial M_f}{\partial b_0} = \sum Y_i + nb_0 + \left(b_{11}\sum z_{11_i} + b_{12}\sum z_{12_i} + \ldots + b_{1P}\sum z_{1P_i}\right) + \left(b_{21}\sum z_{21_i} + b_{22}\sum z_{22_i} + \ldots + b_{2P}\sum z_{2P_i}\right) + \ldots + \left(b_{N1}\sum z_{N1_i} + b_{N2}\sum z_{N2_i} + \ldots + b_{NP}\sum z_{NP_i}\right) = 0 \; . \tag{44}$$

Now, by multiplying and dividing equation (44) by n and recalling the relation for mean values, the following results

$$\frac{\partial M_f}{\partial b_0} = -n\bar{Y} + nb_0 + \left(nb_{11}\bar{z}_{11} + nb_{12}\bar{z}_{12} + \ldots + nb_{1P}\bar{z}_{1P}\right)$$

$$+ \left(nb_{21}\bar{z}_{21} + nb_{22}\bar{z}_{22} + \ldots + nb_{2P}\bar{z}_{2P}\right)$$

$$+ \ldots + \left(nb_{N1}\bar{z}_{N1} + nb_{N2}\bar{z}_{N2} + \ldots + nb_{NP}\bar{z}_{NP}\right) = 0 \ . \tag{45}$$

It is also noted that $\bar{z}_{11}$ can be written in the following forms:

$$z_{11} = \frac{\sum z_{11i}}{n} = \frac{\sum \left(z_{1i} - \bar{z}_1\right)}{n} \tag{46}$$

where the right-hand relationship stems from equation (A-6). Thus, it follows that

$$\bar{z}_{11} = \frac{\left(z_{11} - \bar{z}_1\right) + \left(z_{12} - \bar{z}_1\right) + \ldots + \left(z_{NP} - \bar{z}_1\right)}{n}$$

$$= \frac{\sum z_{1i}}{n} - \frac{n\bar{z}_1}{n} = 0 \ . \tag{47}$$

Similar results may be obtained for $\bar{z}_{21}$, $\bar{z}_{31}$, $\ldots$ $\bar{z}_{N1}$:

$$\bar{z}_{21} = \frac{\sum z_{2i}}{n} - \frac{n\bar{z}_2}{n} = 0 \ , \tag{48}$$

$$\bar{z}_{31} = \frac{\sum z_{3i}}{n} - \frac{n\bar{z}_3}{n} = 0 \ , \tag{49}$$

$$\bar{z}_{N1} = \frac{\sum z_{Ni}}{n} - \frac{n\bar{z}_N}{n} = 0 \ . \tag{50}$$

Now considering the terms in equation (45) containing Z^2 and Z^P, it is noted that

$$\bar{z}_{12} = \frac{\sum z_{12i}}{n} = \frac{\sum Z_{1i}^2 - \bar{Z}_1^2}{n}$$

$$= \frac{Z_{11}^2 - \bar{Z}_1^2 + Z_{12}^2 - \bar{Z}_1^2 + \ldots + Z_{1n}^2 - \bar{Z}_1^2}{n}$$

$$= \frac{\sum Z_{1i}^2}{n} - \frac{n\bar{Z}_1^2}{n} = 0 \quad . \tag{51}$$

Similar results hold for $\bar{z}_{22}$, $\bar{z}_{32}$, ... $\bar{Z}_{N2}$ and for $\bar{z}_{1P}$, $\bar{z}_{2P}$, ... $\bar{z}_{NP}$:

$$\bar{z}_{22} = \frac{\sum Z_{2i}^2}{n} - \frac{n\bar{Z}_2^2}{n} = 0 \quad , \tag{52}$$

$$\bar{z}_{32} = \frac{\sum Z_{3i}^2}{n} - \frac{n\bar{Z}_3^2}{n} = 0 \quad , \tag{53}$$

$$\bar{z}_{N2} = \frac{\sum Z_{Ni}^2}{n} - \frac{n\bar{Z}_N^2}{n} = 0 \quad , \tag{54}$$

$$\bar{z}_{1P} = \frac{\sum Z_{1i}^P}{n} - \frac{n\bar{Z}_1^P}{n} = 0 \quad , \tag{55}$$

$$\bar{z}_{2P} = \frac{\sum Z_{2i}^P}{n} - \frac{n\bar{Z}_2^P}{n} = 0 \quad , \tag{56}$$

$$\bar{z}_{NP} = \frac{\sum Z_{Ni}^{P}}{n} - \frac{n \bar{Z}_{N}^{P}}{n} = 0 \qquad (57)$$

Then, realizing that all the z terms in equation (45) are equal to zero, equation (A-12) can be written as

$$\frac{\partial M_f}{\partial b_0} = - n \bar{Y} + n b_0 = 0, \qquad (58)$$

Hence, b_0 can be determined from equation (58) as follows:

$$b_0 = \bar{Y} = \frac{\sum Y_i}{n} \quad , \qquad (59)$$

which when substituted into equation (40) yields

$$Y_1^C = \bar{Y} + \left(b_{11} z_{11i} + b_{12} z_{12i} + \ldots + b_{1P} z_{1Pi}\right)$$

$$+ \left(b_{12} z_{21i} + b_{22} z_{22i} + \ldots + b_{2P} z_{2Pi}\right)$$

$$+ \ldots + \left(b_{N1} z_{N1i} + b_{N2} z_{N2i} + \ldots + b_{NP} z_{NPi}\right) \quad . \qquad (60)$$

The following quantity is now defined for the difference in the observed value of Y_i and the mean value of the observed values:

$$y_i = Y_i - \bar{Y} \quad . \qquad (61)$$

To treat the remaining normal equations, equation (61) is substituted into equation (60). Then substituting this result in equation (61) for the minimizing function and forming the partial derivatives called for in equation (42), which are identically equal to zero yields

$$\frac{\partial M_f}{\partial b_{11}} = \sum \Big[z_{11_i} y_i - z_{11_i} \left(b_{11} z_{11_i} + b_{12} z_{12_i} + \cdots b_{1P} z_{1P_i} \right) - z_{11_i} \left(b_{21} z_{21_i} + b_{22} z_{22_i} + \cdots + b_{2P} z_{2P_i} \right) - \cdots - z_{11_i} \left(b_{N1} z_{N1_i} + b_{N2} z_{N2_i} + \cdots + b_{NP} z_{NPi} \right) \Big] = 0 , \tag{62}$$

$$\frac{\partial M_f}{\partial b_{12}} = \sum \Big[z_{12_i} y_i - z_{12_i} \left(b_{11} z_{11_i} + b_{12} z_{12_i} + \cdots + b_{1P} z_{1P_i} \right) - z_{12_i} \left(b_{21} z_{21_i} + b_{22} z_{22_i} + \cdots + b_{2P} z_{2P_i} \right) - \cdots - z_{12_i} \left(b_{N1} z_{N1_i} + b_{N2} z_{N2_i} + \cdots + b_{NP} z_{NP_i} \right) \Big] = 0 , \tag{63}$$

$$\frac{\partial M_f}{\partial b_{1P}} = \sum \Big[z_{1P_i} y_i - z_{1P_i} \left(b_{11} z_{11_i} + b_{12} z_{12_i} + \cdots + b_{1P} z_{1P_i} \right) - z_{1P_i} \left(b_{21} z_{21_i} + b_{22} z_{22_i} + \cdots + b_{2P} z_{2P_i} \right) - \cdots - z_{1P_i} \left(b_{N1} z_{N1_i} + b_{N2} z_{N2_i} + \cdots + b_{NP} z_{NP_i} \right) \Big] = 0 , \tag{64}$$

$$\frac{\partial M_f}{\partial b_{21}} = \sum \Big[z_{21_i} y_i - z_{21_i} \left(b_{11} z_{11_i} + b_{12} z_{12_i} + \ldots + b_{1P} z_{1P_i} \right)$$

$$- z_{21_i} \left(b_{21} z_{21_i} + b_{22} z_{22_i} + \ldots + b_{2P} z_{2P_i} \right)$$

$$- \ldots - z_{21_i} \left(b_{N1} z_{N1_i} + b_{N2} z_{N2_i} + \ldots + b_{NP} z_{NP_i} \right) \Big] = 0, \tag{65}$$

$$\frac{\partial M_f}{\partial b_{22}} = \sum \Big[z_{22_i} y_i - z_{22_i} \left(b_{11} z_{11_i} + b_{12} z_{12_i} + \ldots + b_{1P} z_{1P_i} \right)$$

$$- z_{22_i} \left(b_{21} z_{21_i} + b_{22} z_{22_i} + \ldots + b_{2P} z_{2P_i} \right)$$

$$- \ldots - z_{22_i} \left(b_{N1} z_{N1_i} + b_{N2} z_{N2_i} + \ldots + b_{NP} z_{NP_i} \right) \Big] = 0 \ , \tag{66}$$

$$\frac{\partial M_f}{\partial b_{2P}} = \sum \Big[z_{2P_i} y_i - z_{2P_i} \left(b_{11} z_{11_i} + b_{12} z_{12_i} + \ldots + b_{1P} z_{1P_i} \right)$$

$$- z_{2P_i} \left(b_{21} z_{21_i} + b_{22} z_{22_i} + \ldots + b_{2P} z_{2P_i} \right)$$

$$- \ldots - z_{2P_i} \left(b_{N1} z_{N1_i} + b_{N2} z_{N2_i} + \ldots + b_{NP} z_{NP_i} \right) \Big] = 0 \ , \tag{67}$$

$$\frac{\partial M_f}{\partial b_{N1}} = \sum \Big[z_{N1_i} y_i - z_{N1_i} \left(b_{11} z_{11_i} + b_{12} z_{12_i} + \ldots + b_{1P} z_{1P_i} \right)$$

$$- z_{N1_i} \left(b_{21} z_{21_i} + b_{22} z_{12_i} + \ldots + b_{2P} z_{2P_i} \right)$$

$$- \ldots - z_{N1_i} \left(b_{N1} z_{N1_i} + b_{N2} z_{N2_i} + \ldots + b_{NP} z_{NP_i} \right) \Big] = 0 \quad , \tag{68}$$

$$\frac{\partial M_f}{\partial b_{N2}} = \sum \Big[z_{N2_i} y_i - z_{N2_i} \left(b_{11} z_{11_i} + b_{12} z_{12_i} + \ldots + b_{1P} z_{1P_i} \right)$$

$$- z_{N2_i} \left(b_{21} z_{21_i} + b_{22} z_{22_i} + \ldots + b_{2P} z_{2P_i} \right)$$

$$- \ldots - z_{N2_i} \left(b_{N1} z_{N1_i} + b_{N2} z_{N2_i} + \ldots + b_{NP} z_{NP_i} \right) \Big] = 0 \quad , \tag{69}$$

$$\frac{\partial M_f}{\partial b_{NP}} = \sum \Big[z_{NP_i} y_i - z_{NP_i} \left(b_{11} z_{11_i} + b_{12} z_{12_i} + \ldots + b_{1P} z_{1P_i} \right)$$

$$- z_{NP_i} \left(b_{21} z_{21_i} + b_{22} z_{22_i} + \ldots + b_{2P} z_{2P_i} \right)$$

$$- \ldots - z_{NP_i} \left(b_{N1} z_{N1_i} + b_{N2} z_{N2_i} + \ldots + b_{NP} z_{NP_i} \right) \Big] = 0 \quad , \tag{70}$$

Regrouping equations (62) through (70) in a manner which suggests a matrix solution yields

$$\sum \Big[\Big(b_{11} z_{11}^{\,2} + b_{12} z_{11_i} z_{12_i} + \cdots + b_{1P} z_{11_i} z_{1P_i} \Big)$$

$$+ \Big(b_{21} z_{11_i} z_{21_i} + b_{22} z_{11_i} z_{22_i} + \cdots + b_{2P} z_{11_i} z_{2P_i} \Big)$$

$$+ \cdots + \Big(b_{N1} z_{11_i} z_{N1_i} + b_{N2} z_{11_i} z_{N2_i} + \cdots + b_{NP} z_{11_i} z_{NP_i} \Big) \Big] = \sum z_{11_i} y_i \tag{71}$$

$$\sum \Big[\Big(b_{11} z_{12_i} z_{11_i} + b_{12} z_{12_i}^{\,2} + \cdots + b_{1P} z_{12_i} z_{1P_i} \Big)$$

$$+ \Big(b_{21} z_{12_i} z_{21_i} + b_{22} z_{12_i} z_{22_i} + \cdots + b_{2P} z_{12_i} z_{2P_i} \Big)$$

$$+ \cdots + \Big(b_{N1} z_{12_i} z_{N1_i} + b_{N2} z_{12_i} z_{N2_i} + \cdots + b_{NP} z_{12_i} z_{NP_i} \Big) \Big] = \sum z_{12_i} y_i \tag{72}$$

$$\sum \Big[\Big(b_{11} z_{1P_i} z_{11_i} + b_{12} z_{1P_i} z_{12_i} + \cdots + b_{1P} z_{1P_i}^{\,2} \Big)$$

$$+ \Big(b_{21} z_{1P_i} z_{21_i} + b_{22} z_{1P_i} z_{22_i} + \cdots + b_{2P} z_{1P_i} z_{2P_i} \Big)$$

$$+ \cdots + \Big(b_{N1} z_{1P_i} z_{N1_i} + b_{N2} z_{1P_i} z_{N2_i} + \cdots + b_{NP} z_{1P_i} z_{NP_i} \Big) \Big] = \sum z_{1P_i} y_i \tag{73}$$

$$\sum \left(b_{11} z_{11_i} z_{21_i} + b_{12} z_{21_i} z_{12_i} + \ldots + b_{1P} z_{21_i} z_{1P_i}\right)$$

$$+\left(b_{21} z_{21_i}^{2} + b_{22} z_{21_i} z_{22_i} + \ldots + b_{2P} z_{21_i} z_{2P_i}\right)$$

$$+ \ldots + \left(b_{N1} z_{21_i} z_{N1_i} + b_{N_2} z_{21_i} z_{N2_i} + \ldots + b_{NP} z_{21_i} z_{NP_i}\right) = \sum z_{21_i} y_i \tag{74}$$

$$\sum \left(b_{11} z_{11_i} z_{22_i} + b_{12} z_{22_i} z_{12_i} + \ldots + b_{1P} z_{22_i} z_{1P_i}\right)$$

$$+\left(b_{21} z_{22_i} z_{21_i} + b_{22} z_{22_i}^{2} + \ldots + b_{2P} z_{22_i} z_{2P_i}\right)$$

$$+ \ldots + \left(b_{N1} z_{22_i} z_{N1_i} + b_{N2} z_{22_i} z_{N2_i} + \ldots + b_{NP} z_{22_i} z_{NP_i}\right) = \sum z_{22_i} y_i \tag{75}$$

$$\sum \left(b_{11} z_{11_i} z_{2P_i} + b_{12} z_{2P_i} z_{12_i} + \ldots + b_{1P} z_{2P_i} z_{1P_i}\right)$$

$$+\left(b_{21} z_{2P_i} z_{21_i} + b_{22} z_{2P_i} z_{22_i} + \ldots + b_{2P} z_{2P_i}^{2}\right)$$

$$+ \ldots + \left(b_{N1} z_{2P_i} z_{N1_i} + b_{N2} z_{2P_i} z_{N2_i} + \ldots + b_{NP} z_{2P_i} z_{NP_i}\right) = \sum z_{2P_i} y_i \tag{76}$$

$$\sum \Big[\Big(b_{11} z_{N1_i} z_{11_i} + b_{12} z_{N1_i} z_{12_i} + \ldots + b_{1P} z_{N1_i} z_{1P_i} \Big)$$

$$+ \Big(b_{21} z_{N1_i} z_{21_i} + b_{22} z_{N1_i} z_{22_i} + \ldots + b_{2P} z_{N1_i} z_{2P_i} \Big)$$

$$+ \ldots + \Big(b_{N1} z_{N1_i}^2 + b_{N2} z_{N1_i} z_{N2_i} + \ldots + b_{NP} z_{N1_i} z_{NP_i} \Big) \Big] = \sum z_{N1_i} y_i \tag{77}$$

$$\sum \Big[\Big(b_{11} z_{N2_i} z_{11_i} + b_{12} z_{N2_i} z_{12_i} + \ldots + b_{1P} z_{N2_i} z_{1P_i} \Big)$$

$$+ \Big(b_{21} z_{N2_i} z_{21_i} + b_{22} z_{N2_i} z_{22_i} + \ldots + b_{2P} z_{N2_i} z_{2P_i} \Big)$$

$$+ \ldots + \Big(b_{N1} z_{N1_i} z_{N2_i} + b_{N2} z_{N2_i}^2 + \ldots + b_{NP} z_{N2_i} z_{NP_i} \Big) \Big] = \sum z_{N2_i} y_i \tag{78}$$

$$\sum \Big[\Big(b_{11} z_{NP_i} z_{11_i} + b_{12} z_{NP_i} z_{12_i} + \ldots + b_{1P} z_{NP_i} z_{1P_i} \Big)$$

$$+ \Big(b_{21} z_{NP_i} z_{21_i} + b_{22} z_{NP_i} z_{22_i} + \ldots + b_{2P} z_{NP_i} z_{2P_i} \Big)$$

$$+ \ldots + \Big(b_{N1} z_{N1_i} z_{NP_i} + b_{N2} z_{N2_i} z_{NP_i} + \ldots + b_{NP} z_{NP_i}^2 \Big) \Big] = \sum z_{NP_i} y_i \tag{79}$$

Inspection of equations (71) through (79) indicates the desirability of defining the following matrix quantities:

$$S_{11} = \begin{bmatrix} \sum z_{11_i}^2 & \sum z_{11_i} z_{12_i} & \cdots & \sum z_{11_i} z_{1P_i} \\ \sum z_{12_i} z_{11_i} & \sum z_{12_i}^2 & \cdots & \sum z_{12_i} z_{1P_i} \\ \vdots & \vdots & & \vdots \\ \sum z_{1P_i} z_{11_i} & \sum z_{1P_i} z_{12_i} & \cdots & \sum z_{1P_i}^2 \end{bmatrix} \tag{80}$$

$$S_{12} = \begin{bmatrix} \sum z_{11_i} z_{21_i} & \sum z_{11_i} z_{22_i} & \cdots & \sum z_{11_i} z_{2P_i} \\ \sum z_{12_i} z_{21_i} & \sum z_{12_i} z_{22_i} & \cdots & \sum z_{12_i} z_{2P_i} \\ \vdots & \vdots & & \vdots \\ \sum z_{1P_i} z_{21_i} & \sum z_{1P_i} z_{22_i} & \cdots & \sum z_{1P_i} z_{2P_i} \end{bmatrix} \tag{81}$$

$$S_{IN} = \begin{bmatrix} \sum z_{11_i} z_{N1_i} & \sum z_{11_i} z_{N2_i} & \cdots & \sum z_{11_i} z_{NP_i} \\ \sum z_{12_i} z_{N1_i} & \sum z_{12_i} z_{N2_i} & \cdots & \sum z_{12_i} z_{NP_i} \\ \vdots & \vdots & & \vdots \\ \sum z_{1P_i} z_{N1_i} & \sum z_{1P_i} z_{N2_i} & \cdots & \sum z_{1P_i} z_{NP_i} \end{bmatrix} \tag{82}$$

$$S_{21} = \begin{bmatrix} \sum z_{21_i} z_{11_i} & \sum z_{21_i} z_{12_i} & \cdots & \sum z_{21_i} z_{1P_i} \\ \sum z_{22_i} z_{11_i} & \sum z_{22_i} z_{12_i} & \cdots & \sum z_{22_i} z_{1P_i} \\ \vdots & \vdots & & \vdots \\ \sum z_{2P_i} z_{11_i} & \sum z_{2P_i} z_{12_i} & \cdots & \sum z_{2P_i} z_{1P_i} \end{bmatrix} \quad (83)$$

$$S_{22} = \begin{bmatrix} \sum z_{21_i}^2 & \sum z_{21_i} z_{22_i} & \cdots & \sum z_{21_i} z_{2P_i} \\ \sum z_{22_i} z_{21_i} & \sum z_{22_i} z_{22_i} & \cdots & \sum z_{22_i} z_{2P_i} \\ \vdots & \vdots & & \vdots \\ \sum z_{2P_i} z_{21_i} & \sum z_{2P_i} z_{22_i} & \cdots & \sum z_{2P_i} z_{2P_i} \end{bmatrix} \quad (84)$$

$$S_{2N} = \begin{bmatrix} \sum z_{21_i} z_{N1_i} & \sum z_{21_i} z_{N2_i} & \cdots & \sum z_{21_i} z_{NP_i} \\ \sum z_{22_i} z_{N1_i} & \sum z_{22_i} z_{N2_i} & \cdots & \sum z_{22_i} z_{NP_i} \\ \vdots & \vdots & & \vdots \\ \sum z_{2P_i} z_{N1_i} & \sum z_{2P_i} z_{N2_i} & \cdots & \sum z_{2P_i} z_{NP_i} \end{bmatrix} \quad (85)$$

$$S_{N1} = \begin{bmatrix} \sum z_{N1_i} z_{11_i} & \sum z_{N1_i} z_{12_i} & \cdots & \sum z_{N1_i} z_{1P_i} \\ \sum z_{N2_i} z_{11_i} & \sum z_{N2_i} z_{12_i} & \cdots & \sum z_{N2_i} z_{1P_i} \\ \vdots & \vdots & & \vdots \\ \sum z_{NP_i} z_{11_i} & \sum z_{NP_i} z_{12_i} & \cdots & \sum z_{NP_i} z_{1P_i} \end{bmatrix} \quad (86)$$

$$S_{N2} = \begin{bmatrix} \sum z_{N1_i} z_{21_i} & \sum z_{N1_i} z_{22_i} & \cdots & \sum z_{N1_i} z_{2P_i} \\ \sum z_{N2_i} z_{21_i} & \sum z_{N2_i} z_{22_i} & \cdots & \sum z_{N2_i} z_{2P_i} \\ \vdots & \vdots & & \vdots \\ \sum z_{NP_i} z_{21_i} & \sum z_{NP_i} z_{22_i} & \cdots & \sum z_{NP_i} z_{2P_i} \end{bmatrix} \quad (87)$$

$$S_{NN} = \begin{bmatrix} \sum z_{N1_i}^2 & \sum z_{N1_i} z_{N2_i} & \cdots & \sum z_{N1_i} z_{NP_i} \\ \sum z_{N2_i} z_{N1_i} & \sum z_{N2_i}^2 & \cdots & \sum z_{N2_i} z_{NP_i} \\ \vdots & \vdots & & \vdots \\ \sum z_{NP_i} z_{N1_i} & \sum z_{NP_i} z_{N2_i} & \cdots & \sum z_{NP_i}^2 \end{bmatrix} \quad (88)$$

$$B_1 = \begin{bmatrix} b_{11} \\ b_{12} \\ \vdots \\ b_{1P} \end{bmatrix} \quad (89)$$

$$B_2 = \begin{bmatrix} b_{21} \\ b_{22} \\ \vdots \\ b_{2P} \end{bmatrix} \tag{90}$$

$$B_N = \begin{bmatrix} b_{N1} \\ b_{N2} \\ \vdots \\ b_{NP} \end{bmatrix} \tag{91}$$

$$S_{1y} = \begin{bmatrix} \sum z_{11_i} y_i \\ \sum z_{12_i} y_i \\ \vdots \\ \sum z_{1P_i} y_i \end{bmatrix} \tag{92}$$

$$S_{2y} = \begin{bmatrix} \sum z_{21_i} y_i \\ \sum z_{22_i} y_i \\ \vdots \\ \sum z_{2P_i} y_i \end{bmatrix} \tag{93}$$

$$S_{Ny} = \begin{bmatrix} \sum z_{N1_i} y_i \\ \sum z_{N2_i} y_i \\ \vdots \\ \sum z_{NP_i} y_i \end{bmatrix} . \qquad (94)$$

Hence, using equations (80) through (94), equations (71) through (79) can be written in matrix form as follows:

$$\left.\begin{aligned} S_{11} B_1 + S_{12} B_2 + \ldots + S_{1N} B_N &= S_{1y} \\ S_{21} B_1 + S_{22} B_2 + \ldots + S_{2N} B_N &= S_{2y} \\ &\vdots \\ S_{N1} B_1 + S_{N2} B_2 + \ldots + S_{NN} B_N &= S_{Ny} \end{aligned}\right\} \qquad (95)$$

or

$$\begin{bmatrix} S_{11} & S_{12} & \cdots & S_{1N} \\ S_{21} & S_{22} & \cdots & S_{2N} \\ \vdots & \vdots & & \vdots \\ S_{N1} & S_{N2} & \cdots & S_{NN} \end{bmatrix} \begin{bmatrix} B_1 \\ B_2 \\ \vdots \\ B_N \end{bmatrix} = \begin{bmatrix} S_{1y} \\ S_{2y} \\ \vdots \\ S_{Ny} \end{bmatrix} . \qquad (96)$$

NP × NP NP × 1 NP × 1

Then the matrix solution for the unknown constants in the transformed model equation (60) is

$$\begin{bmatrix} B_1 \\ B_2 \\ \vdots \\ B_N \end{bmatrix} = \begin{bmatrix} S_{11} & S_{12} & \cdots & S_{1N} \\ S_{21} & S_{22} & \cdots & S_{2N} \\ \vdots & \vdots & & \vdots \\ S_{N1} & S_{N2} & \cdots & S_{NN} \end{bmatrix}^{-1} \begin{bmatrix} S_{1y} \\ S_{2y} \\ \vdots \\ S_{Ny} \end{bmatrix} . \qquad (97)$$

Having determined the matrix solution indicated by equation (97), the intercept A_o of the fitted expression may be determined by substitution of equation (59) into equation (38) as

$$A_o = \bar{X} - b_{11}\bar{Z}_1 + b_{12}\bar{Z}_1^2 + \cdots + b_{1P}\bar{Z}_1^P$$

$$- b_{21}\bar{Z}_2 + b_{22}\bar{Z}_2^2 + \cdots + b_{2P}\bar{Z}_2^P$$

$$- \cdots - b_{N1}\bar{Z}_N + b_{N2}\bar{Z}_N^2 + \cdots + b_{NP}\bar{Z}_N^P \qquad (98)$$

As noted by Graybill [37], there is an infinite number of solutions to such a relationship. However, only one such solution must be found to have a useful result. Also note that this solution to the quasi-linear multiple regression problem is a function of parameters such as the sum of the squares, cross-products and mean values similar to previously developed solutions for linear

regression. In this case, one finds a more complex result with nested matrices, which becomes practical only in combination with digital computer techniques.

A computer program has been developed to evaluate the unknown constants in the model equation with the solution specified by equation (97) [24]. It is required in application of this technique that the S matrix be nonsingular and that the input data are reasonably well-behaved. It is also required that $n \geqq NP$. That is, the number of data points n must be equal to or greater than the number of unknown parameters in the model equation.

C. Significance of the Estimated Regression Equation

To determine if the solution matrix is a useful representation of the input data, it is also desirable to determine the standard deviation of the observed data with respect to the fitted equation and the average error. Furthermore, the multiple correlation coefficient and the F statistic are of value in assessing the goodness of fit and, hence, the usefulness of the fitted model equation in estimating the observed phenomena.

The significance of the estimated regression equation can be considered from the viewpoint of an analysis of variance as summarized below, where the total sum of squares is resolved into a component measuring the residual fitting error, and a component which measures the regression variation being tested.

Analysis of Variance

Degrees of Freedom	Type Variation	Sum of Squares (SS)	Mean Square (MS)	F Value
n - 1	Total	$S_{YY} = \sum\left(Y_i - \bar{Y}\right)^2$		
NP - 1	Residual	$S(RES) = \sum\left(Y_i - Y_i^C\right)^2$	$M(RES) = \frac{S(RES)}{NP - 1}$	
n - NP	Regression	$S(REG) = \sum\left(Y_i^C - \bar{Y}\right)^2$	$M(REG) = \frac{S(REG)}{n - NP}$	$\frac{M(REG)}{M(RES)}$

where MS = SS/degrees of freedom

$S_{YY} = S(RES) + S(REG)$

$\bar{Y}$ = average of observed values

As noted by Smille [38], the results of such an analysis of variance can be used to test the combined effect of all of the independent variables on the dependent variable. That is, the hypothesis that all of the population regression coefficients in the model regression equation are zero can be tested since the ratio of the regression mean square to the residual mean square are distributed in an F distribution with n - NP numerator degrees of freedom and NP - 1 denominator degrees of freedom as shown below:

$$F = \frac{S(REG) \,/\, n - NP}{S(RES) \,/\, NP - 1} \tag{99}$$

where it is assumed that the observations are selected at random from a

normally distributed population with zero mean and constant variance, that Z_1, Z_2, ... Z_N are independent variables following χ^2 distributions, and that only random errors are associated with the observations.

The F ratio calculated from equation (99) can be used to test the statistical significance of the regression equation under consideration by comparing it with the appropriate F_{table} value at the desired probability level with n - NP numerator degrees of freedom and NP-1 denominator degrees of freedom. That is, the following test of the null hypothesis may be performed:

$$H_0 : b_{10} = \ldots = b_{NP} = 0$$

accept when $F_c < F_{table}$ and conclude the regression equation is not statistically significant

reject when $F_c > F_{table}$ and conclude the regression equation is statistically significant.

Since the regression equations under consideration have generally yielded large F values somewhat beyond the range of most F tables, it is of interest to determine the significance level and probability value when F calculated is substituted into the analytical F distribution function used to calculate the F table (i.e., $F_c = F_{TABLE}$). As noted by Abromowitz and Stegun [39], the probability value can be obtained by evaluating the integral of the F distribution density function as follows for $F \geq 0$:

$$P\left(F_{V_1, V_2}\right) = \frac{V_1^{\frac{1}{2}V_1} + V_2^{\frac{1}{2}V_2}}{B\left(\frac{1}{2}V_1, \frac{1}{2}V_2\right)} \int_0^F t^{\frac{1}{2}\left(V_1 - 2\right)} \left(V_2 + V_1 t\right)^{-\frac{1}{2}\left(V_1 + V_2\right)} dt, \tag{100}$$

where

$$B(\tfrac{1}{2}V_1, \tfrac{1}{2}V_2) = \frac{\Gamma\left(\frac{V_1 + V_2}{2}\right)}{\Gamma\left(\frac{V_1}{2}\right)\Gamma\left(\frac{V_2}{2}\right)} ,$$

Γ is the gamma integral function, V_1 is the numerator degrees of freedom, and V_2 is the denominator degrees of freedom. It follows that the significance level is

$$Q = 1 - P(F) \quad . \tag{101}$$

Another useful parameter in testing the significance of the regression equation is the standard deviation which is estimated by

$$s = \left[\frac{\sum\left(Y_i - Y_i^C\right)^2}{n - NP - 1}\right]^{\frac{1}{2}} = \left[\frac{S(RES)}{n - NP - 1}\right]^{\frac{1}{2}} \quad . \tag{102}$$

Previously, the analysis of variance technique was used to test the combined effect of the independent variables on the dependent variable using the F statistic. A closely related statistic is the multiple correlation coefficient R. Smille [38] defines this statistic as the simple correlation coefficient between

the observed values of the dependent variable and those values estimated by the multiple regression function as given by

$$R = \left[\frac{S(REG)}{S_{YY}} \right]^{1/2} \quad . \tag{103}$$

If the observed and estimated values are completely unrelated, R will be zero and, if they are identical, the multiple correlation coefficient will be unity. Values in between these limits represent different degrees of correlation or the closeness within which the regression equation describes the original data.

Also of interest is the average of the absolute values of the percent error of the dependent variable considering each fitted observation:

$$|\epsilon|_{AVG} = \frac{1}{n} \sum \left| \frac{Y_i - Y_i^C}{Y_i} \right| \times 100 \quad . \tag{104}$$

During this calculation, the maximum absolute error condition can be determined for evaluation purposes.

D. Summary

A powerful quasi-linear multiple regression technique has been developed with which the nonlinear behavior of identified independent variables can be related to a given dependent variable. The polynomial expression can be of Pth degree and can incorporate N independent variables. The resulting surface fit can be used to summarize trends for a given phenomenon, and the analytic

results can be used to seek information concerning optimum values on a mathematical basis.

To implement this technique, a computer program has been developed to evaluate the various constants in the model regression equation, the standard deviation, the multiple correlation coefficient, the F statistic, the maximum absolute percent error, and the average of the absolute values of the percent error [24]. Furthermore, included in the program is the solution for the identity matrix to identify any problems in the original matrix inversion process and a means of obtaining machine plots comparing the computer results to each set of input data.

REFERENCES

1. Wright, R. H. and Ward, V. G.: NASA Transonic Wind Tunnel Sections. RM L8506, NACA, 1948.

2. Capone, F. J. and Coates, E. M.: Determination of Boundary-Reflected Disturbance Lengths in the Langley 16-Foot Transonic Tunnel. TND-4153, NASA, 1950.

3. DeHart, J.: Calibration of the Transonic Test Section of the MSFC's 14 x 14-Inch Trisonic Wind Tunnel. Report No. M-1046, Northrop-Huntsville, February 1972.

4. Theodorsen, T.: The Theory of Wind Tunnel Wall Interferences. Report 410, NACA, 1932.

5. Goodman, T. R.: The Porous Wall Wind Tunnel, Part II, Interference Effect on a Cylindrical Body in a Two Dimensional Tunnel at Subsonic Speed, Report No. AD-594-A-3, Cornell, Aeronautical Laboratory, 1950.

6. Pindzola, M. and Lo, C. F.: Boundary Interference at Subsonic Speeds in Wind Tunnels with Ventilated Walls. AEDC-TR-69-47, 1969.

7. Goethert, B. H.: Transonic Wind Tunnel Testing. Pergamon Press, 1961.

8. Goin, K. L.: The History, Evolution and Use of Wind Tunnels. AIAA Student Journal, February, 1971.

9. Kondo, K.: Boundary Interference of Partially Closed Wind Tunnel. Report No. 137, Aeronautical Research Institute Tokyo XI.

10. Wieselburger, C.: On the Influence of the Wind Tunnel Boundary on the Drag, Particularly in the Region of the Compressible Flow. Technical Report 1172, DVL, Berlin, 1939.

11. Goodman, T. R.: The Porous Wall Wind Tunnel, Part III, Reflection and Absorption of Shock Waves at Supersonic Speeds. Report No. AD-706-A-1, Cornell Aeronautical Laboratory, 1950.

12. Estabrooks, Bruce, B.: Wall Interference Effects of Axisymmetric Bodies in Transonic Wind Tunnels with Perforated Wall Test Sections. TR-59-12, AEDC, 1959.

REFERENCES (Continued)

13. Chew, W. L.: Experimental and Theoretical Studies on Three Dimensonal Wave Reflection in Transonic Flow — Part III Characteristics of Perforated Test Section Walls with Different Resistance to Cross Flow. TN-55-44, AEDC, March 1956.

14. Felix, A. R.: Variable Porosity Walls for Transonic Wind Tunnels. TMX-53295, NASA, April 1965, pp. 54-58.

15. Davis, J. W. and Graham, R. F.: Flow Interference in a Variable Porosity Trisonic Wind Tunnel. AIAA 7th Aerodynamic Testing Conference, September, 1972.

16. Davis J. W.: AGARD Model B Transonic Blockage Investigation. Presented at the 39th Semi-Annual Meeting of the Supersonic Tunnel Association, March, 1973.

17. Gardenier, H. E.: The Extent and Decay of Pressure Disturbances Created by the Holes in Perforated Walls at Transonic Speeds. TN-56-1, AEDC, April 1956.

18. Chew, W. L.: Cross Flow Calibration at Transonic Speeds of Fourteen Perforated Plates with Air Flow Parallel to the Plates. TR-54-65, AEDC, July, 1955.

19. Chew, W. L.: Characteristics of Perforated Plates with Conventional and Differential Resistance to Cross Flow and Air Flow Parallel to the Plates. AEDC, July, 1956.

20. Equations, Tables, and Charts for Compressible Flow. NACA Report 1135, 1953.

21. Sims, J. L.: Tables for Supersonic Flow Around Right Circular Cones at Zero Angle of Attack. SP-3004, NASA, 1964.

22. Jacocks, J. L.: Determination of Optimum Operating Parameters for the AEDC-PWT 4 Ft. Transonic Tunnel with Variable Porosity Test Section Walls. TR-69-164, AEDC, 1969.

23. Ferri, A.: Report of Ad Hoc Committee on Engine Airplane Interference and Wall Corrections in Transonic Wind Tunnel Tests. Presented at the AGARD Advisory Groups for Aerospace Research and Development Meeting, April 26-28, 1971.

REFERENCES (Continued)

24. Davis, J. W.: Multiple Regression Technique for Pth Degree Polynomials With and Without Linear Cross Products. NASA TN D-7422, May 10, 1970.

25. Pun, L.: Introduction to Optimization Practice. New York: John Wiley and Sons, 1969.

26. Robertson, J. E. and Chevalier, H. L.: Characteristics of Steady-State Pressures on the Cylindrical Portion of Cone-Cylinder Bodies at Transonic Speeds. TDR-63-104, AEDC, August 1963.

27. Anderson, C. F., Anderson, A. and Credle, O. P.: The Effect of Plenum Volume on The Test Section Flow Characteristics of a Perforated Wall Transonic Wind Tunnel. TR-70-220, AEDC, 1970.

28. Jacocks, J. L.: Determination of Optimum Operating Parameters for the AEDC-PWT 4-Foot Transonic Tunnel with Variable Porosity Test Section Walls. TR-69-164, AEDC, August 1969.

29. Mitchel, G. A.: Blockage Effects of Cone Cylinder Bodies on Perforated Wind Tunnel Wall Interference. TMX-1655, NASA, October 1968.

30. Hartley, M. S. and Jacocks, J. L.: Static Pressure Distributions on Various Bodies of Revolution at Mach Numbers from 0.60 to 1.60 TR-68-37, AEDC, March 1968.

31. Erickson, E. W. and Dowling, E. D.: Transonic Pressure Tests on a Series of 3.480 Inch Diameter Cone-Cylinder Models in the Convair High Speed Wind Tunnel. HST-TR-021-0, Convair Division of General Dynamics, April 1961.

32. Hartley, M. S. and Nickols, J. H.: Model Blockage Study Test Results from the NASA Huntsville 14 X 14-Inch Trisonic Tunnel. AEDC-PWT Aerodynamics Branch Departmental Correspondence, September 23, 1965.

33. Houser, R. J.: Experimental Pressure and Normal Force Distribution Data for a Family of Cone-Cylinder Configurations at Test Mach Numbers from 0.7 to 2.0. LMSC/HREC-A710143, Lockheed Missiles and Space Company, March 1965.

34. Page, W. A.: Experimental Study of the Equivalence of Transonic Flow about Slender Cone-Cylinders of Circular and Elliptic Cross Section. TN-4233, NACA, April 1968.

REFERENCES (Concluded)

35. Coe, C. F. and Kashey, A. J.: The Effects of Nose Bluntness on the Pressure Fluctuations Measured on 15 and 20 Degree Cone Cylinders at Transonic Speeds. TMX-779, NASA, January 1963.

36. Snedecor, G. W. and Cochran, W. G.: Statistical Methods. Ames, Iowa: The Iowa State University Press, 1967.

37. Graybill, F. A.: An Introduction to Linear Statistical Models, Volume I. New York: McGraw-Hill, 1961.

38. Smille, K. W.: An Introduction to Regression and Correlation. New York: The Ryerson Press, 1966.

39. Abromowitz, M. and Stegun, I. A.: Handbook of Mathematical Functions. National Bureau of Standards, 1964.

*U.S. GOVERNMENT PRINTING OFFICE: 1973-739-153/52